NASA CONTRACTOR REPORT 177355

ACOUSTIC CHARACTERISTICS OF 1/20-SCALE MODEL HELICOPTER ROTORS

RAJARAMA K. SHENOY
FRED W. KOHLHEPP
KENNETH P. LEIGHTON

CONTRACT NAS2-11310
August 1986

NASA

NASA CONTRACTOR REPORT

Acoustic Characteristics of 1/20-Scale Model Helicopter Rotors

R.K. Shenoy
F.W. Kohlhepp
K.P. Leighton

Sikorsky Aircraft Division
United Technologies Corporation
Stratford, Connecticut

Prepared for
Ames Research Center
under Contract NAS2-11310

National Aeronautics and
Space Administration

Ames Research Center
Moffett Field, California 94035

Table of Contents

ABSTRACT

Results of an investigation of rotor acoustics using small scale models conducted in the United Technologies Research Center (UTRC) Acoustic Research Tunnel is presented here. Main rotor models of approximately 1/20-scale for the S-76 and the UH-60 systems were used to evaluate the extent to which small scale models can be used to predict the noise characteristics of larger scale and full-scale rotors. The effect of blade design parameters such as twist and tip design (airfoil, planform, sweep and taper) were studied. Operating parameters such as forward speed, rotor loading, tip speed, and rotor tip path plane were systematically varied to determine their effect on various rotor noise mechanisms. In all, four rotors were tested under the contract NAS2-11310 and three additional rotors were tested under the Sikorsky IR&D funds. For the sake of completeness data from all the seven rotors have been made available in this report.

Tests were conducted at low-speed (50-70 knots) and at higher speeds. The results of the 1/20-scale model low-speed tests are extensively compared with those of approximately 1/5-scale model tests conducted in the NASA Langley Research Center's 4mx7m Wind tunnel. Two microphone locations, one under the rotor disk and one in the forward direction at approximately 30° below the tip path plane are chosen for these comparisons. The high-speed test results are only compared with full-scale rotor acoustic data since the 1/5-scale model tests could not be conducted at high tunnel speeds in the 4mx7m tunnel in an open throat configuration.

The results show that the Reynolds number effects significantly alter the acoustic signature during Blade-Vortex Interaction (BVI) conditions. This is observed as a single sided impulse rather than a positive-negative impulse of high frequency content. In the spectral domain, these effects appear as enhanced low frequency and subdued high frequency content. At higher advance ratio conditions, in the absence of BVI, the 1/20-scale model noise trends with rotational Mach number are similar to those of the larger scale models. However, at high thrust and large advance ratio conditions, the 1/20-scale model acoustic trends appear to indicate early stall.

List of Figures

List of Figures (Cont'd)

List of Figures (Cont'd)

List of Figures (Cont'd)

List of Figures (Cont'd)

List of Figures (Cont'd)

List of Figures (Cont'd)

List of Figures (Cont'd)

List of Figures (Cont'd)

List of Tables

List of Symbols

BVI	-	Blade Vortex Interaction
C	-	Chord Length (m), (ft)
C_L	-	Lift Coefficient
C_T	-	Thrust Coefficient
D	-	Rotor Diameter
dBA	-	A-Weighted Sound Pressure Level
dBD	-	D-weighted Sound Pressure Level
M	-	Mach Number
$M_{\Omega R}$	-	Rotational Tip Mach Number
$M_{1,90}$	-	Advancing Blade Tip Mach Number
OASPL	-	Overall Sound Pressure Level
R	-	Radial Distance
Re	-	Reynold's Number
Re_c	-	Critical Reynold's Number
T	-	Temperature (°C)
U	-	Characteristic Velocity (m/sec) (ft/sec)
V_f	-	Forward Velocity (m/sec), (ft/sec)
V_T	-	Tunnel Speed (m/sec) (knots)
V_{tip}	-	Rotor Tip Velocity (m/sec), (ft/sec)
X	-	Chordwise Coordinate
Y	-	Thickness Position
α_{TPP}	-	Tip Path Plane Angle (degrees)
μ	-	Advance Ratio
σ	-	Solidity

1.0 INTRODUCTION

The rotorcraft of today generate complex acoustic signatures. Contributions from both the main and tail rotors arise from a number of complex aerodynamic events. Main rotor wake interactions with main and tail rotors, turbulence ingestion, volume displacement, and tail rotor/pylon interaction effects are just a part of the complex environment that the rotorcraft aeroacoustician must face. The apparent intractability of this situation leads one to utilize a phenomenon-oriented approach to understand the problem and propose solutions. In this way, important steps may be taken to reduce the noise in spite of the lack of a first principles, all-encompassing aeroacoustic theory.

One technique which is utilized to reduce the complexity of the problem and provide direct control of the important parameters is wind tunnel testing of isolated components. Many tests have been conducted on various scales in various facilities. Acoustic measurements of a full-scale rotor have been made in the NASA Ames wind tunnel by M. Mosher[1]. Acoustic treatments to the tunnel were not incorporated at the time of these tests. Four tip shapes were studied, and the test identified a low noise configuration. Schmitz, et al, [2] have conducted anechoic wind tunnel (DNW) tests to compare model scale data with data acquired utilizing their in-flight technique [3].

Model scale testing in wind tunnels for explicit acoustic purposes have taken place since 1966, when Leverton [4] conducted his initial tests to study "Blade Slap" utilizing a small scale model. Harris and his co-workers at Massachusetts Institute of Technology have conducted a number of anechoic wind tunnel tests on a 1/10-th scale model [4,5]. Although valuable insights into the rotor noise problem were gained, the low Mach numbers together with the low Reynold's numbers involved raise questions with respect to the direct applicability of their results to full-scale rotors. It is known that important aerodynamic factors such as the boundary layer thickness and the vortex structure are sensitive to the Reynold's number. Unfortunately, no definitive experiment has been conducted to date which determines the critical transition region for various aeroacoustic phenomena.

Because of the importance of the radiated acoustics to the military detection and the community annoyance problems, it is expected that acoustic wind tunnel testing will be an important component of future rotorcraft technology development. Although anechoic wind tunnel facilities exist at the United Technologies Research Center [6] and Massachusetts Institute of Technology, the test section size limits the scale of models which can be tested.

It is therefore important to determine if any of the rotorcraft noise mechanisms can be re-produced at these small scales.

This report provides an account of the series of small (0.76 meter diameter) model rotors tested in the U.T.R.C. Acoustic Research Tunnel (ART). The effects of several design and operating parameters on the noise characteristics are evaluated. Test conditions representive of low speed descent are included to study the blade/vortex interaction noise phenomenon. High speed noise is evaluated for a number of level flight conditions up to high speed cruise (140 kts, 71.4 m/sec). Overall noise and integrated flight-scaled metrics are used to evaluate the noise level for all conditions.

A cooperative program to study the main rotor/tail rotor interaction noise problem under the NASA contract NAS1-17146 is presently underway. Under this NASA/ARMY/SIKORSKY effort an isolated 1/5-scale main rotor wind tunnel test in the Langley 4 x 7 meter wind tunnel was conducted in 1983 [7]. The results of those tests are compared with the 1/20-th scale low speed acoustic data taken in the U.T.R.C. (ART). Since it has been shown that blade-vortex interaction noise may be successfully scaled [8] on a rotor of approximately the same geometric scale (1/7-th scale model of the AH-1G helicopter rotor) and that the 4 x 7 m tunnel can be used for BVI acoustic investigations [9], the 4 x 7 meter tunnel results are used as the benchmark by which the usefulness of the 1/20-th scale test is determined.

2.0 TEST FACILITIES, APPARATUS AND PROCEDURES

2.1 UTRC Acoustic Research Tunnel

The investigation was conducted in the UTRC Acoustic Research Tunnel (ART). This anechoic wind tunnel has been extensively used for various aeroacoustic research projects involving small scale helicopter rotors [6], propellers, jet engine fans and exhaust nozzles. A picture of the experimental model installed in the ART is shown in figure 1. Fiberglass wedges cover all walls, the ceiling, the floor, and the turntable mechanism supporting the model rotor system. These wedges may also be seen in Figure 1.

The wind tunnel is an open-circuit, open-jet facility. A number of (circular) nozzles of various geometries may be installed in the tunnel. For this experiment the 1.27 m (50 inch) diameter nozzle was used. This allows an upper limit of tunnel speed of 72 m/sec (140 kts). Figure 2 provides the dimensions of the ART and the microphone locations used during the test. The background noise at two in-flow microphones are provided in Appendix A. Since the out-of-flow microphones have much lower ambient noise levels, their background noise has not been shown.

2.2 Acoustic Test Rig

The experiment was conducted utilizing Sikorsky's Acoustic Test Rig (ATR). A schematic of the ATR is shown in Figure 3. The system consists of a rotor hub and swashplate assembly attached to the front end of a variable frequency drive motor which is cantilevered from the metric side of a six component strain gage balance. The ground side of the balance is supported from the upper end of the main vertical support strut. The lower end of the support strut attaches to the turntable mechanism which provides rotor shaft tilt capability. The motor housing was faired and the vertical support strut remained outside of the flow for all test conditions.

The rotor hub had blade flapping capability, but had no lead-lag hinge. Blade flapping motion can be measured on one blade by means of a flapping potentiometer mounted from a bracket on the hub and a sector gear attached to the spindle. Collective pitch is set remotely by movement of the swashplate assembly by a linear actuator mounted to the drive motor. A potentiometer is provided to calibrate swashplate travel and blade pitch. A support housing is bolted to the front plate of the drive motor which acts as a guide for movement of the swashplate and also houses a bearing

just below the rotor hub to support over hung loads developed by the rotor system. The rotating element of the swashplate is driven by two studs, acting as rotating scissors, which are located at a 180 degree spacing on the unit. These studs extend upwards and slide through two bushings in the rotor hub. The non-rotating swashplate is restrained by the collective drive pinion. The rotor system has no cyclic pitch capability.

The drive motor is a Task (subsidiary of Able Corporation) variable frequency 4 pole motor rated at 20 horsepower at 12,000 RPM, 400 cycles and 1.2 volts/Hz. The motor is equipped with a hole drilled through the length of the armature shaft to permit routing of the instrumentation wiring. The rear of the armature shaft is threaded to permit installation of the slip ring used for measurements on the rotating components.

The motor with swashplate assembly and rotor is supported from a Task Corporation six-component internal strain gage balance. The raw balance signals are sent to the data acquisition/control unit. A schematic of the system used for processing the balance data and the other non-acoustic data is shown in Figure 4. The HP 3497A Data Acquisition/Control unit has a 20 channel multiplexer with thermocouple compensation and a 100 kHz reciprocal counter. Acting as a digital volt meter, the units A-to-D converters relay all balance and thermocouple signals to the HP86 desktop computer system. The HP86 applies a calibration matrix to the signals to obtain the relevant loads in engineering units. Control system software then displays this information on the HP82913A monitor. The pilot, interacting with this display, adjusts shaft tilt and collective pitch to set the desired operating conditions. When the conditions specified in the test plan have been reached, final data acquision is begun. These data points are stored on floppy disks within the HP 9130A disk drive, and a hard copy is produced by the HP 82905B printer. A sample of this printout is shown in Figure 5.

2.3 Acoustic Data Acquisition System

A schematic of the acoustic data acquisition system is shown in Figure 6. Six 0.635cm (0.25 in) B&K type 4135 condenser microphones were used. Their location in the wind tunnel is shown in Figure 2. The three microphones located in the flow (mics 2, 8 and 9) are fitted with B&K type UA0385 nose cones. B&K type 2633 preamplifiers are connected to B&K type 2807 power supplies. These power supplies are connected via BNC cables to custom built amplifiers/attenuators in the control room. The output of the amp/attenuator system is then split. Each microphone signal is fed

directly to the EMI 9000 28-channel tape deck. Also the signals for each microphone are sent to Krohn-Hite 3342 high pass filters, where a 30 kHz high pass filter was applied. These filtered channels were then amplified by NEFF model #124A amplifiers. These filtered signals were then recorded on separate channels of the EMI 9000 tape deck. The filtered signals provide an improved signal to noise ratio for the higher frequencies present during BVI conditions, where the lower frequencies are of very high level. On-line monitoring of the acoustic measurements was provided by a Nicolet 4094 digital oscilloscope (time histories) and a Nicolet 444 spectrum analyzer (narrow-band spectra). Selected time waveforms were stored with the Nicolet 4094 floppy disk drive and plots were obtained on an HP 7074A digital plotter. A 32-channel Scan-Scope #1810 was connected to the output of the playback channels of the tape deck to verify that acceptable signal levels were recorded for each test condition.

A once per revolution signal was recorded simultaneously with the acoustic data. The once per revolution signal was generated as follows. A 72 tooth gear was attached to the rotor shaft. One of the teeth on this gear was removed. A magnetic pick-up was mounted in the fixed frame. The low-level signal generated by the rotating gear was amplified and conditioned by a "missing pulse" detector circuit. The missing pulse, which was generated by the missing gear tooth, was recorded as the once per revolution timing pulse. The missing tooth on the gear was aligned with the blade which drove the flapping potentiometer. This permitted orienting the flapping trace to blade azimuth. The flapping trace in conjunction with shaft angles could then be used to determine blade tip path plane angle.

To verify the adequacy of the acoustic data acquisition system frequency response characteristics a "white noise" signal (2 Hz to 200 kHz bandwidth) was inserted into each channel. The resulting spectra were flat from 2 Hz - 80 kHz, which was the frequency range of interest for this test program. A B&K type 4220 pistonphone was used to apply a 123.8 dB, 250 Hz calibration tone to each microphone channel prior to and upon completion of acoustic data acquisition for the day.

2.4 Data Reduction Techniques

The primary data reduction format used was a 1/12-th octave spectrum, with the equipment required for this reduction technique shown in Figure 7. The FM magnetic tape, which was recorded at 120 ips and IRIG wideband group I, was Ampex type 797. The test condition selected is located on the tape and the relevant micro-

phone signal is sent to either a B&K 2131 Digital Frequency Analyzer or a combination of a B&K 2134 Sound Intensity unit and a B&K 4715 Display unit. There the data is digitized and digital filters provide the 1/12-octave spectral components of the signal. These 1/12-octave levels are then used to compute flight scaled A-weighted, D-weighted and Overall Sound Pressure Levels (OASPL) using a program developed at Sikorsky Aircraft. This flight scaling is achieved by shifting the weighting functions by the ratio of the model scale frequency to the full scale frequency. These shifted weighting functions are then applied to the 1/12-octave spectral components. Typically the data reduction is conducted at 30 ips tape speed. Not only does this enhance the accuracy by bringing the higher frequencies within the capability of the analyzer, it also facilitates the comparison of the 1/20-th scale model rotor data with data from the 1/5-th scale rotor. The resulting spectrum and metrics are then plotted on an HP 9872A 4-pen digital plotter. A sample of the 1/12-th octave spectrum and metrics is shown in Figure 8. Tunnel background noise spectra (1/12-th octave bands) with model installed without rotor blades are shown in Appendix A for various tunnel speeds.

Acoustic time histories and narrow band spectra were acquired for selected test points to provide supplementary information for data analysis. Narrow band spectra are shown in Appendix B. For the acoustic time histories, a HP 5423 analyzer replaces the desktop computer and the B&K frequency analyzers as shown in the schematic of figure 7. The acoustic data is processed for instantaneous time history. For acquisition of bandwidth adjustable narrow band acoustic data an HP 5420 Spectral Analyzer is used. Once again the HP 5420 replaces the desktop computer and B&K analyzer as shown in the schematic of Figure 7. Average power spectral density plots are obtained with "free run" sampling (without synchronizing with rotor RPM) and using a Hanning window.

2.5 Model Rotor Blades

Table I summarizes the rotor configurations tested. Figure 9 shows the planforms of the seven (7) rotor systems tested, along with the twist and airfoil information. Essentially two different airfoils have been used in the tip region of various configurations. The SC1095 airfoil, in use on many Sikorsky Aircraft models, is called the standard airfoil. The SSC-A09 airfoil, designed for higher Mach number operation, is called the advanced or the new airfoil. The profiles of these two airfoils are shown in figure 10. The rectangular tip rotor is a scaled version of the UH-1H rotor with NACA0012 airfoil. As the rotor bearings were showing signs of wear, the UH-1H rotor was not tested at high tunnel speed.

The rotor blades have a .76 meter (30 inch) diameter and a 2.54 cm (1.0 inch) chord. Configuration 7, representative of the UH-1H rotor, has a 2.77 cm (1.09 inch) chord. The elastic axis and C.G. of the blades are coincident at the quarter chord. The blades were fabricated using fiberglass (skins), graphite (spar) and foam in a two piece high temperature epoxy. The blades used are not dynamically scaled since dynamic scaling at such a small geometric scale is virtually impossible. Every attempt was made to maintain a close tolerance during the manufacturing process to ensure uniformity of blades.

The Reynolds number on various configurations varied significantly due to the changes in the blade tip chord and rotational speed. The Reynold number at two tunnel speeds for the 1/20-scale model as well as for the 1/5-scale model and the full scale helicopter rotor blades are provided in Table II.

TABLE I
BLADE GEOMETRIC DESCRIPTION

CONFIG NUMBER	TIP	AIRFOIL	TWIST	SWEEP AND TAPER BEGINNING	SWEEP	TAPER
1	Baseline Tip	SC1095	-16°	.94R	20°	.6C
2	S-76 Tip	SC1095	-10°	.95R	30°	.6C
3	Large Swept Tapered Tip	New Airfoil*	-16°	.92R	33°	.6C
4	Large Swept Tapered Tip	SC1095	-16°	.92R	33°	.6C
5	Rectangular	NACA0012	-10°	---	No Sweep	No Taper
6	Parabolic Swept Tip	New Airfoil*	-16°	.92R	30°	.6C
7	Baseline Tip, Low Twist	SC1095	-10°	.94R	20°	No Taper

* NEW AIRFOIL - SSCA09 TIP, SC1095 INBOARD

TABLE II
REYNOLDS NUMBER RANGE OF CONFIGURATIONS TESTED

SCALE	CONFIG #	DESCRIPTION	ΩR m/SEC	Reynolds Number in Millions V=30.7 m/sec (60 kts) @ r = 1.0R	V=30.7 m/sec (60 kts) @ r = 0.9R	V=71.7 m/sec (140 kts) @ r = 1.0R	V=71.7 m/sec (140 kts) @ r = 0.9R
1/20	1	Baseline, -16°	221	0.459	0.418	0.533	0.493
	2	S-76 Tip, -10°	205	0.259	0.393	0.303	0.468
	3	LSTT, New A/F, -16°	221	0.275	0.418	0.32	0.493
	4	LSTT, Std A/F, -16°	221	0.275	0.418	0.32	0.493
	5	Rect. Tip (UH-1H)	248	0.554	0.505	X	X
	6	PST, New A/F,	221	0.275	0.418	0.32	0.493
	7 A	Baseline, -10°	221	0.459	0.418	0.533	0.493
	B	Baseline Tip -10°	205	0.431	0.393	0.505	0.468
1/5	1	Baseline Tip, -16°	221	1.652	1.505	1.919	1.775
	2	S-76 Tip,-10°	205	0.803	1.218	0.939	1.451
FULL		UH-60	221	9.5	8.653	11.033	10.205
		S-76	205	4.04	6.13	4.727	7.3

3.0 RESULTS AND DISCUSSION

The results of the test described in the preceding sections are presented here. The effects of geometric scale on the acoustic pressure time history, spectral characteristics and trends of integrated noise metric with various parameters are shown. In addition, the noise trends with various flight and design variables are provided for both the BVI and high speed level flight conditions.

Though the original intent was to develop noise trending relationships with operational parameters for various rotor blade configurations, as shown in Reference 10 and also later in this section, simulation of the larger scale model acoustic characteristics at lower speeds could not be achieved with confidence. Even while failing to achieve the larger scale representation, this research program highlighted and revealed significant effect of viscosity on various noise source mechanisms of a rotor.

The results are first presented for the low speed condition and later for the high speed condition. The Microphone locations used in these discussions are provided in Table III.

3.1 Low Speed Acoustics

Typically Blade Vortex Interaction (BVI) noise dominates acoustics under descending conditions (positive tip path plane angles) in the low speed flight regime. All the seven rotor configurations shown in Figure 9 were tested at low speeds. Typical test matrix used during these low speed tests is provided in Table IV. In addition to the conditions provided in Table IV, rotational speed, tunnel speed (at constant advance ratio) and thrust coefficient were varied for some of the configurations to study their effect on acoustic characteristics. Results of these tests are provided in this chapter. Details of the narrow band spectra for selected cases are provided in Appendix B and sample 1/12-octave band spectra for both the 1/20 and 1/5-scale models are provided in Appendix C.

TABLE III
MICROPHONE LOCATIONS

1/20 Scale	1/5 Scale	Full Scale
FORWARD, DOWN:		
MIC 2 (r/D=1.0,Ψ=155°,θ=30°)	MIC 5 (r/D=1.6,Ψ=177°,θ=23°)	MIC 1 (r/D=1.5, ψ=178°, θ=15°
UNDER THE ROTOR		
MIC 9 (r/D=0.25,Ψ=110°,θ=35°)	MIC 1 (r/D=0.25,Ψ=110°,θ=35°)	
ON-AXIS, ON THE WAKE SIDE		
MIC 7 (r/D = 3.0) - out of flow MIC 8 (r/D = 0.5) - in flow		

TABLE IV

TYPICAL LOW SPEED TEST MATRIX

CONFIG #	CONFIG DESCRIPTION	TWIST	ΩR m/sec	ΩR ft/sec	TUNNEL m/sec	TUNNEL knots	C_T
1 3 4 6	BASELINE LSTT,SSCA09 LSTT,SC1095 PST,SSCA09	-16°	221	725	30.7	60	0.007
2 7	S-76 BASELINE TIP	-10°	205.6	675	30.7	60	0.007
5	UH-1H	-10°	248.1	814	35.8	70	0.0056

3.1.1 Effect of Geometric Scale:

The acoustic time history for the 1/20-scale model S-76 Configuration (#2) rotor under typical BVI conditions is compared with that of the 1/5-scale model (Ref 10) under similar conditions (with the exception of the microphone location and minor difference in speed of sound) in Figure 11. The 1/5-scale model data was acquired in the NASA 4mx7m wind tunnel under the contract NAS1-17126 and further details can be obtained in Reference 7. Additionally, these data are compared with the acoustic time history of the S-76 helicopter in descent at 6° glide slope and 38 m/sec (74 knots). Unfortunately this is a higher advance ratio condition than the model test conditions. Further, the thrust coefficient of the full-scale flight test is lower than that for the scale models and the time history is obtained at an instance when the S-76 helicopter was estimated to be at a position where the microphone is approximately 30° below the main rotor path plane. Consequently, though one cannot make a direct comparison of the model scale results with the full-scale results, the characteristics of their BVI noise signature can be compared.

It can be seen in Figure 11 that the 1/20-scale model S-76 rotor (config. 2) BVI acoustic time history does not adequately show the multiple impulses of the larger scale rotors. However, the individual blade interactions with the vortex are well defined. This data in spectral domain is shown in Figure 12 together with that of the 1/5-scale model. While the 1/5-scale model spectra shows multiple lobes, the 1/20-scale model spectrum has no lobes. This could be caused by either the reflections in the semi-anechoic NASA 4x7m tunnel used for testing the 1/5-scale model or by the lack of multiple inpulses in the 1/20-scale model BVI acoustic time history. Further, the spectral levels at mid-frequencies relative to the first harmonic level are slightly smaller for the 1/20-scale model than the same for the 1/5-scale model.

While the data at advance ratio of 0.15 for the S-76 configuration showed discrete and well defined BVI impulses, the data at other advance ratio conditions have shown significant unsteadiness and at times drastically different characteristics. Acoustic time histories of the 1/20-scale S-76 configuration at various advance ratios is shown in Figure 13. Though it would have been useful to hold constant Mach number while changing the advance ratio, such a variation was not done. However the BVI time histories at two Mach numbers (0.69 and 0.746) and an advance ratio of 0.15 show similar characteristics (Figure 11 and 13a) indicating that the effect of Mach number on the character of the signature is negligible. Keeping this in mind, one can clearly see from Figure 13 that the advance ratio effects the BVI acoustic signature of the 1/20-scale model significantly.

Acoustic characteristics of the baseline tip configuration 1 at an advance ratio of 0.14 are provided for the 1/5 (mic 5) and 1/20-scales in Figure 14. As in the case of the S-76 configuration 2 (mic 2), the 1/20-scale model BVI does not have the impulsivity exhibited by the 1/5-scale model rotor. Further, the BVI impulse appears as a very large low frequency positive impulse which causes the first few harmonic noise levels to increase in the spectral domain. In the mean time the mid frequency harmonic levels are considerably lower than those for the 1/5-scale model even though the microphone was placed nearer to the 1/20-scale model (1.0 diameter) than the one used in the 1/5-scale model test (1.6 diameter). Once again, the low frequency character does not appreciably change with the Mach Number (Figure 15). It does not appear to change at microphone 9 either (Figure 16).

Acoustic Characteristics similar to the Baseline configuration 1 was obtained for the LSTT with new airfoils (Config. 3) at identical conditions (Figure 17). However, the two bladed UH-1H configuration 5 at an advance ratio of 0.145 yielded slightly more impulsive signature (Figure 18) than the one shown in Figure 17 for the 1/20-scale model. Though the character of the acoustic signature for this configuration is similar to the one obtained for the S-76 configuration at an advance ratio of 0.15 (Figure 11), BVI impulse is wider than that of the S-76 configuration 2.

From the discussion so far, it should be noted that all the 1/20-scale models have lower frequency BVI signature and that the signal character is very sensitive to the advance ratio. Since the advance ratio determines which part of the trailed vortex the blade interacts with, if certain sections of the small scale model trailed vortex wake are in a very turbulent state (with mutual interactions), one can explain why the BVI acoustic signature is sensitive to the advance ratio. Further work is warranted to study this phenomenon.

Even when the higher harmonic noise levels are suppressed by the viscous effects at the 1/20-scale, one can still see discrete tones in the BVI noise spectra (Figures 12, 14 and 17). Appendix B provides a sample of narrow band power spectral density plots for each one of the seven configurations tested. From these it is fairly clear that the BVI noise is a discrete frequency noise and not a broadband noise phenomenon even at as low a Reynolds number (@ 90%R) as 400,000.

3.1.2 Effect of Scale on Noise Trends:

The 1/20-scale model BVI noise trends with thrust coefficient and advancing blade tip Mach number (at a constant advance ratio of 0.14) for the baseline rotor configuration 1 and the LSTT config-

uration 3 are compared with the corresponding 1/5-scale model rotor noise trends in Figures 19 and 20. The noise levels at microphone 2 of the 1/20-scale model data are corrected to account for the distance effect using the inverse square law. Similarly the noise levels at various thrust conditions for the 1/5-scale model are increased to account for the difference in the Mach number between the two scales (due to test temperature difference). This Mach number correction was based on the noise trends with advancing blade tip Mach number. From these two figures one may see that the overall sound pressure level (OASPL) for the 1/20 scale model are 3 to 8 dB higher than the same for the 1/5-scale model. On the other hand, "D" weighted noise levels (dBD) of the 1/20-scale model are lower for the baseline configuration and almost identical for the LSTT configuration. Of course, this is not totally surprising based on the discussions in the preceding section. It may be recalled that the lower frequency levels were enhanced at the 1/20-scale and the mid-frequency levels were suppressed. OASPL, being an unweighted noise metric, is dominated by the increased levels of lower frequency. On the other hand, dBD being weighted higher at the mid to high frequency region, downplays the increase in the lower frequency levels. Fortuitously the increase in the lower harmonic noise levels and the reduction in the higher harmonic noise levels compensate each other in the "D" weighting scheme, resulting in almost equal dBD levels for the two scale models of the LSTT (#3) configurations (Fig. 20). For the baseline configuration the suppression in mid-frequency BVI noise level at the 1/20-scale is far too large and hence the 1/5-scale dBD levels are higher than those of the 1/20-scale (Figure 19). Additionally, the 1/5-scale model dBD noise levels increase with the thrust coefficient at a higher rate than the same for the 1/20-scale. Once again this is the manifestation of the fact that the acoustic levels in the mid-frequency region for 1/20-scale model are suppressed by viscous effects.

Tip path plane angle of the rotor with respect to the free stream determines if the rotor blades encounter strong vortex interactions. Consequently, it is an influential parameter which determines the BVI noise levels. Such noise trends for the baseline tip configuration 1 are provided at two directivity locations for both the 1/5-scale and 1/20-scale models in Figure 21. In these comparisons 1/20-scale microphone 2 data has been corrected (using inverse square law) to a reference distance of 1.6 rotor diameter and the 1/5-scale model test data has been corrected to 15°C. Since the 1/20-scale model test was conducted at approximately 15°C, no temperature correction was applied to it. From Figure 21 one can notice that the OASPL for the 1/20-scale model is higher than the 1/5-scale model in the forward location (mics 2 and 5).

However, the inverse is true under the rotor (mics 9 and 1). On the other hand the weighted noise metrics (dBA and dBD), indicative of the higher frequency BVI noise, remain lower than the 1/5 scale model throughout the test range. In addition, the 1/20 scale model dBA and dBD metrics are far less sensitive to the tip path plane variations than the 1/5-scale model noise.

3.1.3 1/20 Scale Model BVI Noise Trends:

So far it has been shown that the 1/20-scale models do not adequately reproduce the larger scale BVI noise trends. Consequently, additional noise trend data is presented sparingly for BVI conditions. First of all the BVI noise trends with the thrust coefficient at two tip path plane angles and two microphone locations are provided in Figures 22 and 23 for the baseline configuration 1 and the LSTT with new airfoil configuration 3 (quietest in 1/5-scale tests). Very little difference in the BVI noise trends with thrust may be seen from these figures. As discussed in the earlier section, these trends are smaller than the trends obtained at the 1/5th scale.

Another interesting comparison between the 2-bladed UH-1H configuration 5 and the baseline UH-60 configuration 1 is provided in Figure 24. It should be noted that the rotational tip Mach number and the advance ratio for the two tips are different. The intent here is to illustrate the fact that the OASPL for the UH-60 configuration 1 with respect to their dBD and dBA levels are far higher than the same for the UH-1H configuration 5. Once again, this can be related to the acoustic time history characteristics of 1/20-scale models shown in Figures 14 and 18.

3.1.4 Nearfield-Farfield Comparisons:

The relationship between the nearfield (0.5D) measurements and the farfield (3.0D) measurements are shown in Figures 25 and 26 at two on-axis microphones. These on-axis microphone locations are used to minimize the shear layer diffraction effects. Except for the baseline configuration 1, similar noise trends with the tip path plane angles for the nearfield and farfield microphones can be seen in these figures. Indeed difference between the near-field and far-field microphone noise levels for the LSTT configuration 3 with new airfoils and LSTT configuration 4 with SC1095 airfoils is approximately 11 dB in OASPL and 10 dB in dBD at all tip path plane angles. If one were to assume that the BVI noise source is at the hub this translates into $(d)^{-1.3}$ relationship for dBD and $(d)^{-1.4}$ relationship for OASPL. Indeed the BVI noise source is not at the hub and it is probably closer to the blade tip. If we make such an assumption, the BVI noise relationship with distance is approximately $(d)^{-1.6}$ for dBD and $(d)^{-1.7}$ for OASPL.

In the case of the baseline configuration 1, an anomalous behavior in the D weighted noise level can be seen in Figure 25. The 1/12 octave spectra for the in-flow microphone 8 shows (Figure 27) an unusually large "hump" in the near-field spectra. Such a "hump" is not present in the case of the Large Swept Tapered Tip Configuration 3 with new airfoils (Figure 28). For unknown reason, the "humpy" spectra for configuration 1 at microphone 8 was seen at all conditions tested and similar behavior was also present for the lower twist baseline tip configuration 7 and the Parabolic Swept Tip configuration 6. Other configurations did not show such a behavior.

3.2 High Speed Acoustics

In the earlier section the BVI noise dominated low speed acoustic characteristics of the 1/20-scale model main rotors were discussed. In this section the characteristics of these model rotors at high-speed flight are discussed. Since approach and take-off are seldom conducted at high speeds, only the level flight conditions are simulated. The model was typically tested at increasing nose down position (negative tip path plane angles) with the tunnel speed to simulate the propulsive force required to overcome the system drag forces. The tip path plane schedule used with the tunnel speed is shown in Figure 29.

The rotor bearings showed excessive wear during the high-speed test runs of the UH-1H configuration (#5) and hence it was decided not to continue testing them. Consequently, high-speed noise data on this configuration could not be obtained. Additionally, though an in-plane microphone location on the advancing side would have been ideal for high-speed noise measurements, due to the tunnel and model sizes and for fear of flow distortions, decision was made not to place any in-plane microphones. All the data is presented for the same microphone locations (Mics 2 and 9) as in the previous section. Scale comparisons, while being sparse, are typically conducted with the full-scale UH-60 and S-76 flight test data available in the public domain.

3.2.1 Effect of Scale on High-Speed Noise

Unlike the low speed conditions, high-speed noise data on the larger scale configurations of the 1/20-scale models tested are sparse. While 40 x 80 ft wind tunnel (acoustically untreated) test data for the full-scale S-76 rotor (Ref. 1) is available, they are affected by tunnel reverberation and reflection. Indeed, a good account of the effect of wind tunnel walls on discrete frequency noise authored by the same author can be found in

References 13 and 14. Indications from these references are that the measurements at a microphone placed in the forward direction at approximately 1.5 diameter in the tunnel will probably be higher than the same in the free field. Even so, the OASPL and dBD levels for the 1/20, 1/5 and full-scale rotors are compared over a range of Mach numbers for the standard S-76 configuration in Figure 30.

Before drawing any conclusions on the agreement between the various scales, one has to bear in mind a few differences between the scale models tested. For example, the tip path plane schedule used for the 1/20-scale model is shown in Figure 29. However, the same for the full-scale rotor was a constant -5°. In the case of the 1/5-scale model, the data for a tip path plane angle of -2° is used. Further, the microphone placements in the three cases are different (Table III). In spite of these differences, a good agreement between the scale models appears to emerge in terms of OASPL. While the OASPL trends of 1/5 and 1/20-scale models are identical, the full-scale trend appears to be different. The noise levels for the full-scale model are far higher than the other scales at lower speeds and at very high speeds. It is not clear if the tunnel reverberation effects are the cause for this difference in the OASPL trend.

The full-scaled D-weighted noise trends shown in the same figure show significantly higher level for the full-scale model than those for the smaller models. However, the dBD noise trends (not the levels) with Mach number for the three scales become identical at higher speeds. Indeed, the trends are identical for the 1/5 scale and 1/20-scale models even at lower Mach numbers.

As discussed earlier, the high-speed negative tip path plane angle flight conditions represent non-BVI conditions. Though we have concluded that the BVI conditions are not well represented at the 1/20-scale, the general agreement in the noise trends shown in Figure 30 indicates that the non-BVI noise sources prevalent in the high-speed flight conditions are at least qualitatively represented.

Further evidence of this is provided in Figure 31, where the maximum "A" weighted noise trends at the centerline ground plane microphone during the flight tests of the UH-60 and the S-76 helicopters (Ref. 15) are compared with the flight scaled "A" weighted noise trends for the 1/20-scale model configurations 1 and 2. Absolute levels are not provided in these figures since the instance at which the maximum "A" weighted noise levels

occurred during the flight is not known. However, the trends were plotted by normalizing all the flight test data to 4.5 diameters over the microphone at the time of the helicopter's overhead location. The "A" weighted noise trends shown in Figure 31 show a good agreement between the 1/20-scale and the full-scale S-76 configuration considering the crudeness of the method of comparing the two. The 1/20-scale UH-60 model configuration 1 shows trends similar to the S-76 models, but the full-scale UH-60 noise trends are much different.

3.2.2 Effect of Translational Speed on Noise

The effect of design changes on the noise for various advancing blade tip Mach Numbers resulting from tunnel speed variations are shown in Figure 32. Of these configurations, only the S-76 configuration (#2) was operated at a tip speed of 205.7 m/sec (675 ft/sec) whereas the other configurations were operated at 221 m/sec (725 ft/sec). As can be seen, most of the configurations operated at the higher tip speed show decrease in the noise level from Mach 0.783 (90 knots) to 0.798 (100 knots). Indeed this is not surprising since the advance ratio at an advancing blade tip Mach number or 0.783 is only 0.21, which is still the region of vortex interactions.

It can also be noted from Figure 32 that the large swept tapered tip with the new airfoils is the quietest configuration tested. This incidentally is also the quietest of the tips tested at 1/5 scale under BVI conditions.

3.2.3 Effect of Rotational Tip Speed on Noise Trends

The noise levels in terms of OASPL, dBA and dBD at microphones 2 and 9 for various rotational tip speeds and 71.4 m/sec (140 knot) tunnel speed are discussed for various rotor configurations in this section. These levels are plotted in Figures 33 to 38. In these figures, both the baseline tip configurations 1 (Figure 33) and 7 (Figure 38) show steady increase in noise levels with rotational Mach number. On the other hand, the sensitivity of all other configurations to rotational tip Mach number is either fairly low or erratic, specifically at microphone 9 mounted under the disk. On the other hand, such insensitivity to the Mach number was not obvious in Figure 32 where the tunnel Mach number was varied.

Typically, one expects to find similar noise trends with advancing blade tip Mach number irrespective of whether the tunnel speed or rotational speed was changed within a reasonable range. The results shown here for all the rotors show a lower sensitivity to

Mach number when the rotational tip speed is varied and the tunnel speed is held constant. One of the differences of achieving particular Mach number through these means is the advance ratio. The advance ratio influences a number of acoustic phenomena such as the vortex interaction with the blade and retreating blade stall. All the 1/20-scale models tested were operated at low Reynold's numbers. Therefore, they are likely to stall at advance ratios lower than those for the larger scale models and result in increased noise levels. Such an increase appears to have caused higher than normal noise levels at lower rotational tip speeds and caused the models to have lower sensitivity to the tip speed changes. The fact that the larger chord baseline tip configurations 1 (Fig. 33) and 7 (Fig. 38) show a higher sensitivity to the tip speed than the other configurations with smaller chord (2, 3, 4, and 6; see Figs. 34 to 37) provides additional credibility to this hypothesis.

3.2.4 Effect of Rotor Lift Coefficient on Noise

Sound pressure levels in terms of OASPL, dBA and dBD are shown for a rotational tip Mach number of 0.65 and advance ratio of 0.327 in Figures 39 and 40 for a total of 5 configurations. The same for two configurations at a rotational tip Mach number of 0.607 and an advance ratio of 0.35 are shown in Figure 41. The sound pressure levels are provided at microphones 2 and 9 in all these figures. Though it would have been desirable to have data over a wide range of lift coefficients, due to the flapping and stress constraints on these small scale rotor models with no cyclic control, only limited data could be obtained during the tests.

As can be seen in Figures 39 through 41, typically the swept tapered tip configurations 2, 4, and 6, show less sensitivity to lift coefficient variations than the constant chord configurations 1 and 7. Similar behavior of the swept tapered tips was described in the earlier section when the rotational tip speed was varied. Once again the early stall introduced at small Reynolds number is believed to be the cause.

Though the trends obtained in Figures 39 through 41 cannot be reliably applied to larger scale models, one could still qualitatively assess the effect of some of the configuration changes. For example, Figure 39 shows that the higher twist rotor is quieter than the lower twist rotor. Similar comparison among swept tapered tips in Figure 40 shows that the large swept tapered tips (configurations 3 and 4) are quieter than the parabolic swept tip (config. 6).

The S-76 configuration 2 (-10° twist) and the baseline tip configuration 7 with -10° twist operated at a rotational tip Mach number of 0.607 show (Figure 41) that the swept tapered S-76 tip produces less noise than the untapered swept configuration 7.

4.0 CONCLUSIONS

The conclusions drawn from the present study are provided in this chapter. Of the many conclusions listed below, the large effect of viscosity on the acoustic characteristics of small scale models is of primary importance. From the discussions in the previous section on manifestations of viscous effects it can be concluded that very small scale rotor models should not be used to quantify the acoustic characteristics of larger rotors. It can also be concluded that very small scale rotors do not adequately represent the BVI noise characteristics of larger rotors and that only the high speed noise trends with tunnel speed are similar to the larger rotor trends. Much of these differences are believed to be due to viscous effects and in the list of conclusions provided in this chapter, the viscosity is believed to have influence on at least the first six. These and other conclusions from the present investigation are:

1. BVI noise of 1/20-scale model helicopter rotors do not approach the impulsivity of larger scale model rotors.
2. BVI noise of small scale models have higher amplitude at low frequency and smaller amplitude at higher frequency unlike the larger scale models which show a substantial increase in the mid-frequency and high frequency region.
3. The character of the BVI noise of 1/20-scale models change significantly with advance ratio indicating a possibility of significant interaction among the vortices in the wake.
4. 1/20-scale model BVI noise is less sensitive to tip path plane angle and thrust variations than the larger scale models.
5. The high-speed level flight condition noise trends of the 1/20-scale model with the advancing blade tip Mach number are fairly insensitive to the Mach number changes introduced by the rotational tip speed changes, particularly for tapered tip blade configurations.
6. The high-speed level flight condition noise of the 1/20-scale models is not very sensitive to thrust variations.
7. The large swept tapered tip configuration 3 with advanced airfoils was identified as the quietest of the 1/20-scale model tips tested at high-speed level flight conditions. Though this is the configuration identified as the quietest under BVI conditions (1/5-scale tests, Reference 10), it is technically not valid to utilize the 1/20-scale model data to evaluate tips for BVI noise. Since any comparison we obtain cannot be substantiated, such a comparison of tips is not provided.

8. The 1/20-scale model acoustic trends with Mach number are similar to those of the larger scale models when the tunnel speed is varied.

9. The acoustic pressure approximately decays as the inverse of 1.5 power of distance when measured between two on-axis microphones stationed at 0.5 and 3.0 rotor diameters from the hub.

10. BVI noise is dominated by discrete harmonics even for the 1/20-scale model rotor with a Reynolds number of approximately 400,000.

5.0 RECOMMENDATIONS

This study has shown a few similarities and a number of differences between the acoustic characteristics of very small scale (1/20-scale) and larger scale model helicopter rotors. In the process, the effect of viscosity on some of the rotor sound generation mechanisms have been highlighted. Specifically, it has been shown that the BVI noise is significantly altered and the high-speed noise, under certain thrust and advance ratio conditions, is altered. However, the thickness and high-speed impulsive noise mechanisms have not been addressed. Further, while indicating differences between various scales, this study has raised a number of fundamental questions with regard to the way the viscous effects alter various noise sources. It is therefore recommended that a series of experiments, preferably in a variable density tunnel, be conducted to address the following issues:

1. The effect of scale on thickness and high-speed impulsive noise. Specifically the effects on the following:

   a. Noise levels

   b. Boundary layer effects

   c. Shock-boundary layer interaction at transonic speeds

2. The effect of Reynolds number on BVI noise. Specifically the effects on the following:

   a. Vortex structure, strength and stability

   b. Mutual interaction between vortices at various advance ratio

   c. Transient flow-field during vortex interaction

3. The effect of Reynolds number on unsteady loading noise. Specifically the effects on the following:

   a. Stall at high advance ratio

   b. Stall at high lift coefficients

4. The smallest scale allowing adequate representation of various noise source mechanisms.

REFERENCES

1. Mosher, M. "Acoustic Measurements of a Full-Scale Rotor with Four Tip Shapes," NASA TM 85878, Ames Research Center, Moffett Field, California, April 1984.

2. Splettstoesser, W.R., K.J. Schultz, F.H. Schmitz and D.A. Boxwell, "Model Rotor High-Speed Impulsive Noise - Parametric Variations and Full - Scale Comparisons," Paper 83-39-53, 39-th Annual Forum, American Helicopter Society, St. Louis, Missouri, May 1983.

3. Schmitz, F.H. and D.A. Boxwell, "In - Flight Far - Field Measurement of Helicopter Impulsive Noise," J. Am. Helicopter Soc., Vol. 21, No. 4, October, 1976.

4. Widnall, S.E., W.L. Harris, A. Lee, and Drees, H.M., "The Development of Experimental Techniques for the Study of Helicopter Rotor Noise," NASA CR-137684, 1974.

5. Hubbard, J.E., Jr., N.G. Humbad, P. Bauer and W.L. Harris, "Parametric Studies of Model Helicopter Rotor Blade Slap at Low Tip Speeds," M.I.T. Fluid Dynamics Research Laboratory Report No. 79-1, Cambridge, MA, February, 1979.

6. Schlinker, R.H. and R.K. Amiet, "Tail Rotor Blade - Vortex Interaction Noise," Presented at the AIAA 8-th Aeroacoustics Conference, Atlanta, Georgia, April 11-13, 1983.

7. Martin, R.M. and Conner, A.B., "Wind Tunnel Acoustic Results of Two Rotor Models with Several Tip Designs", NASA TM 87698, July 1986.

8. Splettstoesser, W.R., K.J. Schultz, D.A. Boxwell and F.H. Schmitz, "Helicopter Model Rotor Blade-Vortex Interaction Impulsive Noise: Scalability and Parametric Variations", Presented at the tenth European Rotorcraft Forum, The Hague, Netherlands, August 28-31, 1984.

9. Hoad, D.R., "Helicopter Model Scale Results of Blade-Vortex Interaction Impulsive Noise as Affected by Tip Modification", Presented at the 36th AHS Annual Forum, Washington, D.C., May 1980, Preprint #80-62.

10. Shenoy, R. "Role of Scale Models in the Design of 'Low BVI Noise' Rotorcraft," Presented at the 41st Annual A.H.S. Forum, Fort Worth, TX. May 16, 1985.

11. Schmitz, F.H. and Y.H. Yu, "Theoretical Modeling of High - Speed Helicopter Impulsive Noise," Presented at the Third European Rotorcraft and Powered Lift Aircraft Forum, Aix-en-Provence, France, September 7-9, 1977.

12. Schmitz, F.H. and D.A. Boxwell, "In-Flight Far-Field Measurement of Helicopter Impulsive Noise," Presented at the 32nd Annual Forum of the American Helicopter Society, Washington, D.C., May, 1976.

13. Mosher, M., "The Influence of Wind-Tunnel Walls on Discrete Frequency Noise", PhD Dissertation, Stanford University, June 1986.

14. Mosher, M., "Effect of a Wind Tunnel on the Acoustic Field from Various Aeroacoustic Sources", Presented at the 10th AIAA Aeroacoustics Conference, Seattle, WA, July 1986. Preprint No. AIAA-86-1897.

15. Newman, S.J., Rickley, E.J., Ford, D.W., "Helicopter Noise Definition Report: UH-60A, S-76, A-109, 206-L", Report No. FAA-EE-81-16, December 1981.

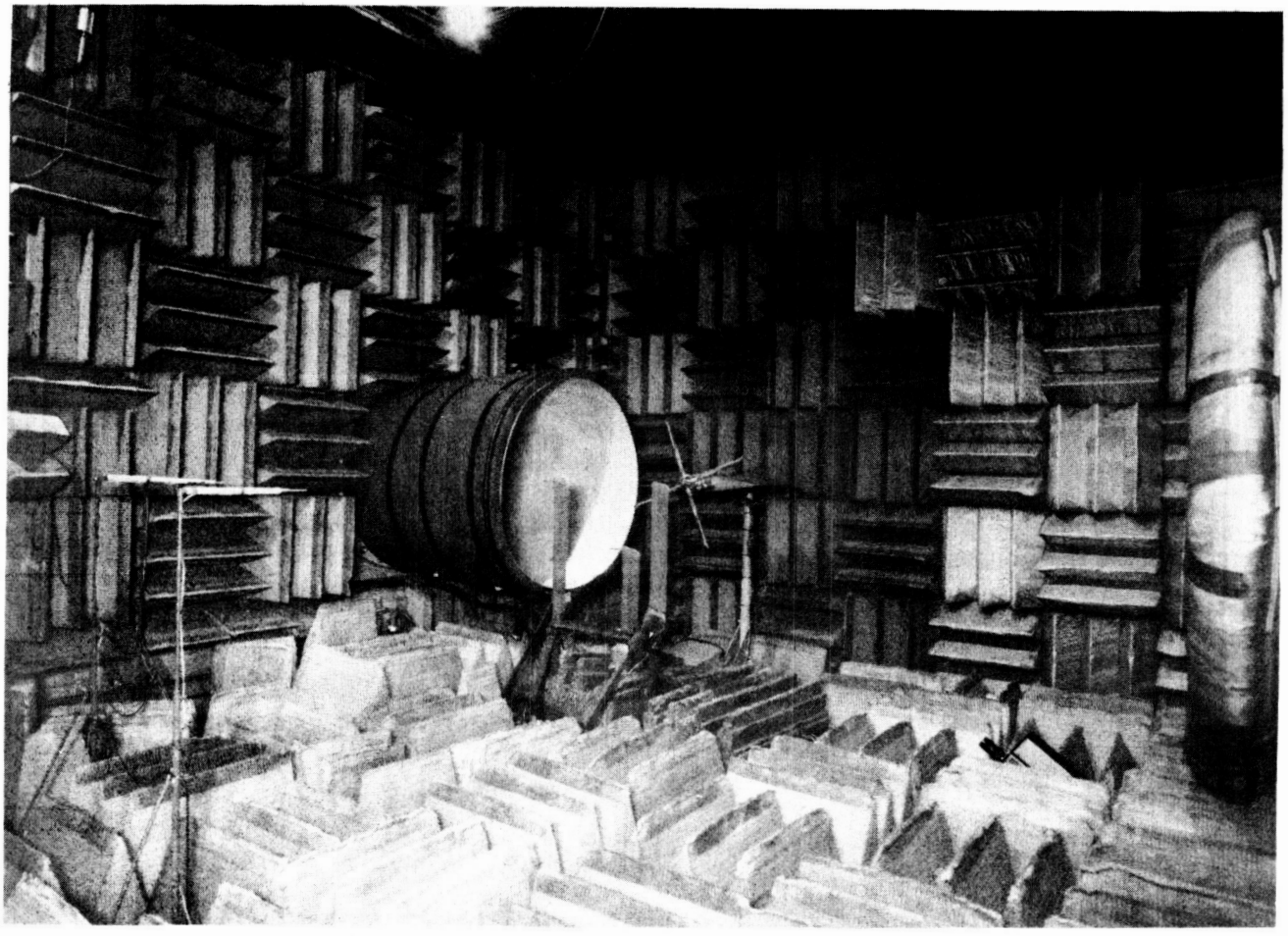

Figure 1. 1/20 Scale Experimental Model Installed in the UTRC Acoustics Research Tunnel

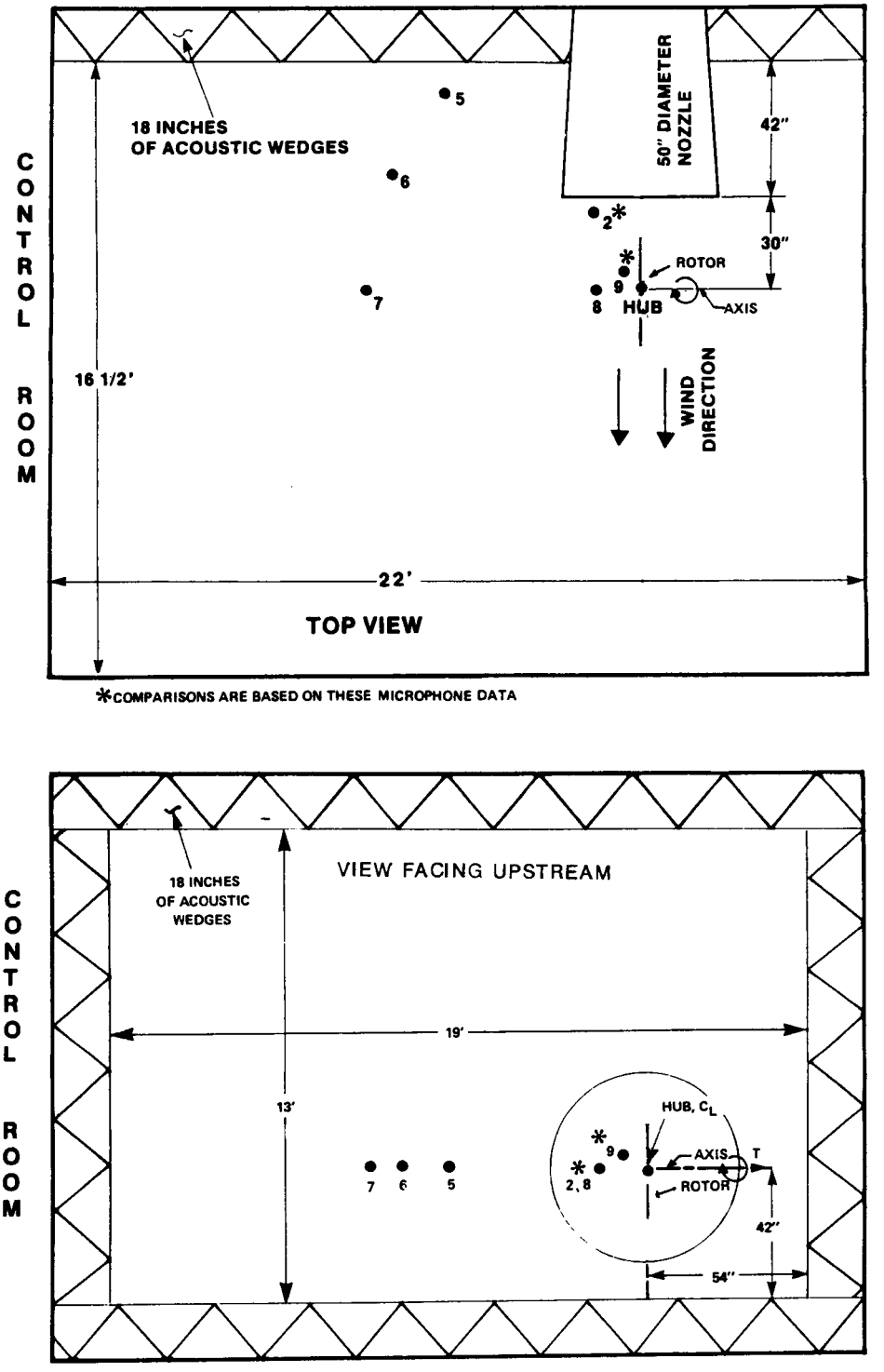

Figure 2. Rotor Test Setup in the UTRC (ART)

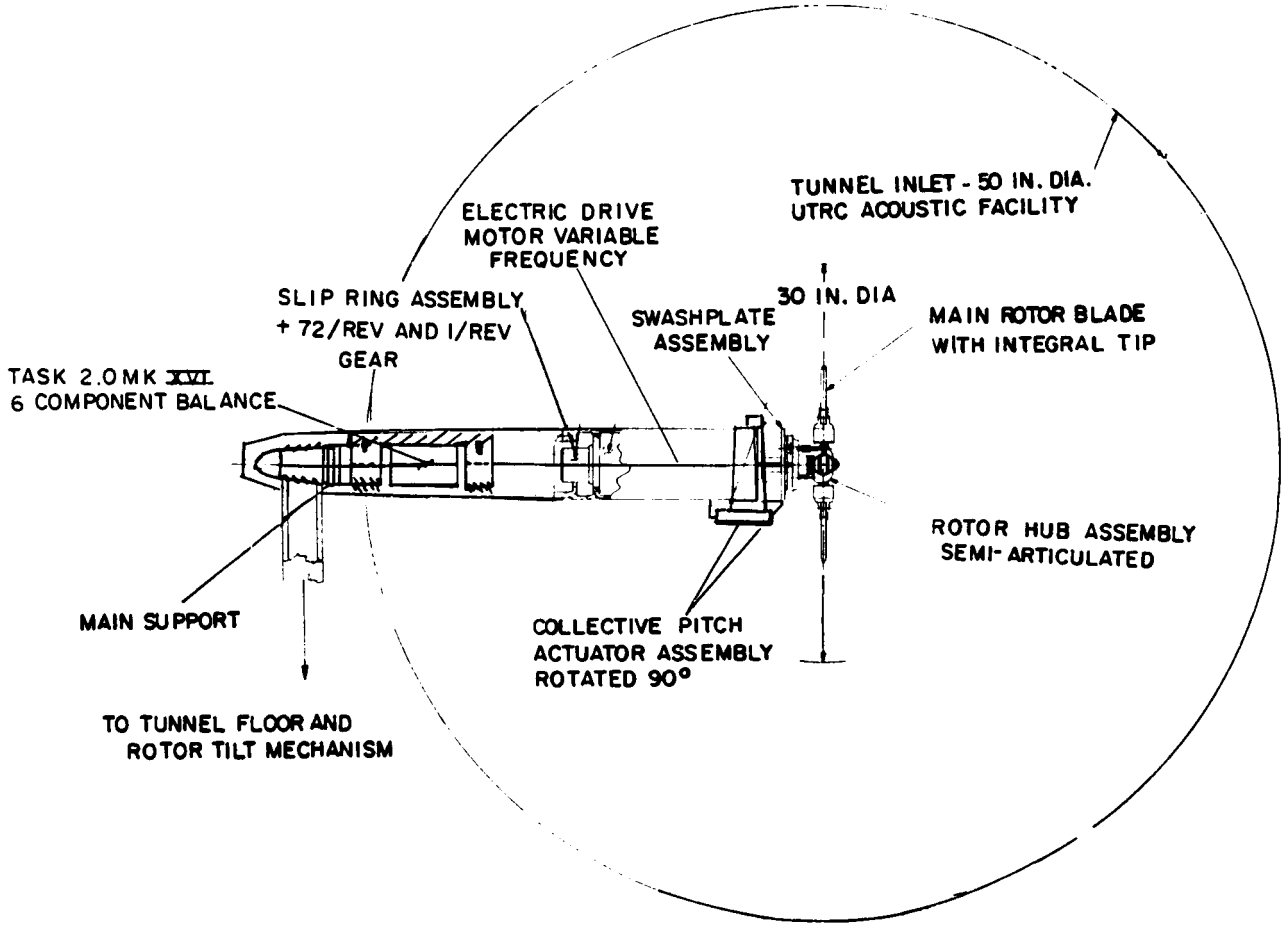

Figure 3. Schematic of the Sikorsky Acoustic Test Rig

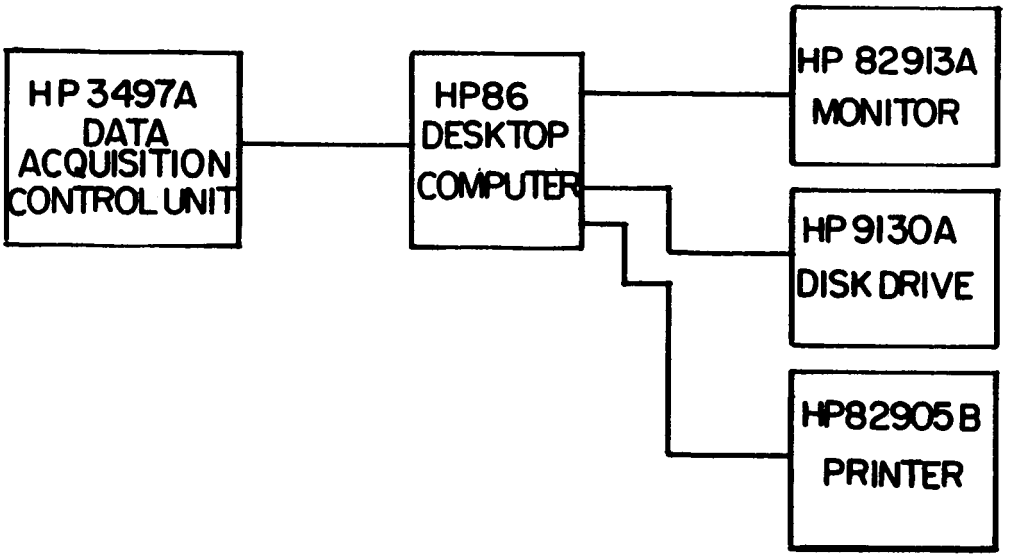

Figure 4. Schematic of the Model Control/Safety and Performance Data Acquisition System

PERFORMANCE DATA FOR CONF# 1 RUN# 99 DATE = 4/12/84

60 KTS 0 TIP PATH PLANE

Pstatic =	29.8243 in-Hg	Tstatic =	65.0000 deg.F
Co =	1122.4364 ft/sec	Vo =	60.0000 knots
Mtip =	.6459	Vo/vtip =	.1398
RPM =	5538.5399 rpm	Sigma =	.0826
Lift =	42.3097 lb	Drag =	-1.8082 lb
Thrust =	42.3482 lb	Torque =	4.9338 lb
Q =	6042.8802 lb	SHP =	.8281 hp
Cl =	.0070	Cd =	-.003
Ct =	.0070	Cq =	.0008
Clsig =	.0848	Cdsig =	-.0036
Ctsig =	.0848	Cqsig =	.0099
Pitch =	7.4088 deg	SHAFT =	-6.8877 deg
Lpha =	-16.6942 deg	Dwash =	17.6436 ft/sec

Balance Loads (lb/ft-lb)		Resolved Loads at Rotor Hub (lb/Ft-lb)	
N1 =	4.00	Forward Force =	-3.2788
N2 =	-3.47	Side Force =	-2.4853
S1 =	-15.69	Vertical Force =	42.2212
S2 =	8.13	Rolling Moment =	-2.9614
Axial =	41.21	Pitching Moment =	-5.2233
Roll =	4.88	Yawing Moment =	4.6120

Figure 5. Sample Printout of the Rotor Operating Conditions

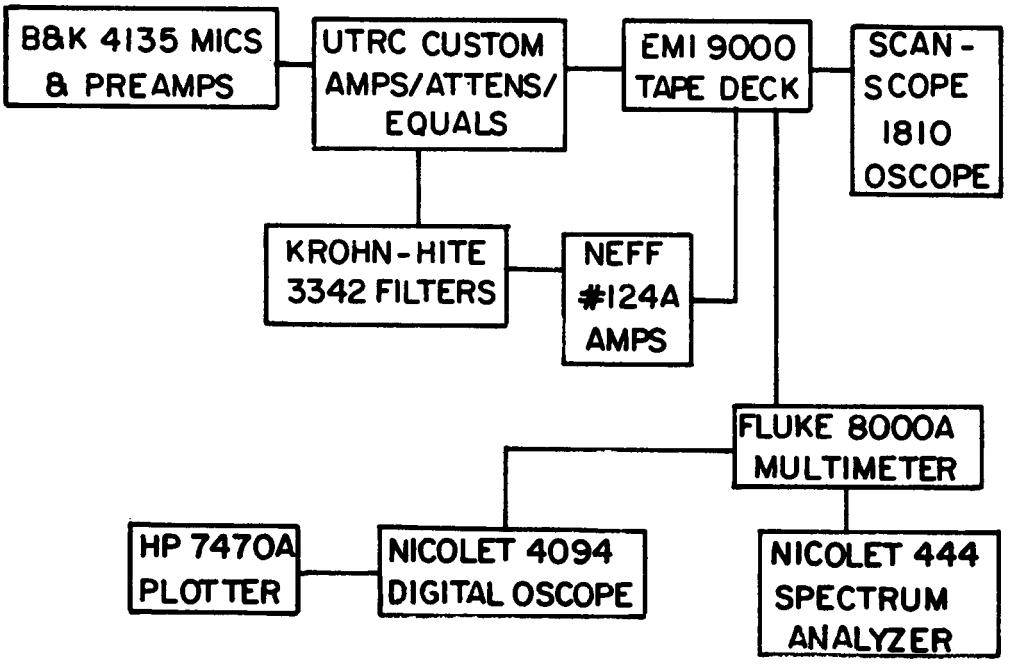

Figure 6 - Schematic of Acoustic Data Acquisition System.

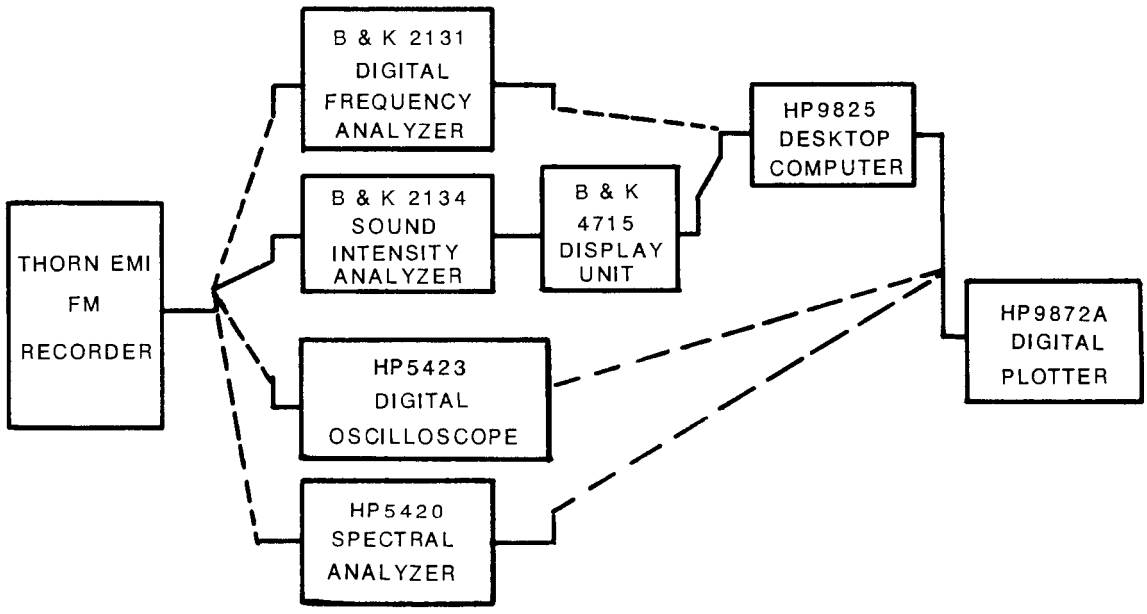

Figure 7. Schematic of Acoustic Data Reduction System

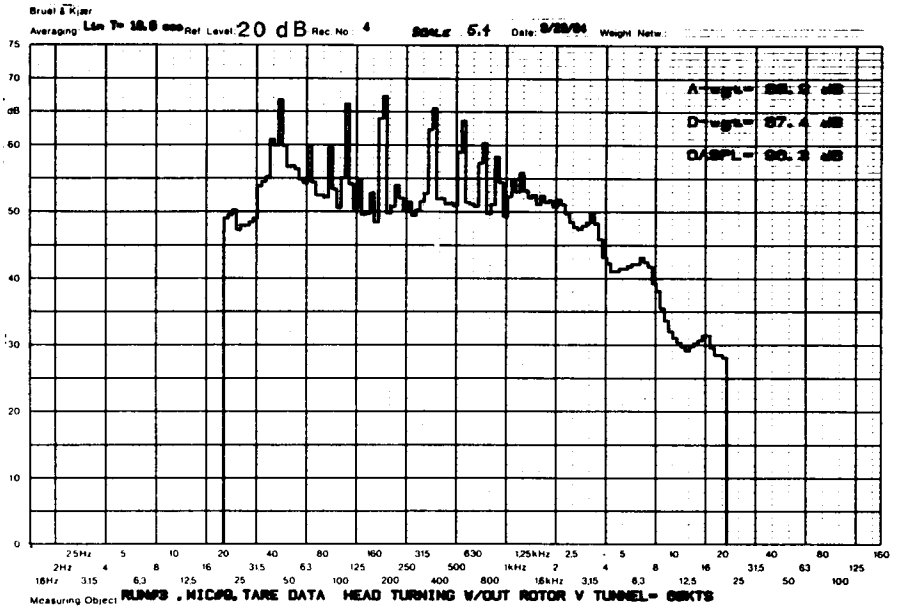

A. 1/12 OCTAVE SPECTRA WITH NO BLADES.

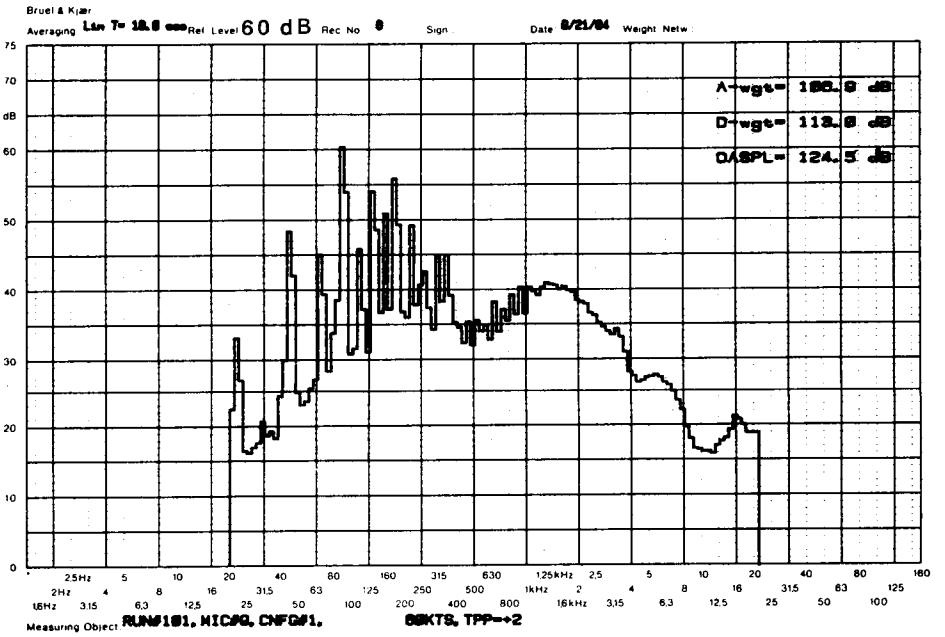

B. 1/12 OCTAVE SPECTRA OF BASELINE ROTOR (#1)

Figure 8. Sample 1/12 Octave Spectra and Noise Metrics

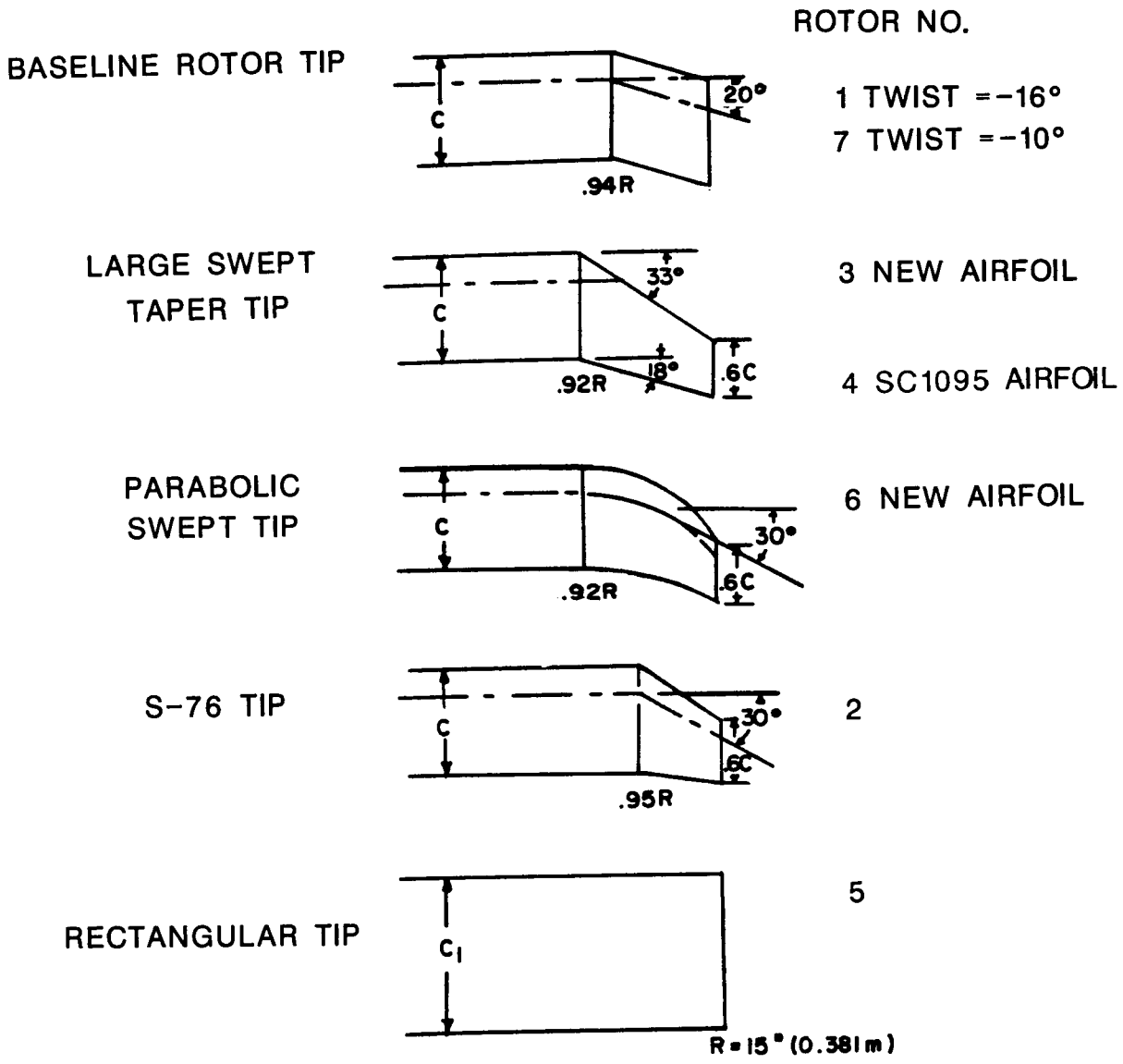

(a)

Figure 9. Rotor Geometric Characteristics

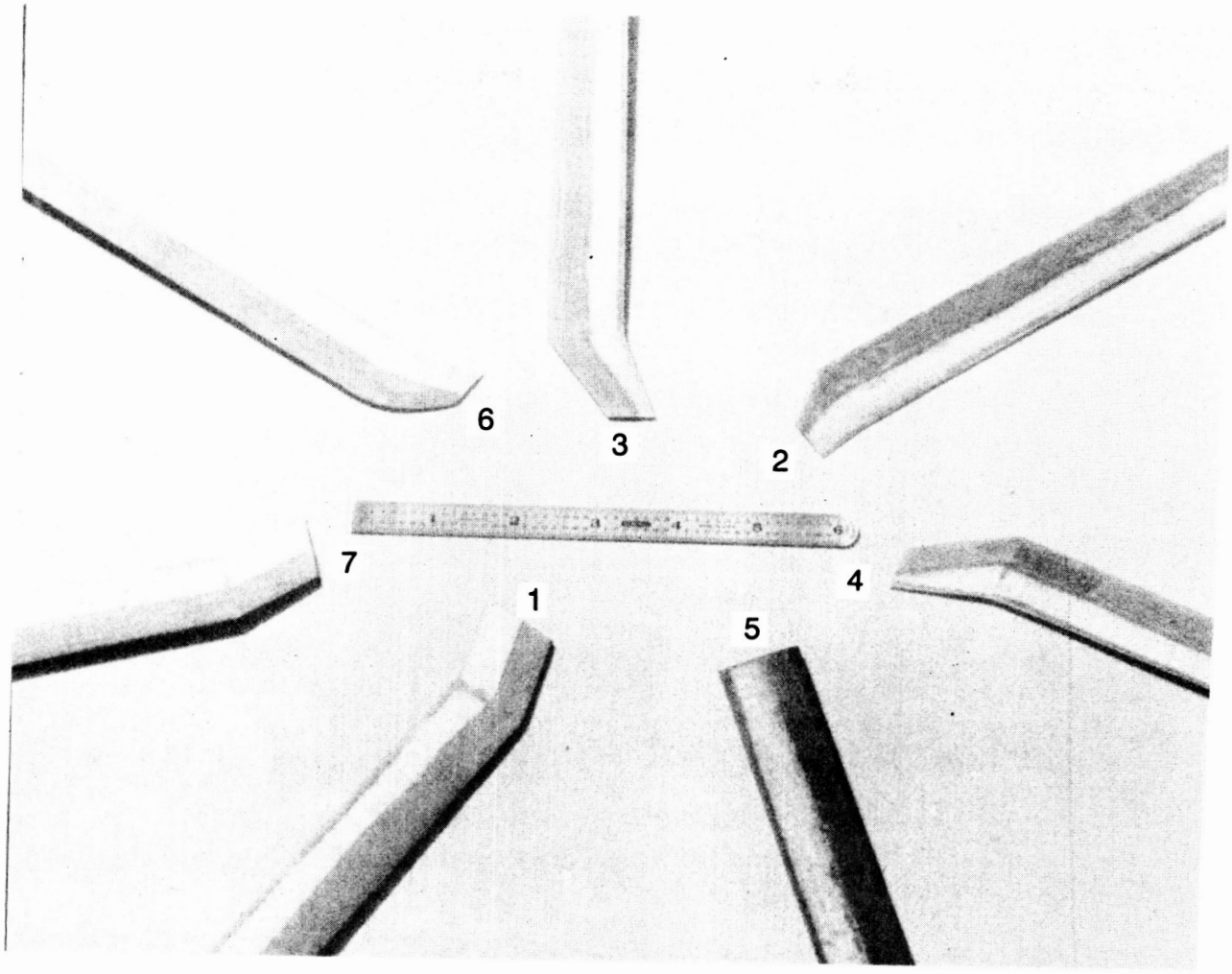

(b)

Figure 9. Rotor Geometric Characteristics (Concluded)

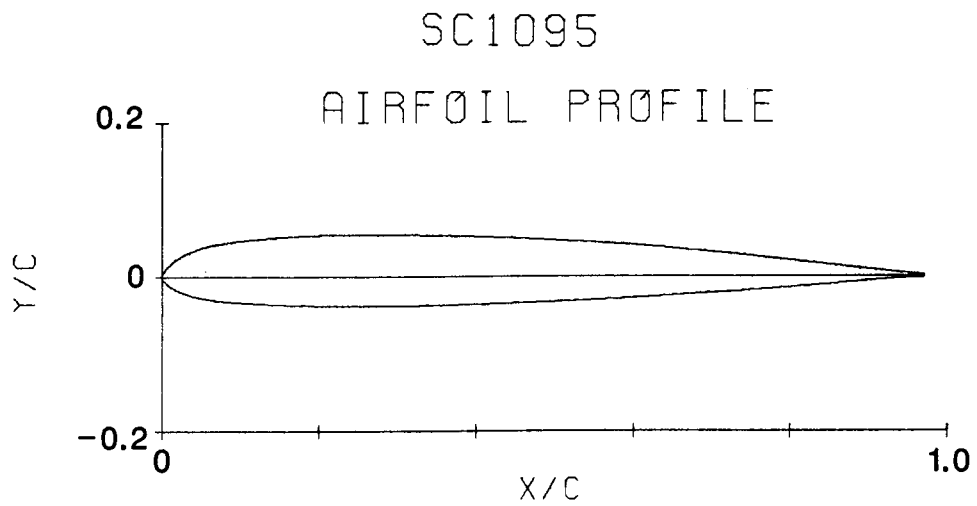

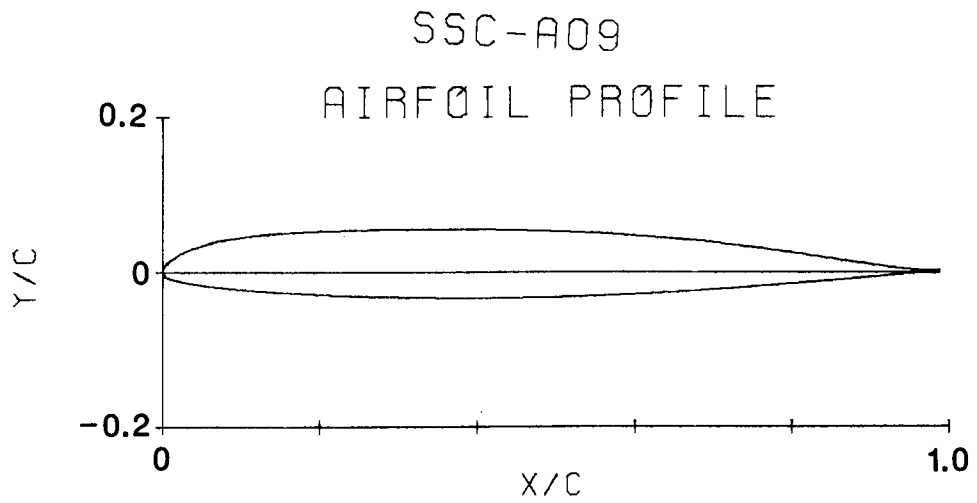

Figure 10. Profiles of SC1095 and SSC-A09 Airfoils

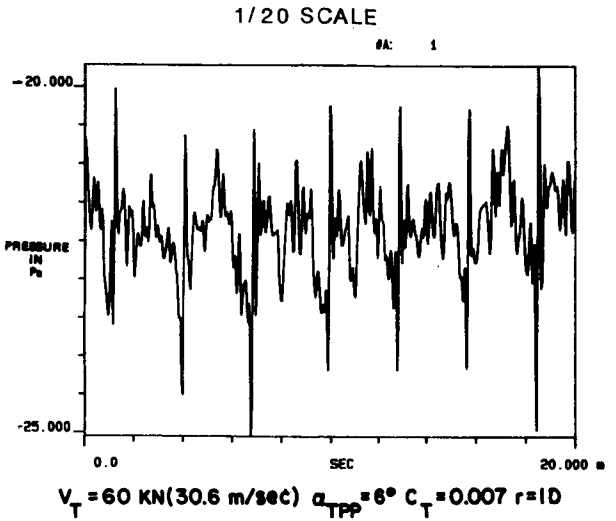

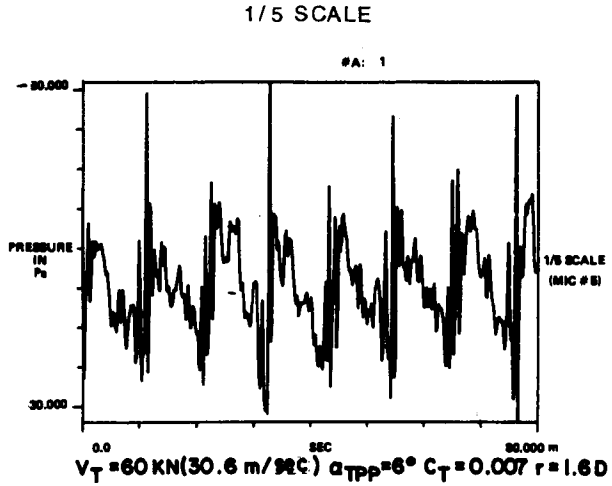

ΩR = 206 m/sec, S-76 CONFIG

SCALE	MIC LOC. r/D	MIC LOC. ELEV	MIC LOC. AZIM	TEMP °C	$M_{1,90}$	μ
1/20	1.0	30°	180°	12°	0.69	.15
1/5	1.6	23°	177°	46°	0.67	.15
FULL	16	30°	180°	19°	0.71	.185

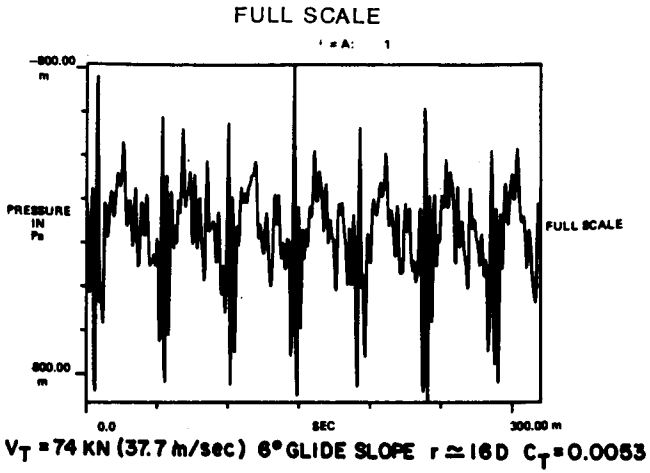

Figure 11. The Effect of Scale on Acoustic Time History for S-76 Configuration

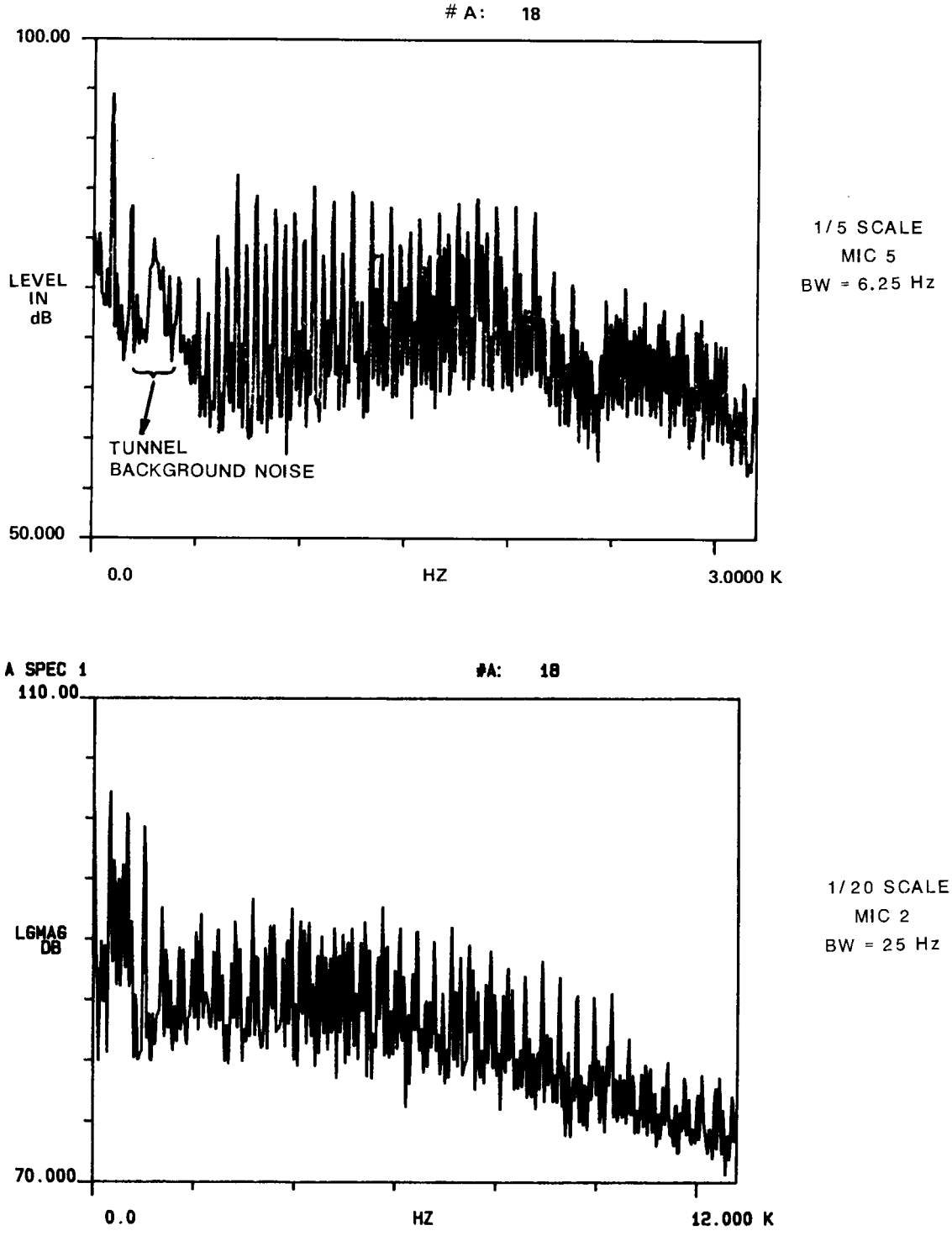

Figure 12. Narrowband Spectra for 1/5 and 1/20 Scale Model S-76 Rotors Corresponding to Figure 11 Conditions

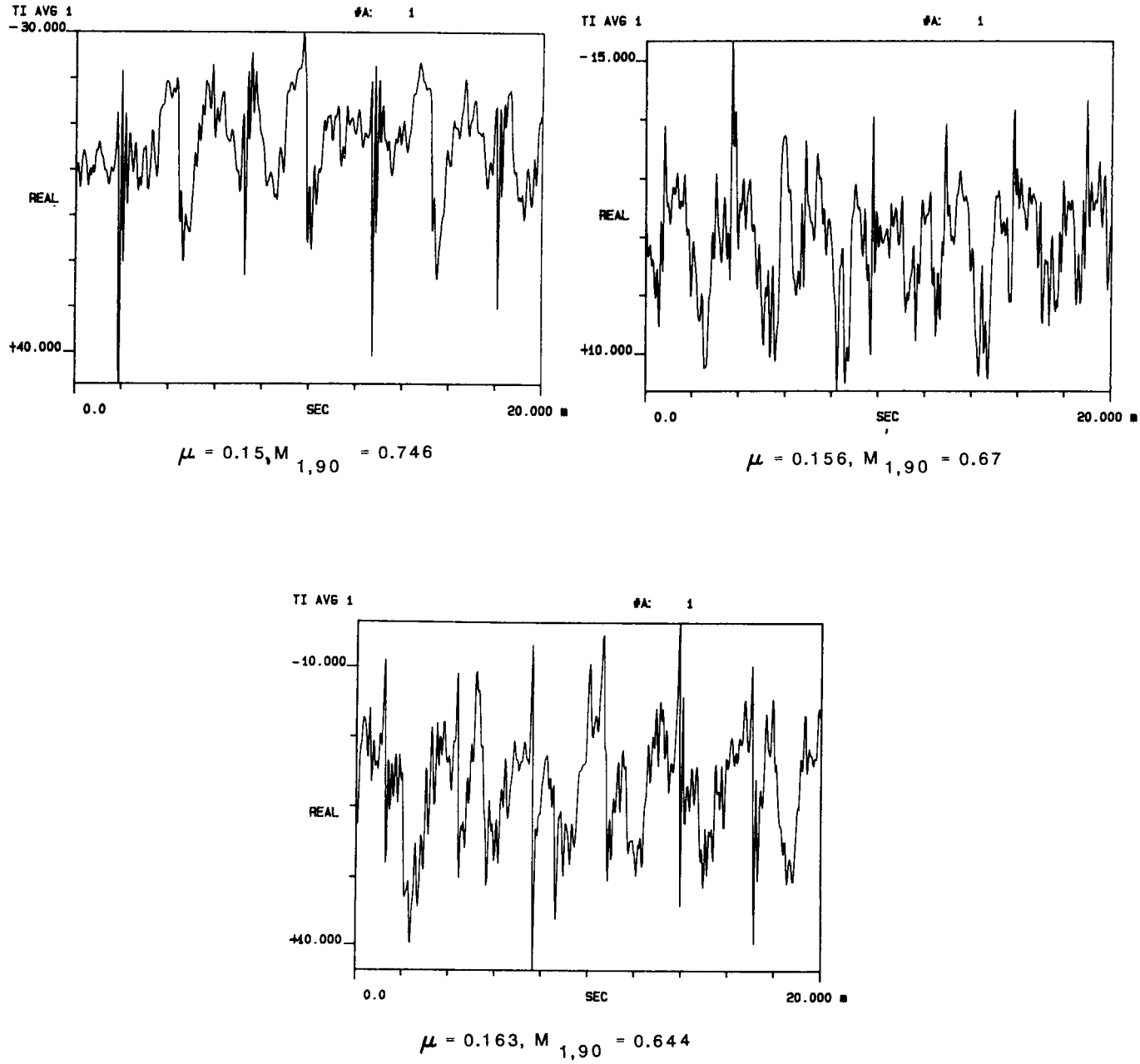

Figure 13. Acoustic Time Histories of the 1/20 Scale S-76 Configuration 2 at C_T = 0.007, α_{TPP} = 2°, Microphone 2

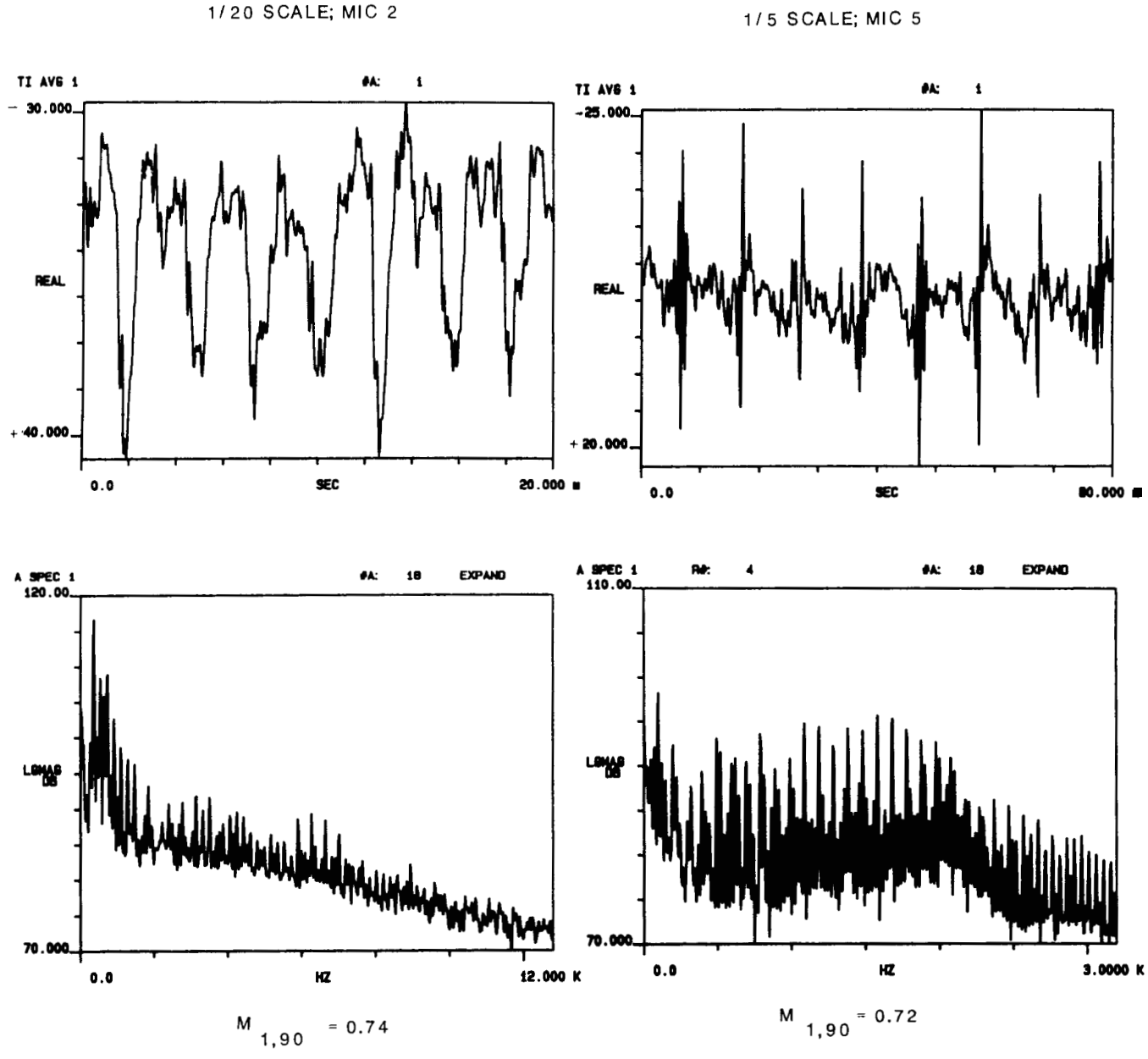

Figure 14. Acoustic Characteristics of 1/20 and 1/5 Scale Model Baseline UH-60 Configuration 1 Rotors at $\mu = 0.14$, $C_T = 0.007$, $\alpha_{TPP} = 6°$

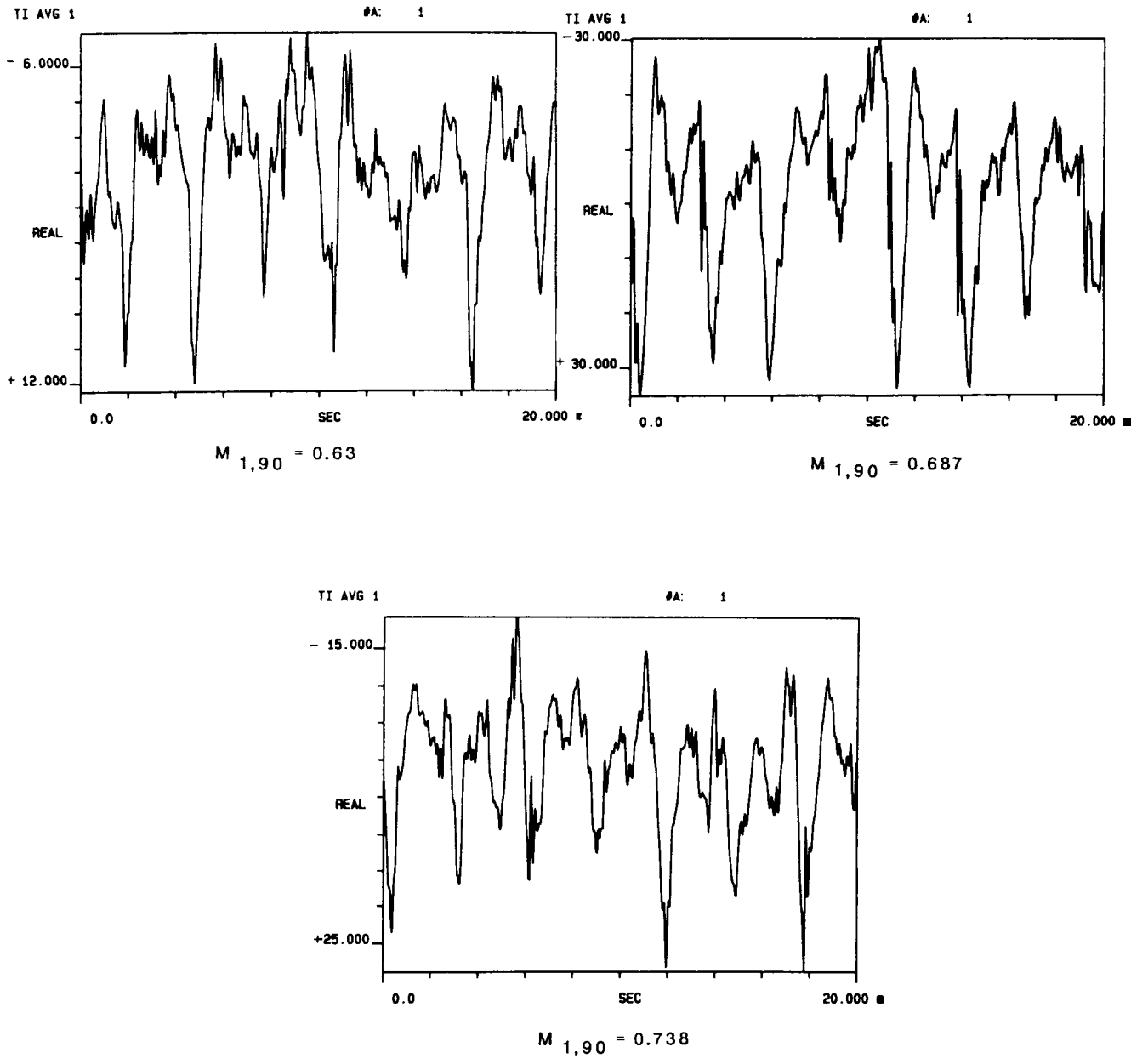

Figure 15. Effect of Mach Number on the BVI Acoustic Time History for the Baseline Configuration 1 at $C_T = 0.007$, $\mu = 0.14$, $\alpha_{TPP} = 2°$ and MIC 2.

MICROPHONE 2

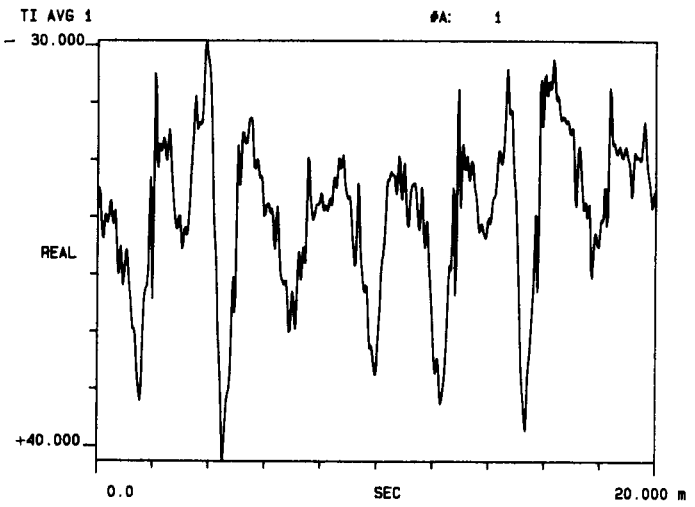

MICROPHONE 9

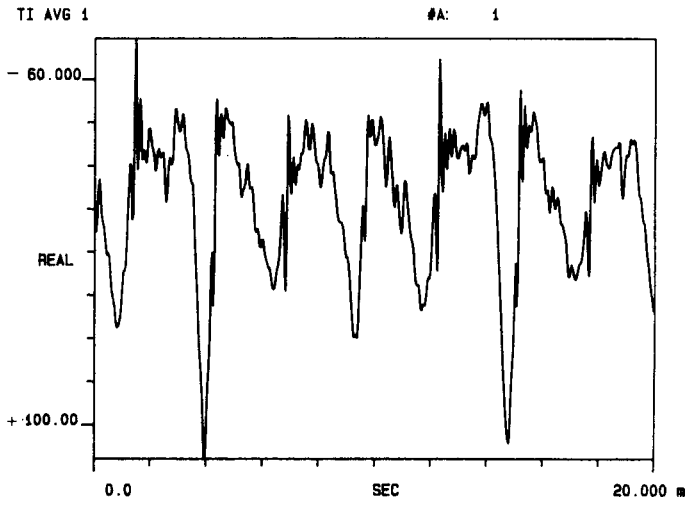

Figure 16. Acoustic Time Histories of the Baseline Configuration 1 at Two Microphone Locations for $M_{1_{90}} = 0.738$, $C_T = 0.007$, $\mu = 0.14$, $\alpha_{TPP} = 2^{\circ}$

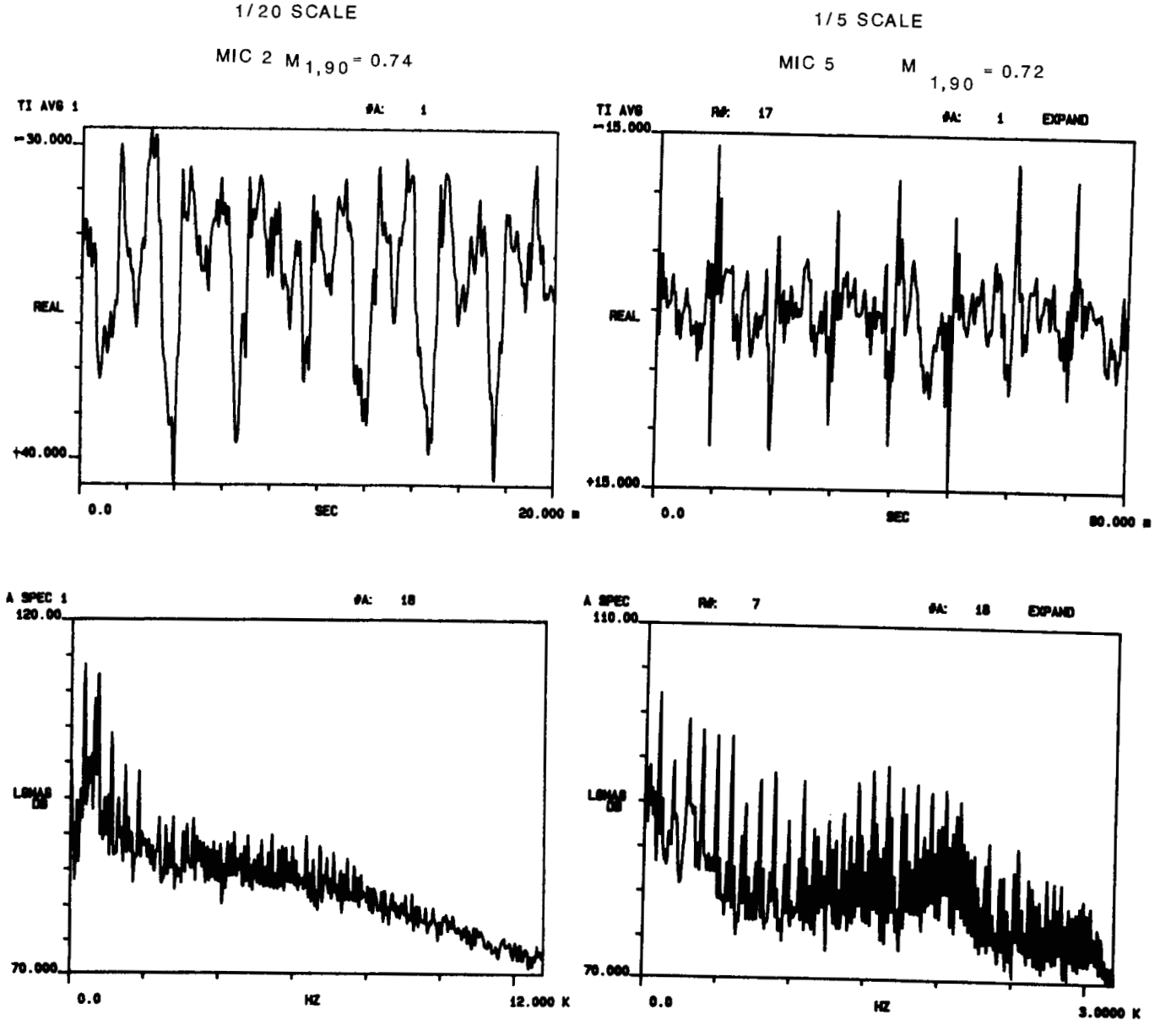

Figure 17. Acoustic Time Histories of 1/20 and 1/5 Scale Model Large Swept Tip Rotor Configurations (#3) with New Airfoil at C_T = 0.007, μ = 0.14, α_{TPP} = 6°

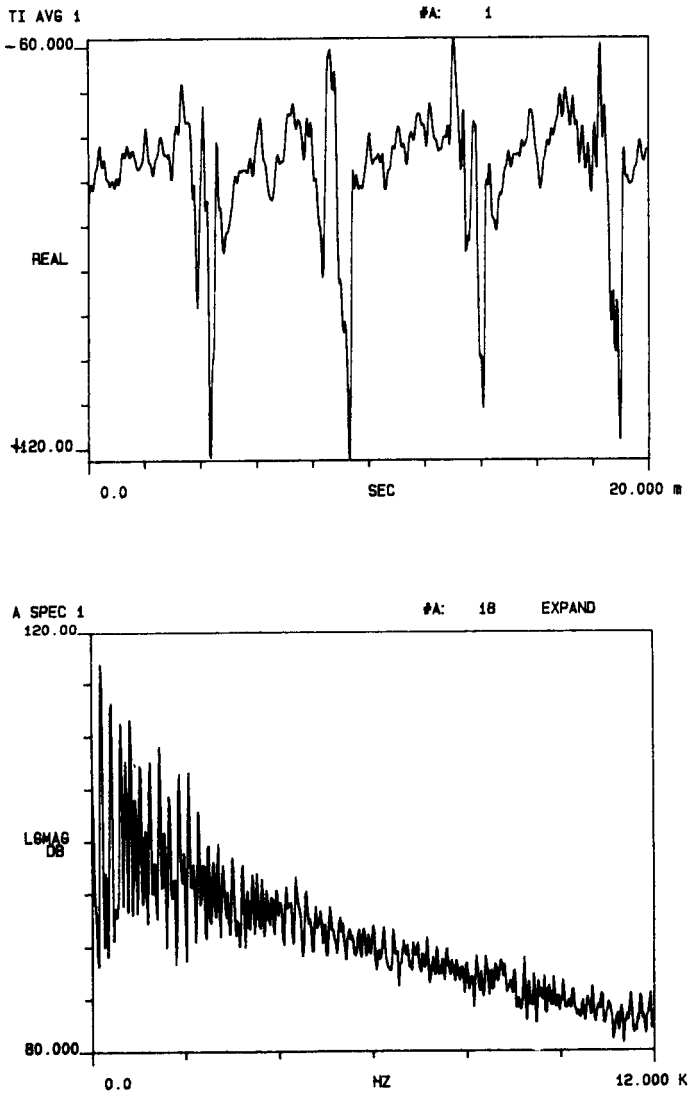

Figure 18. BVI Noise Characteristics of the 2-Bladed UH-1H Configuration 5 at $M_{1_{90}} = 0.833$, $\mu = 0.145$, $\alpha_{TPP} = 3°$, Microphone 2

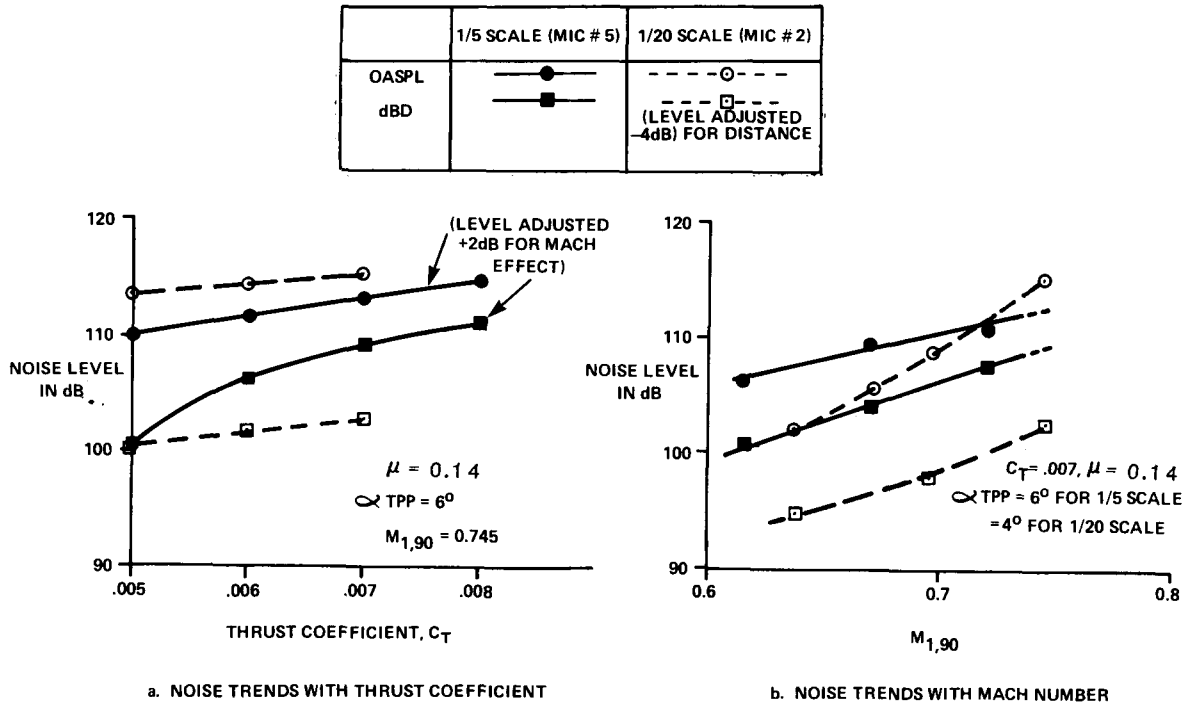

Figure 19. Effect of Thrust Coefficient and Mach Number on the BVI Noise Trends of the Baseline UH-60 Configuration 1

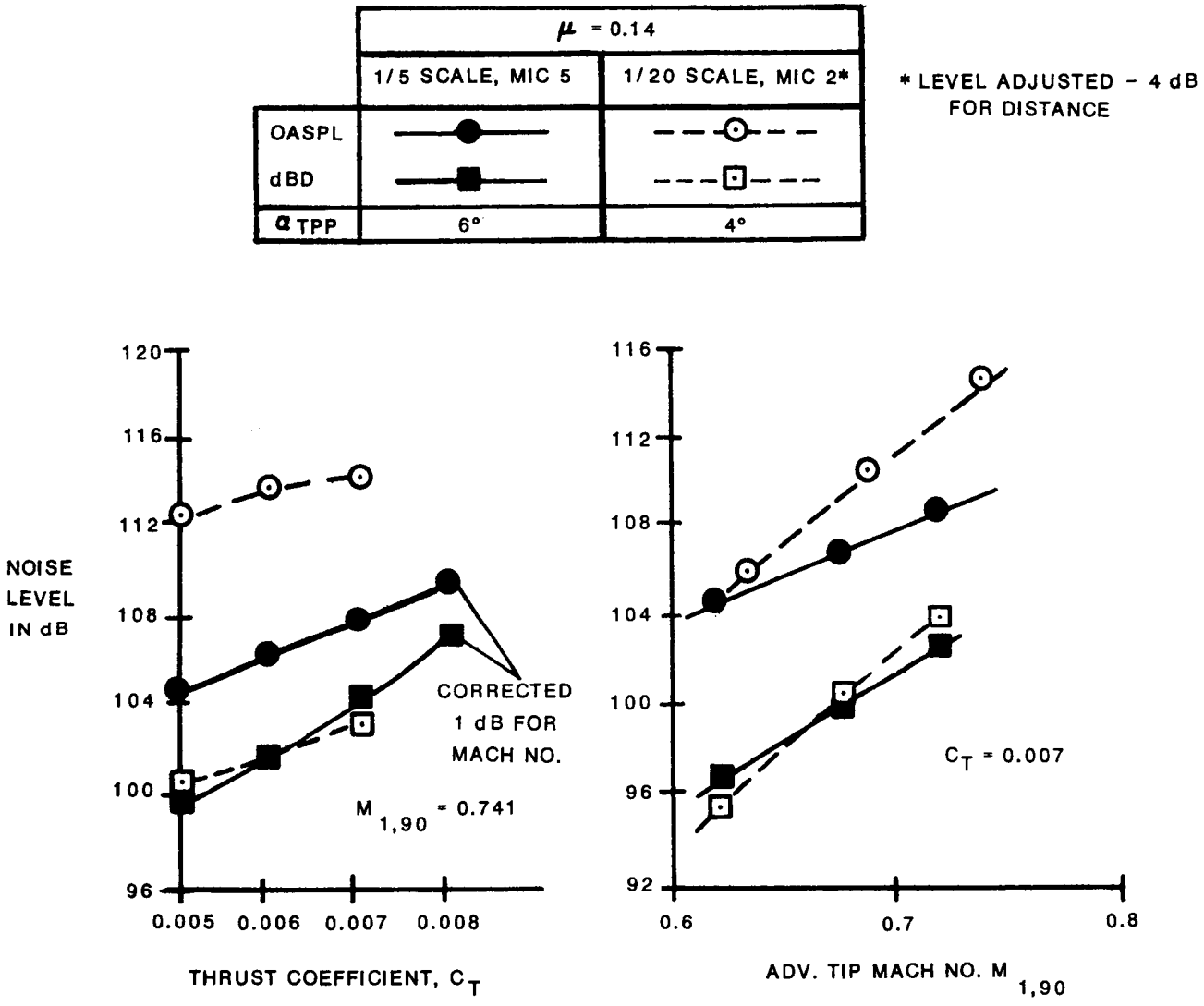

Figure 20. Effect of Thrust Coefficient and Mach Number on BVI Noise Trends of the Large Swept Tapered Tip Configuration (#3) with New Airfoils.

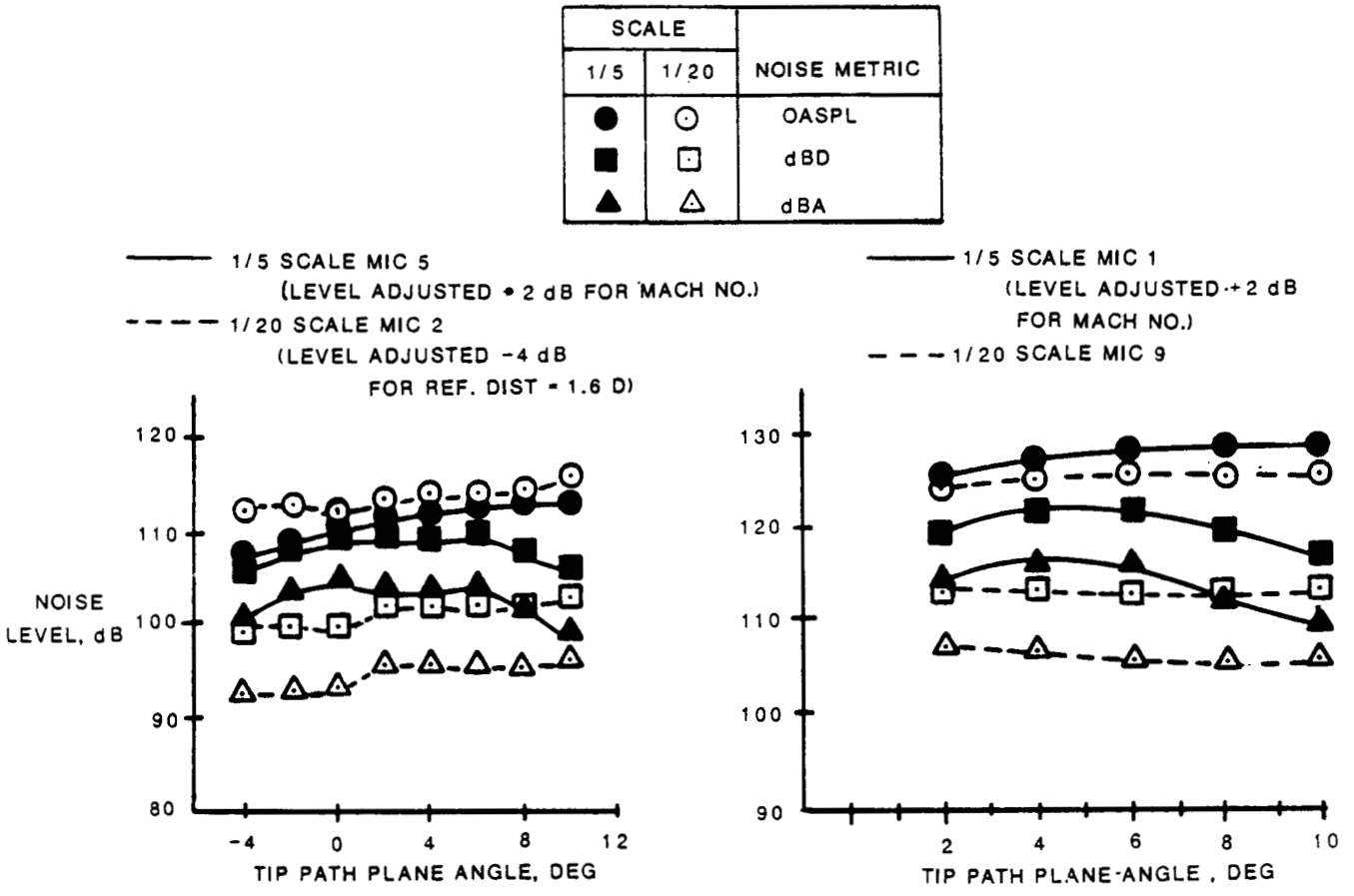

Figure 21. Effect of Rotor Tip Path Plane Orientation on the Noise Trends of the Baseline UH-60 Rotor Configuration 1 at Two Directivity Angles

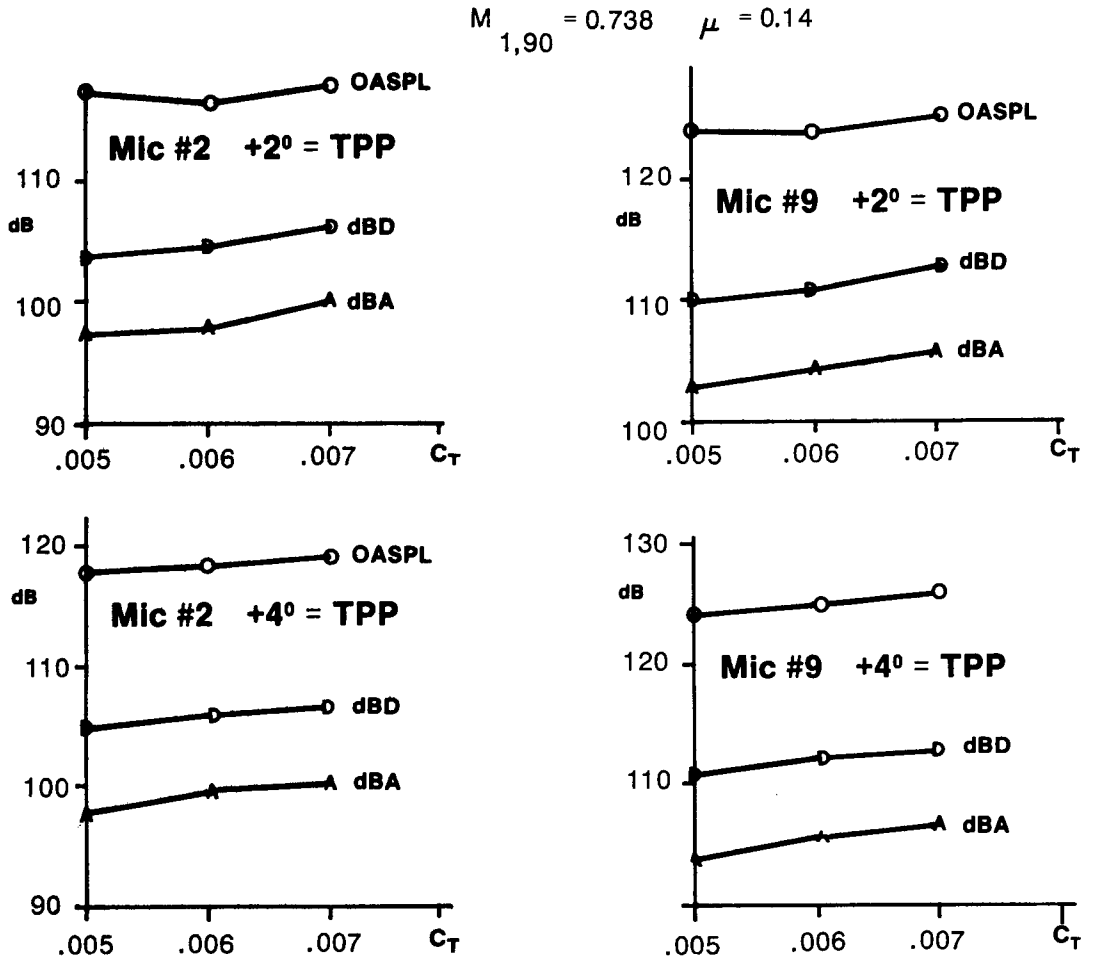

Figure 22. Noise Trends of the Baseline UH-60 Rotor Configuration 1 with Thrust Coefficient

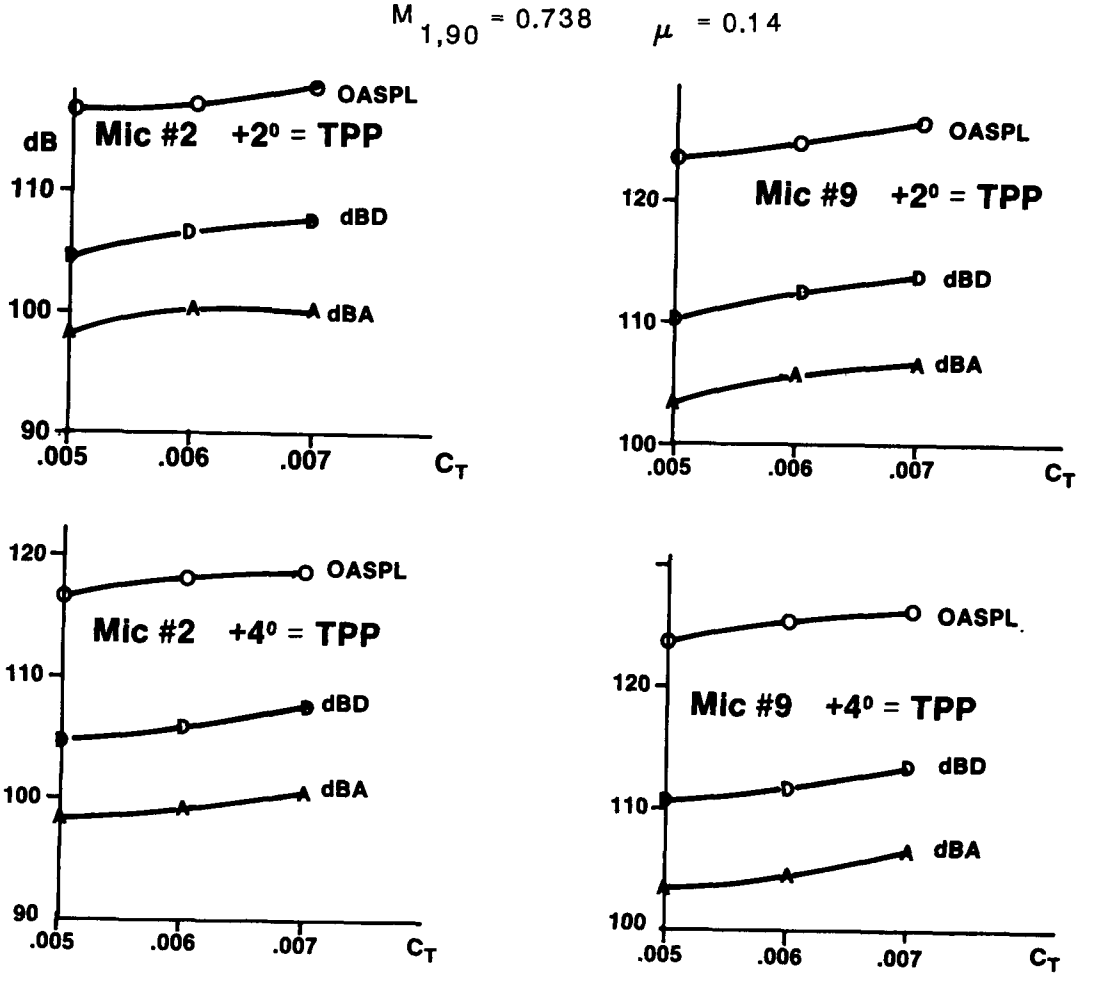

Figure 23. Noise Trends of the Large Swept Tapered Tip Configuration 3 with Thrust Coefficient

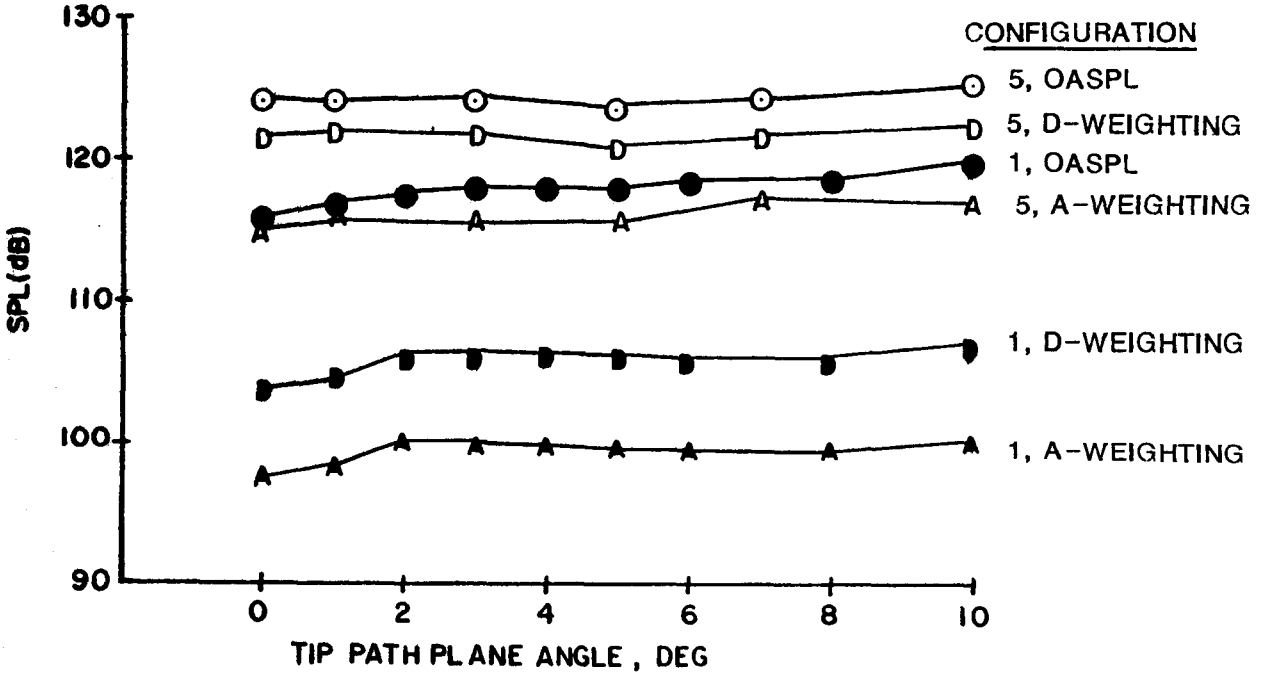

Figure 24. Acoustic Trends of 2-Bladed UH-1H Configuration 5 at $M_{1_{90}} = 0.833$ and $\mu = 0.145$ and 4-Bladed UH-60' Configuration 1 at $M_{1,90} = 0.74$ and $\mu = 0.14$

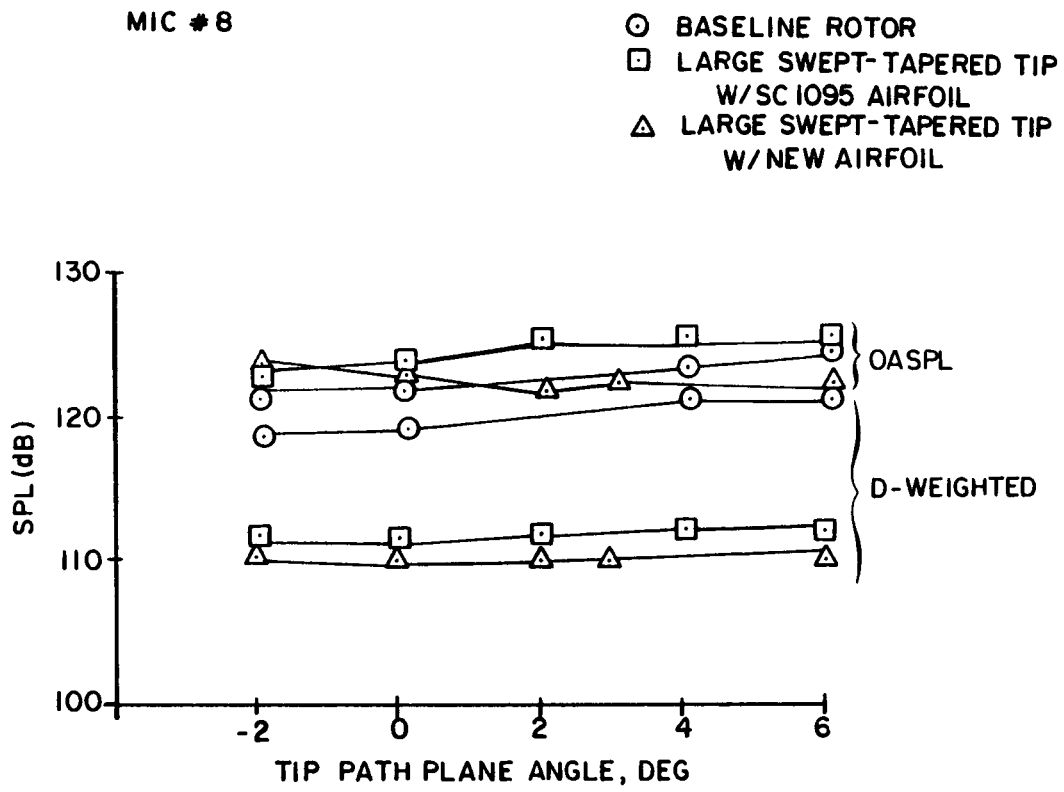

Figure 25. Acoustic Trends at the Near-Field On-Axis, Inflow Microphone 8 for Three Rotor Configurations at $M_{1,90} = 0.74$, $\mu = 0.14$ and $C_T = 0.007$

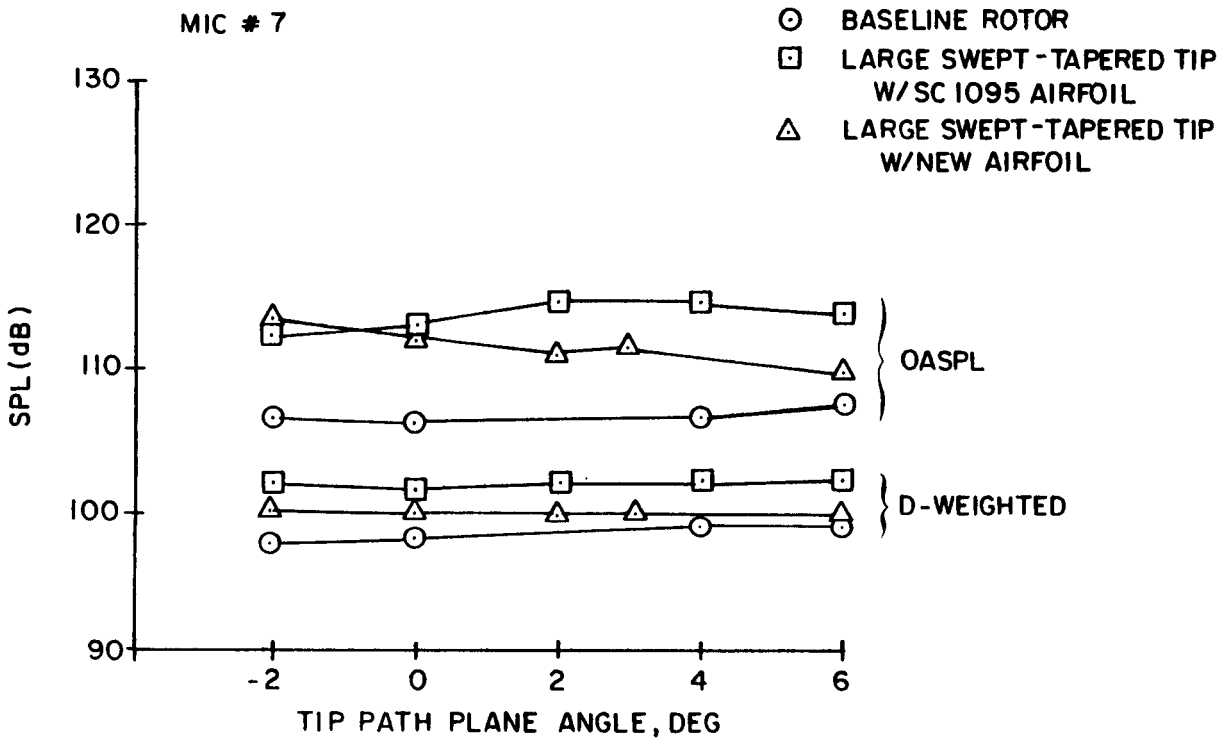

Figure 26. Acoustic Trends at the Far-Field, On-Axis, Out-of-Flow Microphone 7 for Three Rotor Configurations at $M_{1,90} = 0.74$, $\mu = 0.14$ and $C_T = 0.007$

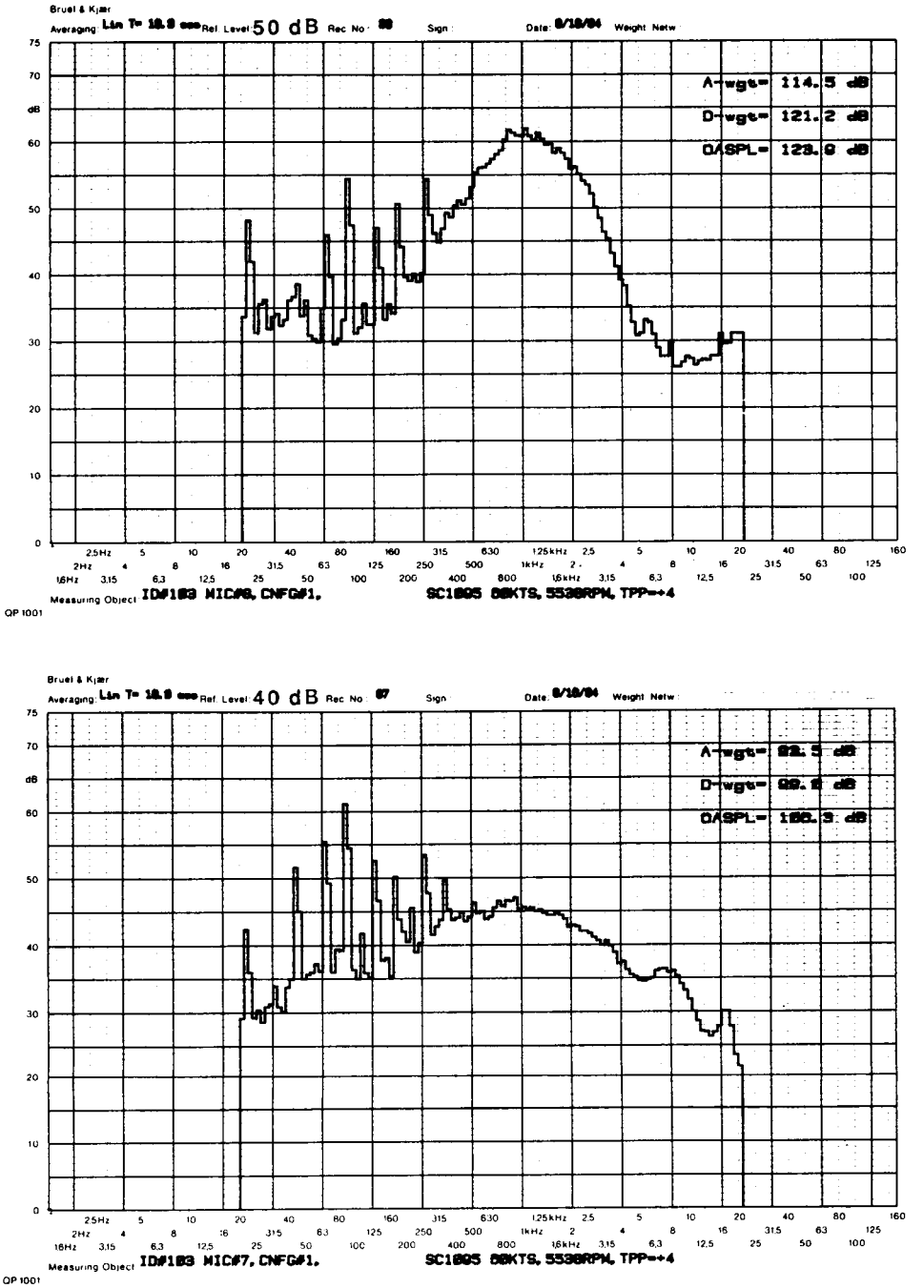

Figure 27. 1/12 Octave Spectra for the Baseline UH-60 Configuration 1 at the Near-Field Microphone 8 and the Far-Field Microphone 7 for $M_{1_{90}} = 0.74$, $\mu = 0.14$, $C_T = 0.007$ and $\alpha_{TPP} = 4°$

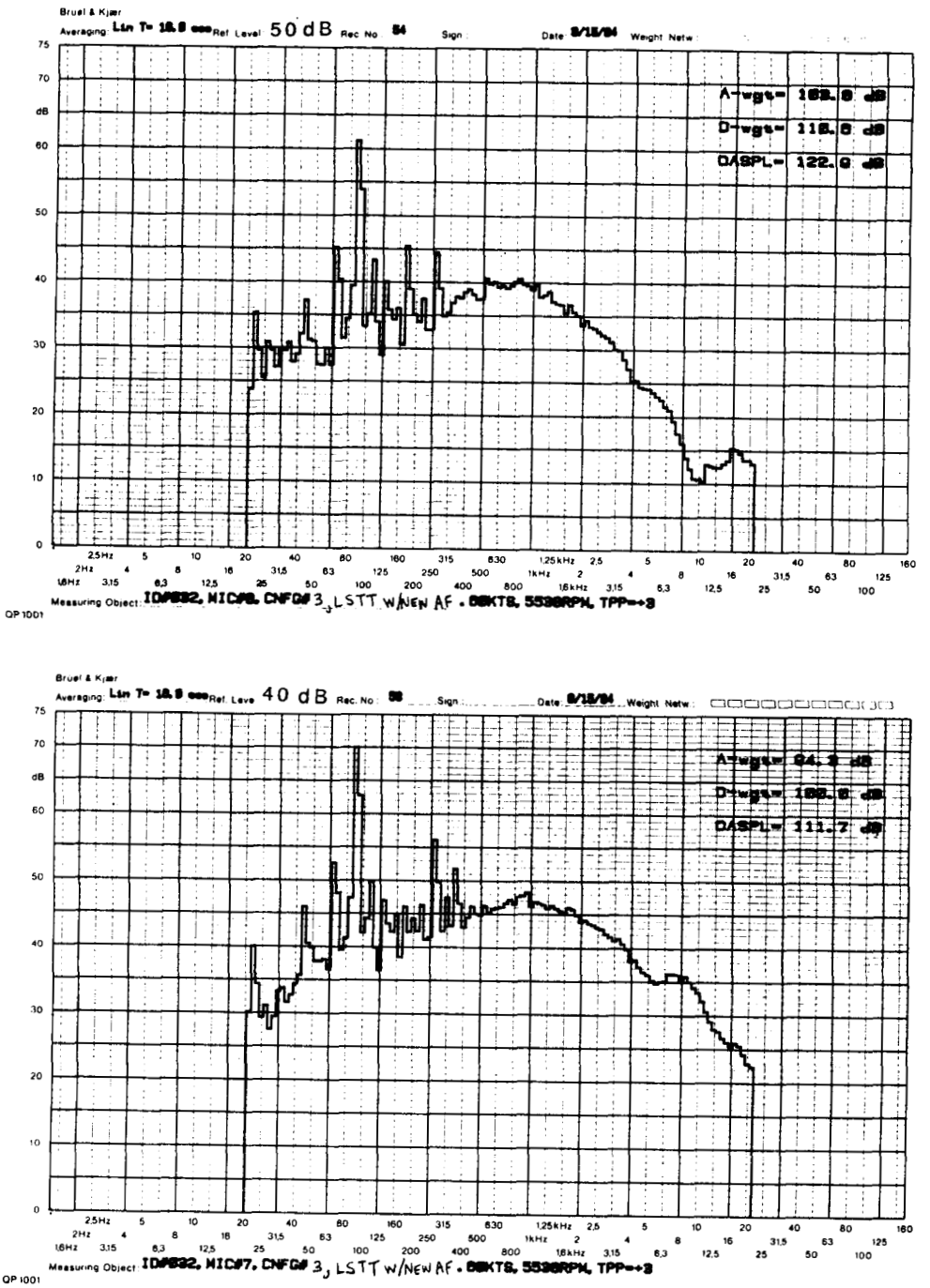

Figure 28. 1/12 Octave Spectra for the Large Swept Tapered Tip Configuration with New Airfoils (#3) at the Near-Field MIC 8 and the Far-Field MIC 7 for $M_{1_{90}} = 0.74$, $\mu = 0.14$, $C_T = 0.007$ and $\alpha_{TPP} = 4°$

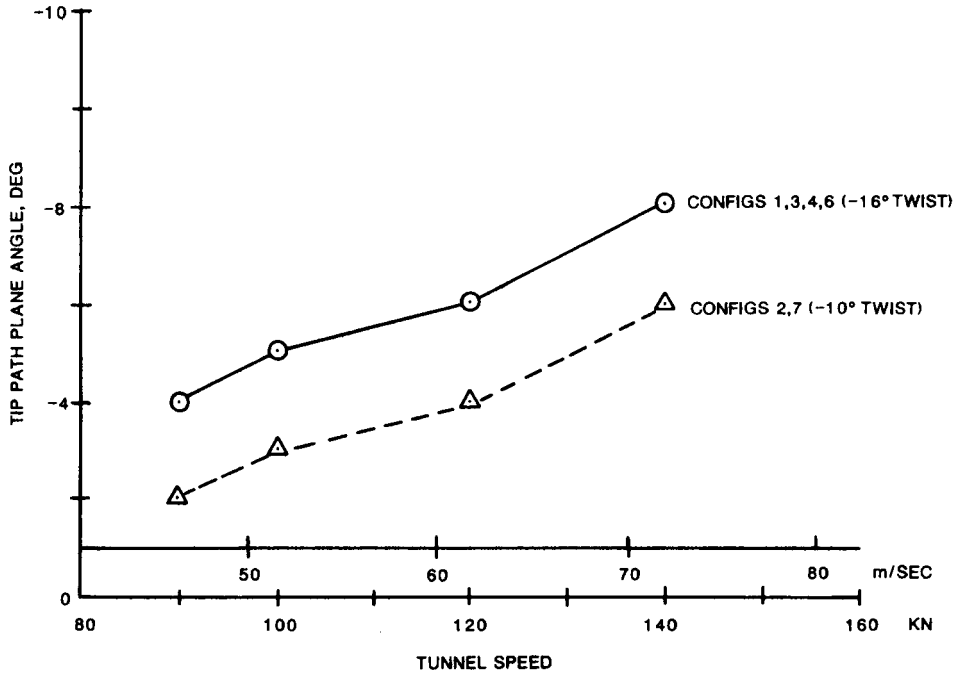

Figure 29. Tip Path Plane Angle Schedule Used During High-Speed Tests

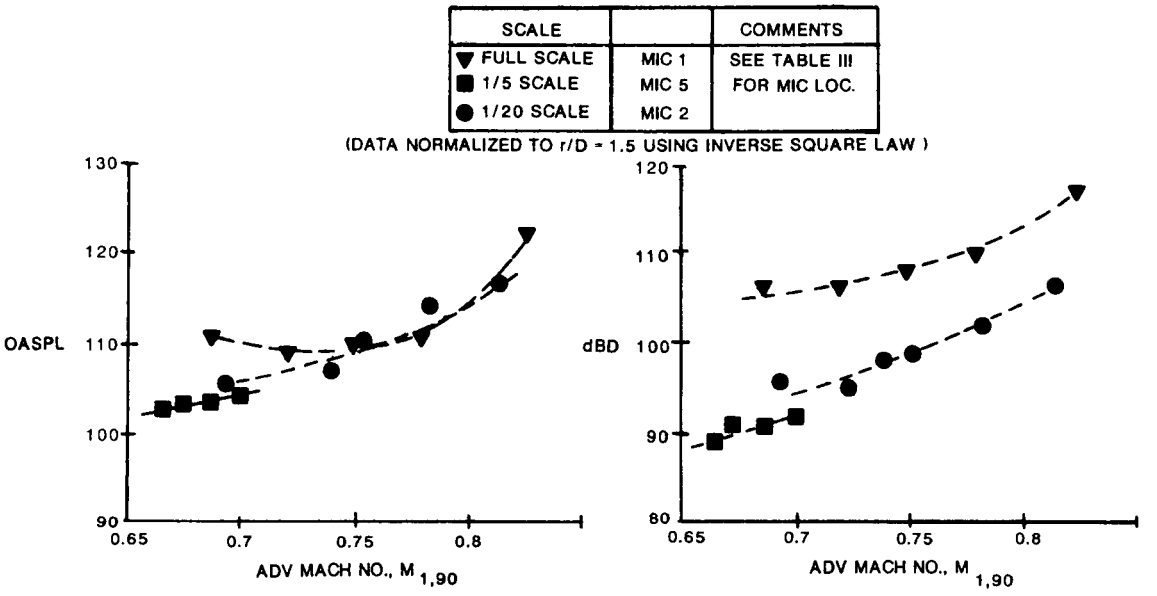

Figure 30. Noise Trends of the S-76 Configuration 2 With Advancing Blade Tip Mach Number at ΩR = 205.7 m/sec (675 ft/sec) for Three Scales

	ROTOR	$M_{\Omega R}$	C_T			COMMENTS
FULL SCALE	S-76	0.6	0.006	dBA(MAX)	TABLE B.2-2.1	LEVELS NORMALIZED TO
	UH-60	0.644	0.007	Ref:12	TABLE B.1-2.10	HEIGHT OF 4.5D ABOVE MIC
1/20 SCALE	CONFIG 2	0.605	0.006	MIC #2		
	CONFIG 1	0.65	0.006			

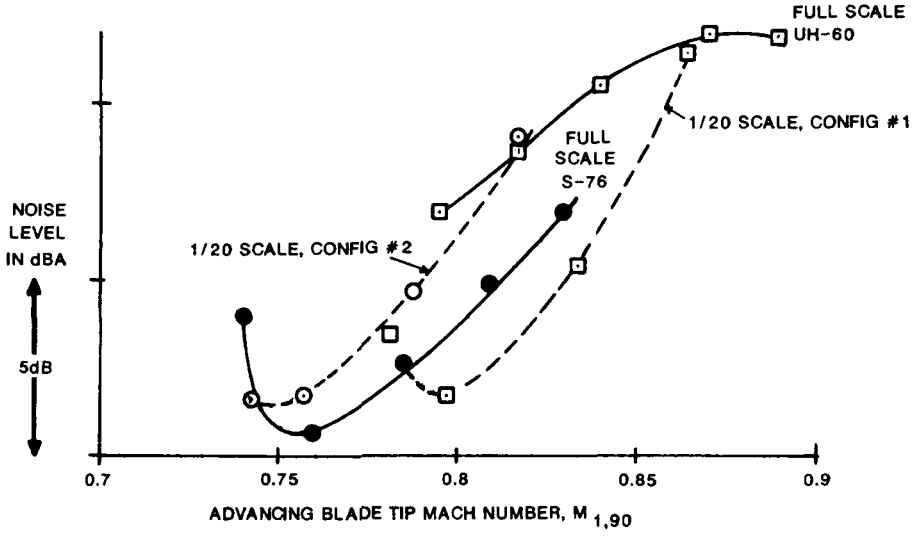

Figure 31. Comparison of the 1/20 Scale and Full Scale Helicopter Noise Trends for the UH-60 Configuration 1 and the S-76 Configuration 2 During Level Flight

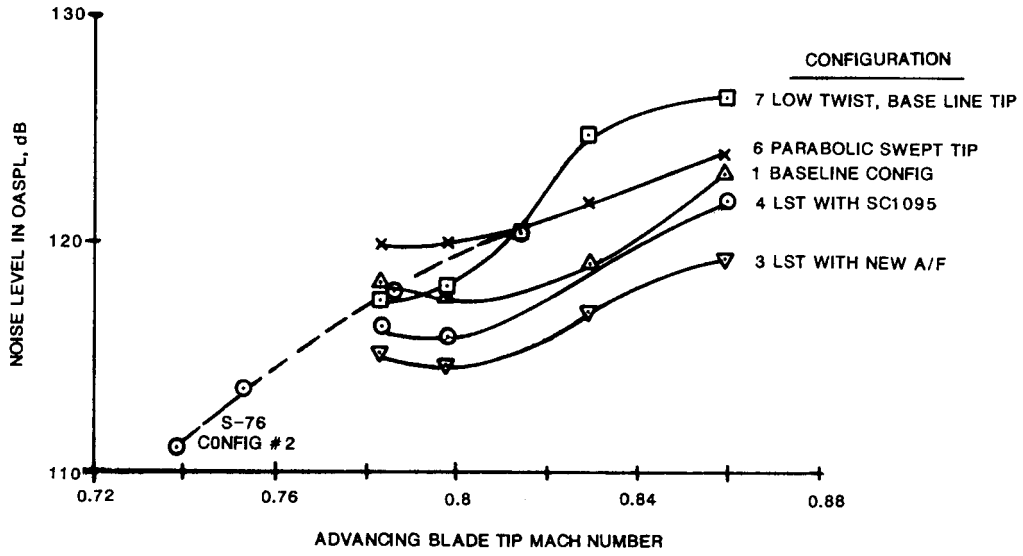

Figure 32. Effect of Blade Design on Noise at Microphone 2 for the 1/20 Scale Model Configurations During Level Flight Conditions (C_T = 0.006)

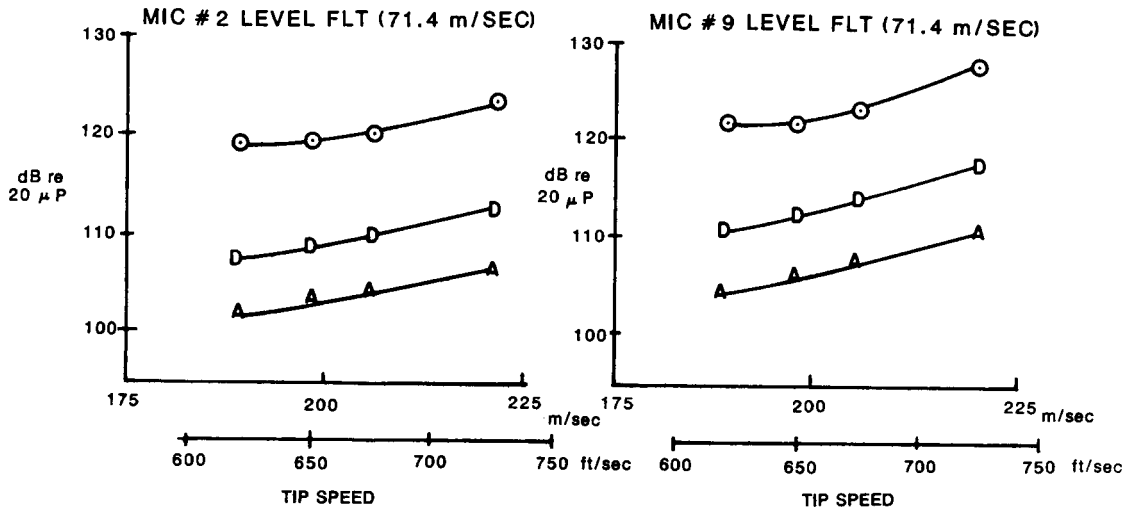

Figure 33. Level Flight Noise Trends with Tip Speed for the Baseline Configuration 1 at 71.4 m/sec (140 Knots), C_T = 0.006, and α_{TPP} = -3°

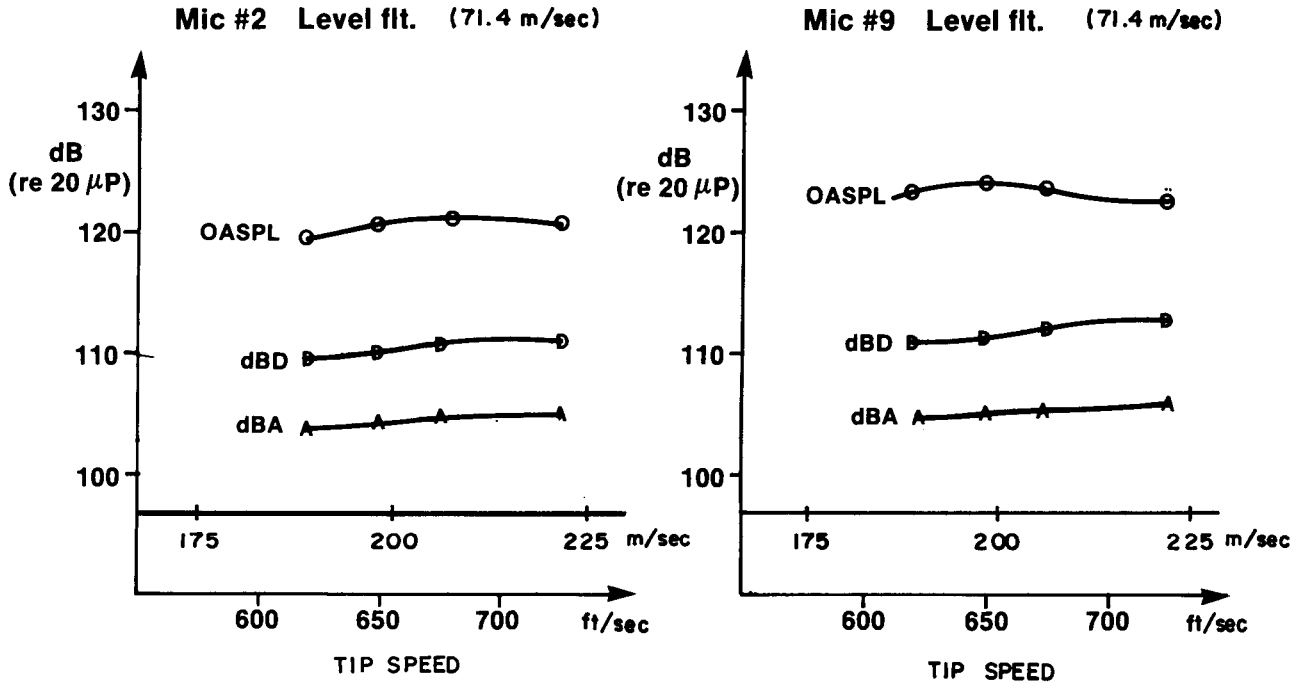

Figure 34. Level Flight Noise Trends with Tip Speed for the S-76 Configuration 2 at 71.4 m/sec (140 Knots), C_T = 0.006, and α_{TPP} = -3°

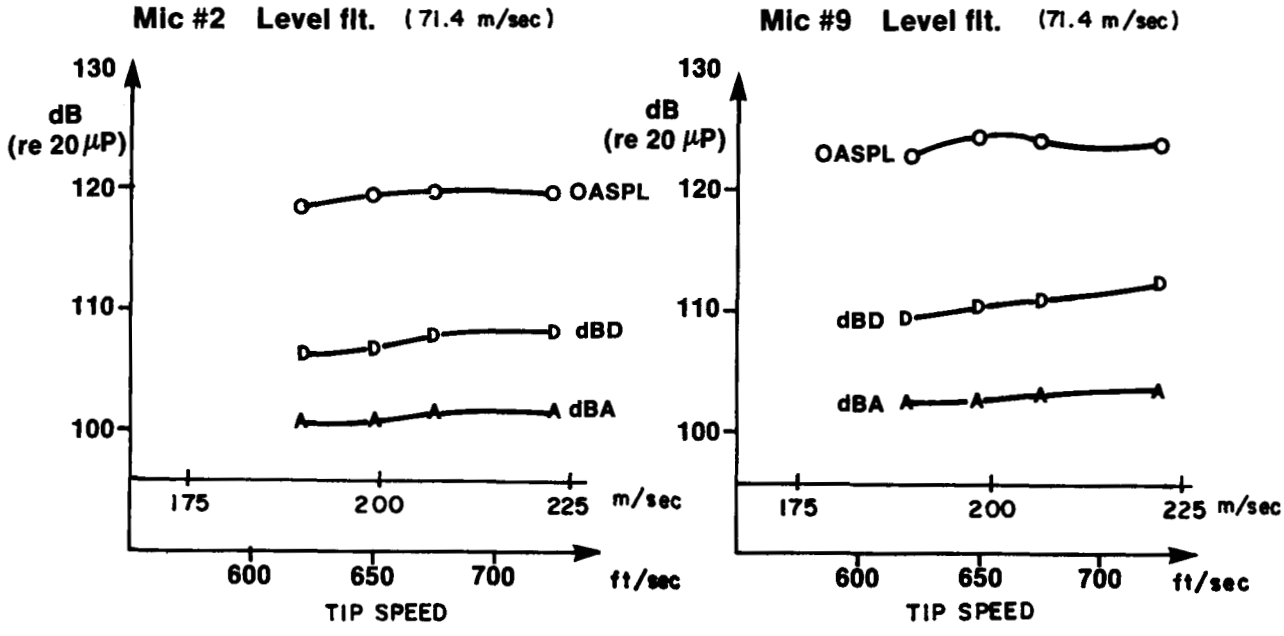

Figure 35. Level Flight Noise Trends with Tip Speed for the Large Tapered Tip Configuration 3 with New Airfoils at 71.4 m/sec, C_T = 0.006, and α_{TPP} = -3°

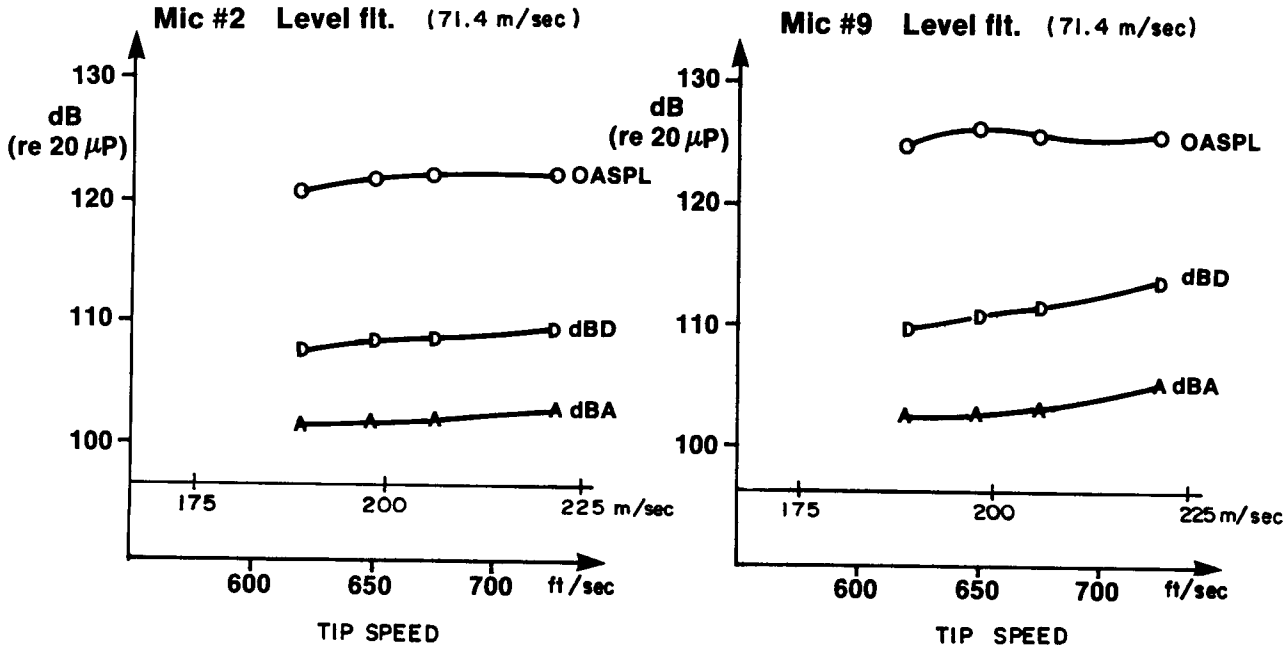

Figure 36. Level Flight Noise Trends with Tip Speed for the Large Tapered Tip Configuration 4 with SC1095 Airfoils at 71.4 m/sec, C_T = 0.006, and α_{TPP} = -3°

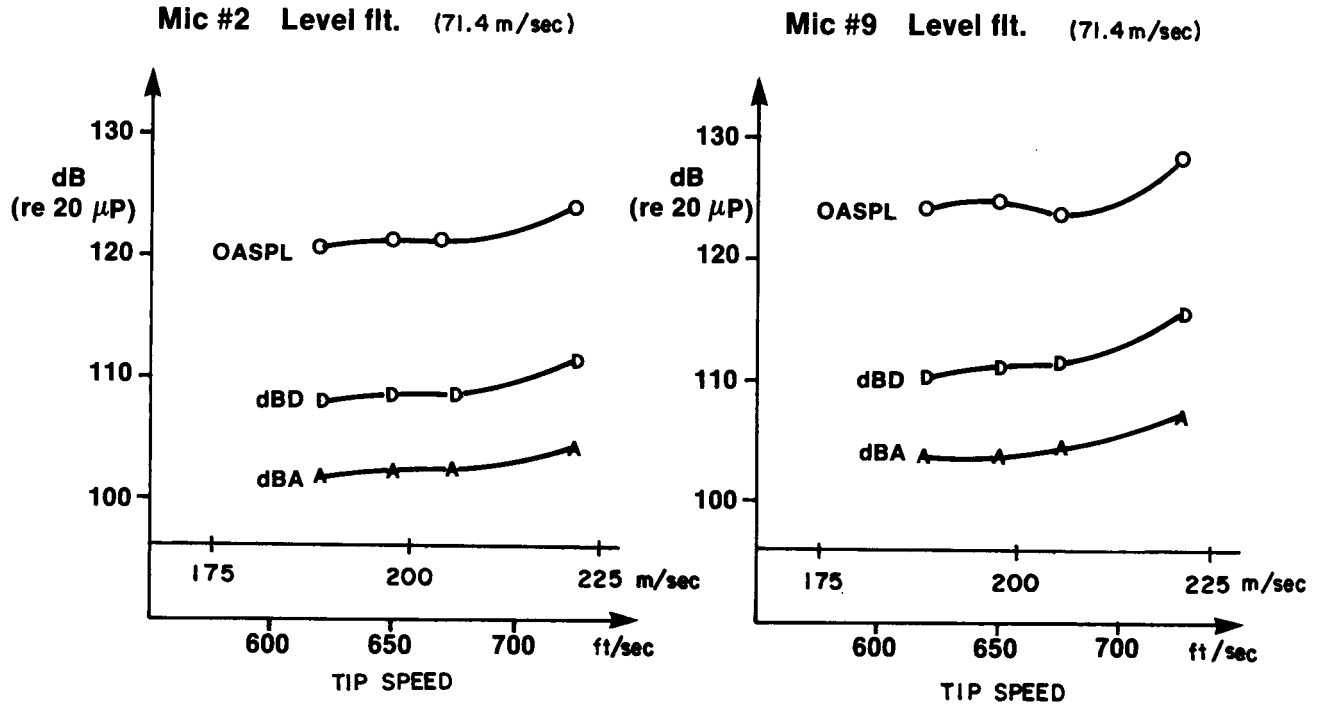

Figure 37. Level Flight Noise Trends with Tip Speed for the Parabolic Swept Tip Configuration 6 at 71.4 m/sec, C_T = 0.006 and α_{TPP} = -3°

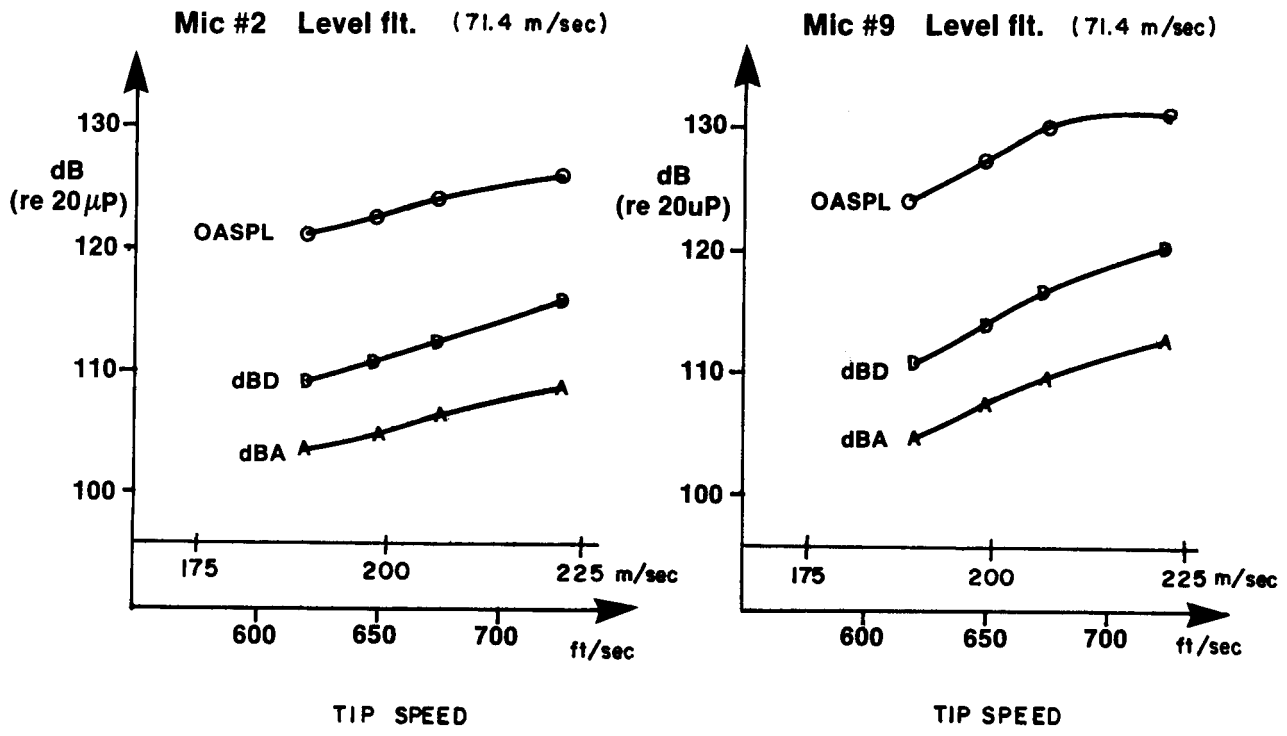

Figure 38. Level Flight Noise Trends with Tip Speed for the Baseline Tip Configuration 7 with -10° Twist at 71.4 m/sec, C_T = 0.006, and α_{TPP} = -3°

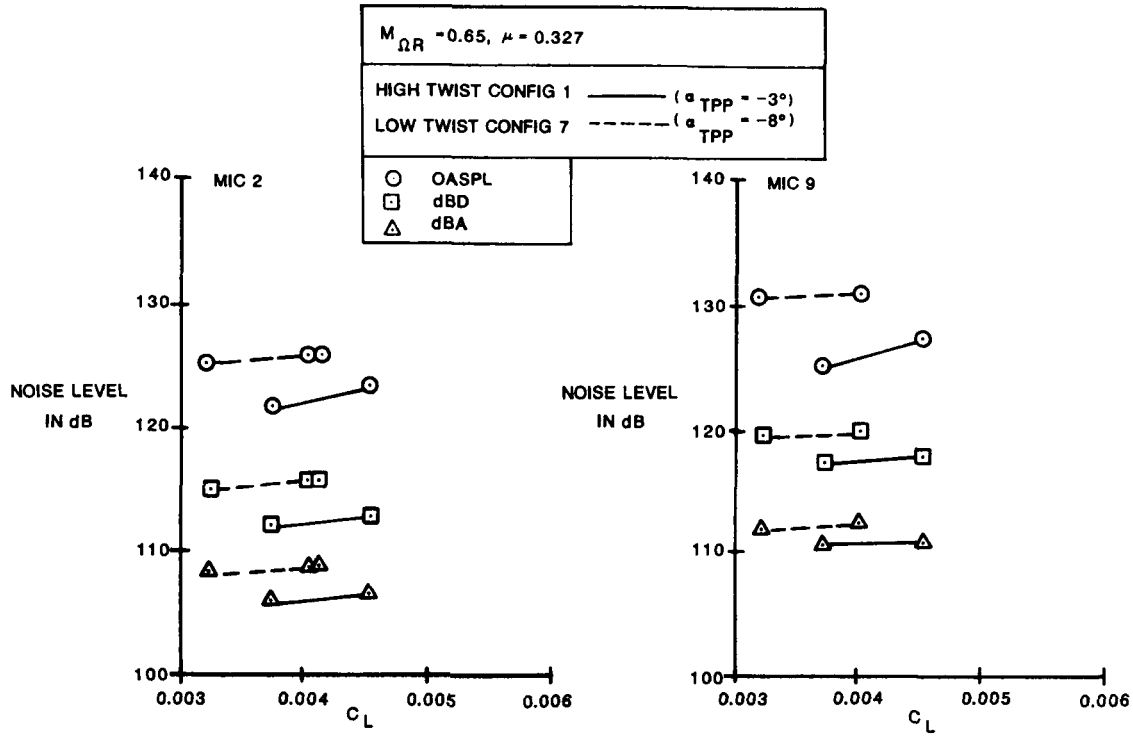

Figure 39. High-Speed Noise Trends with Rotor Lift Coefficient for the Baseline Tip Configurations with -16° Twist and -10° Twist

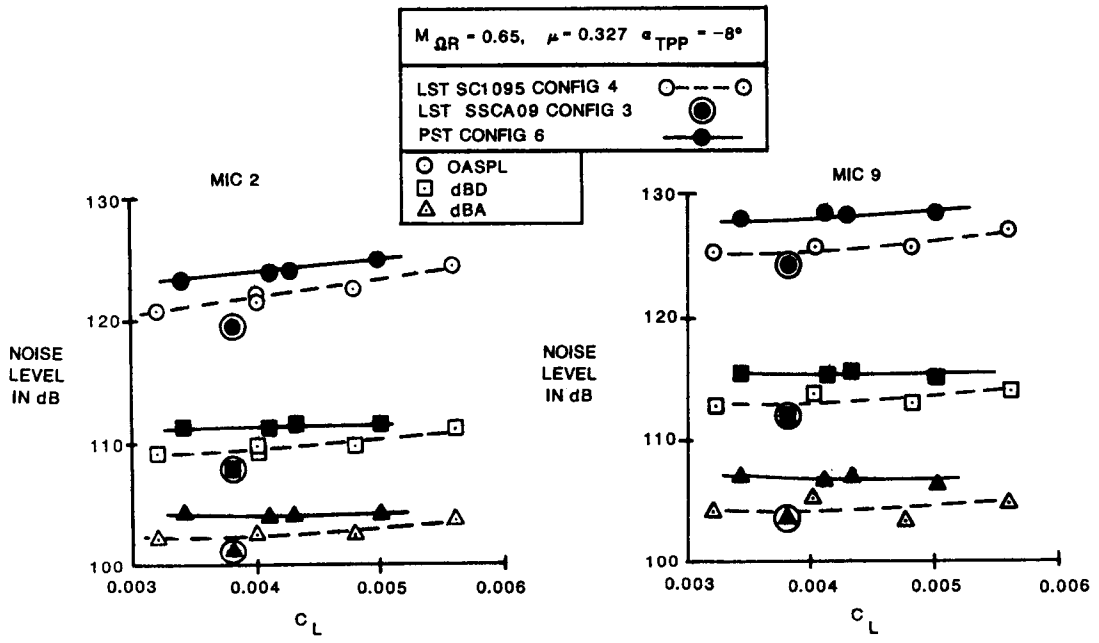

Figure 40. High-Speed Noise Trends with Lift Coefficient for the Large Swept Tapered Tip Configurations with SC1095 and SSCA09 Airfoils

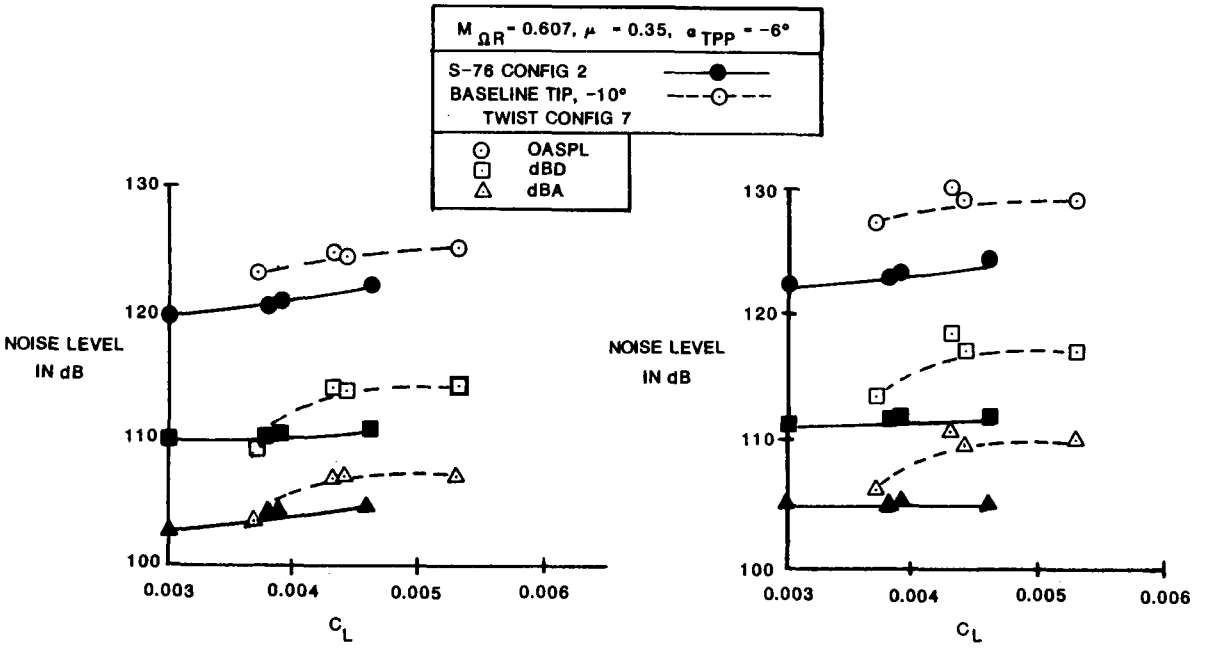

Figure 41. High-Speed Noise Trends with Lift Coefficient for the S-76 Configuration 2 and the Baseline Tip Configuration 7 with -10° Twist

APPENDIX A

TUNNEL BACKGROUND NOISE

The tunnel background noise 1/12-octave band spectra with the bare hub turning are presented at two in-flow microphones (2 and 9). All the spectra provided in this Appendix were obtained by operating the tape recorder at 1/4 the speed of data acquisition. This procedure facilitates easier comparison of 1/12-octave band spectra for the 1/20-scale models with those for the 1/5-scale models.

The tunnel fundamental tone was at 30 Hz (7.5 Hz in the 1/12 octave plots obtained at 1/4 tape speed) and hence it is off the 1/12-octave plots provided here. The plots shown here start at 20X4 = 80Hz at which the higher harmonic tunnel tones appear to have become unimportant. Tones appearing in the 1/12-octave spectra are the harmonics of the rotor hub and they become less pronounced at higher tunnel speeds due to the broadband wind noise. Indeed one can see the classical V^6 relationship in the noise levels (printed on the right hand side in OASPL, dBA and dBD), where V is the tunnel speed.

Comparison of these background noise levels with the rotor noise levels provided in Appendix C show that the background noise levels are far lower than the rotor noise levels.

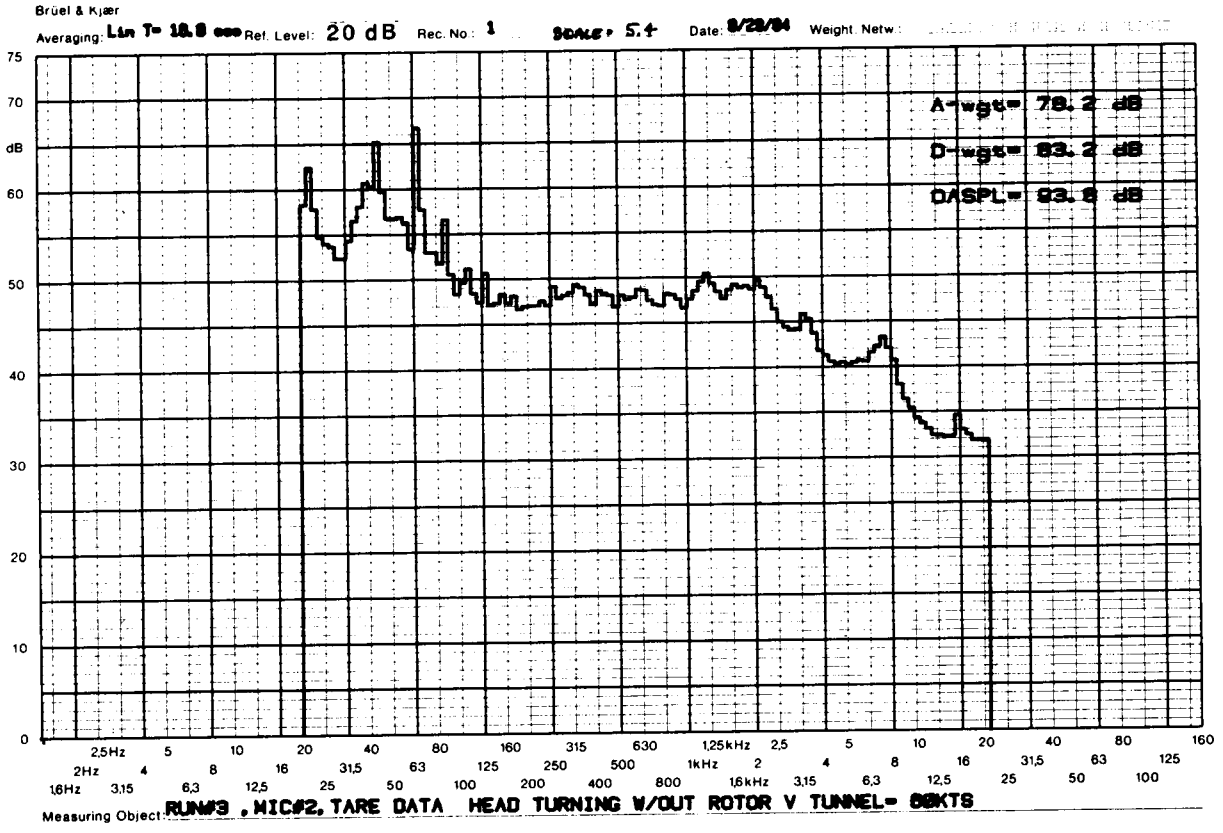

Figure A1. Tunnel Background Noise for 30.6 m/sec (60 Knots) at Microphone 2.

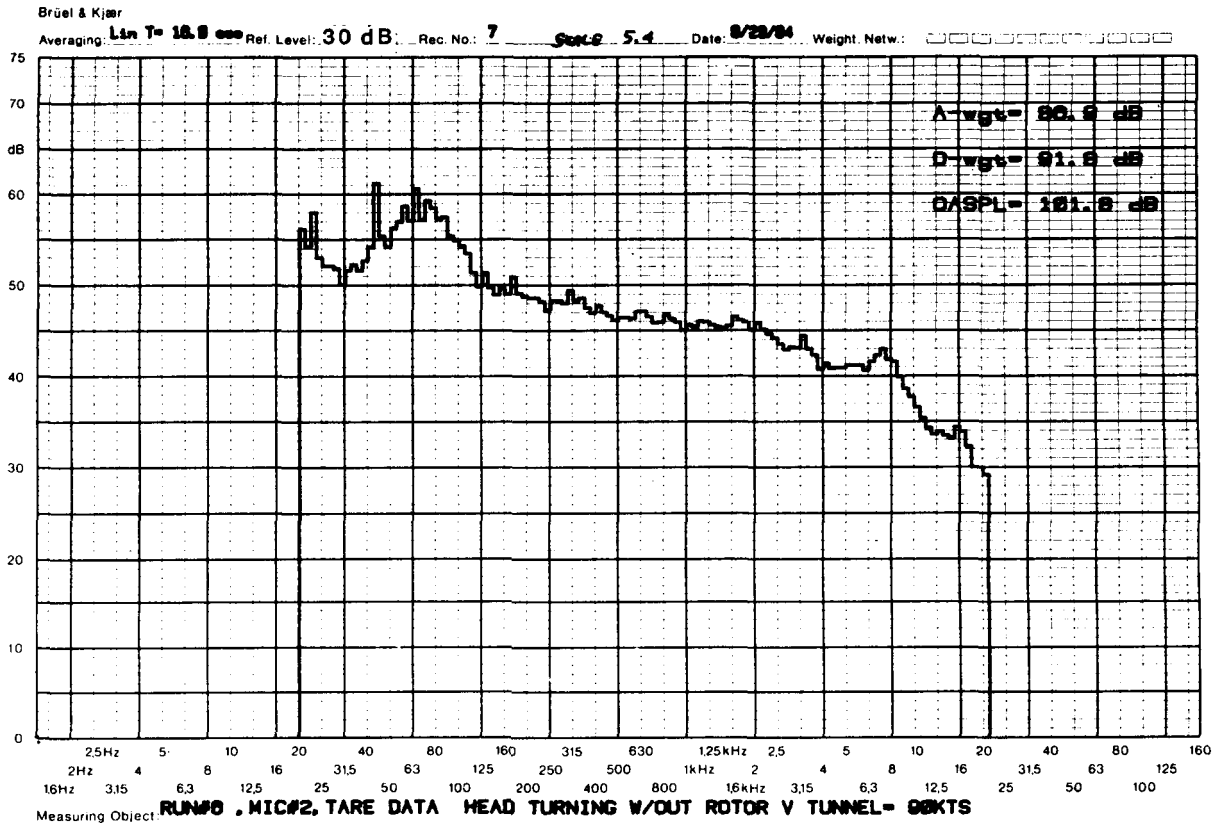

Figure A2. Tunnel Background Noise for 45.9 m/sec (90 Knots) at Microphone 2.

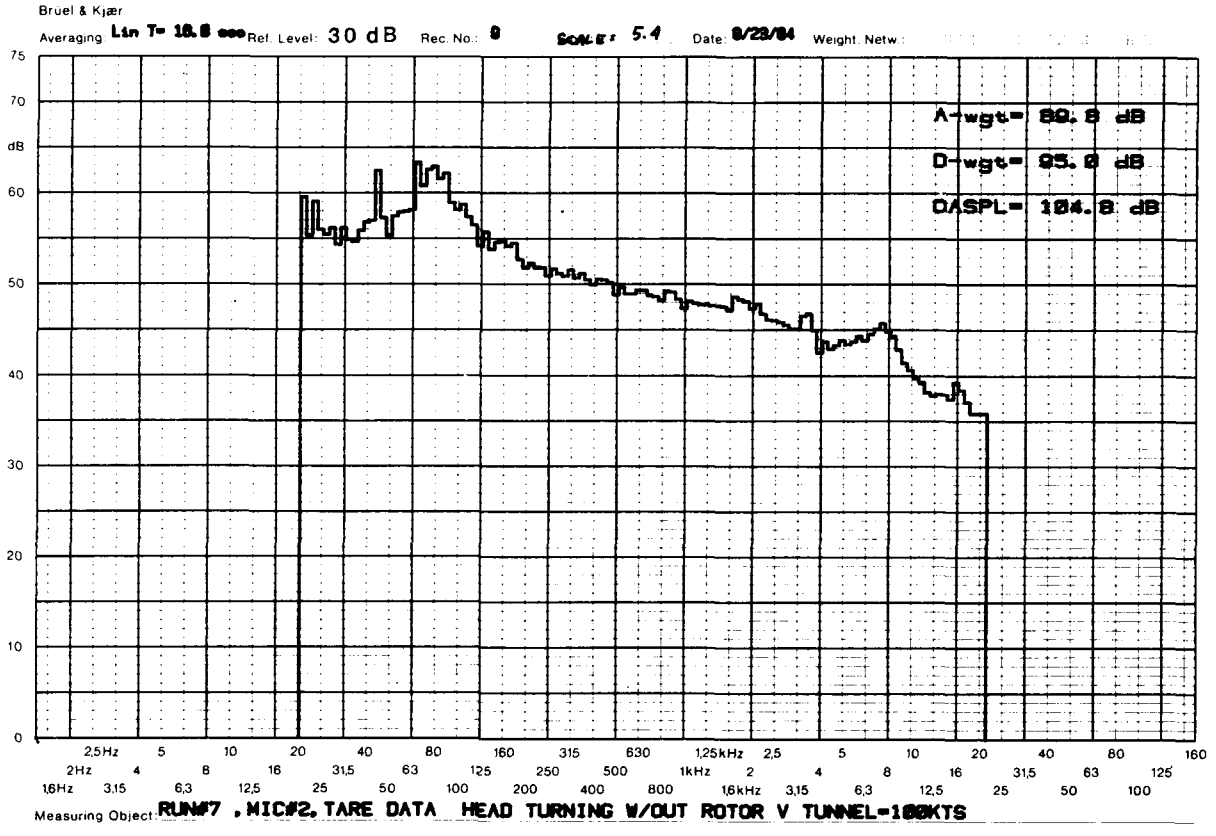

Figure A3. Tunnel Background Noise for 51 m/sec (100 Knots) at Microphone 2.

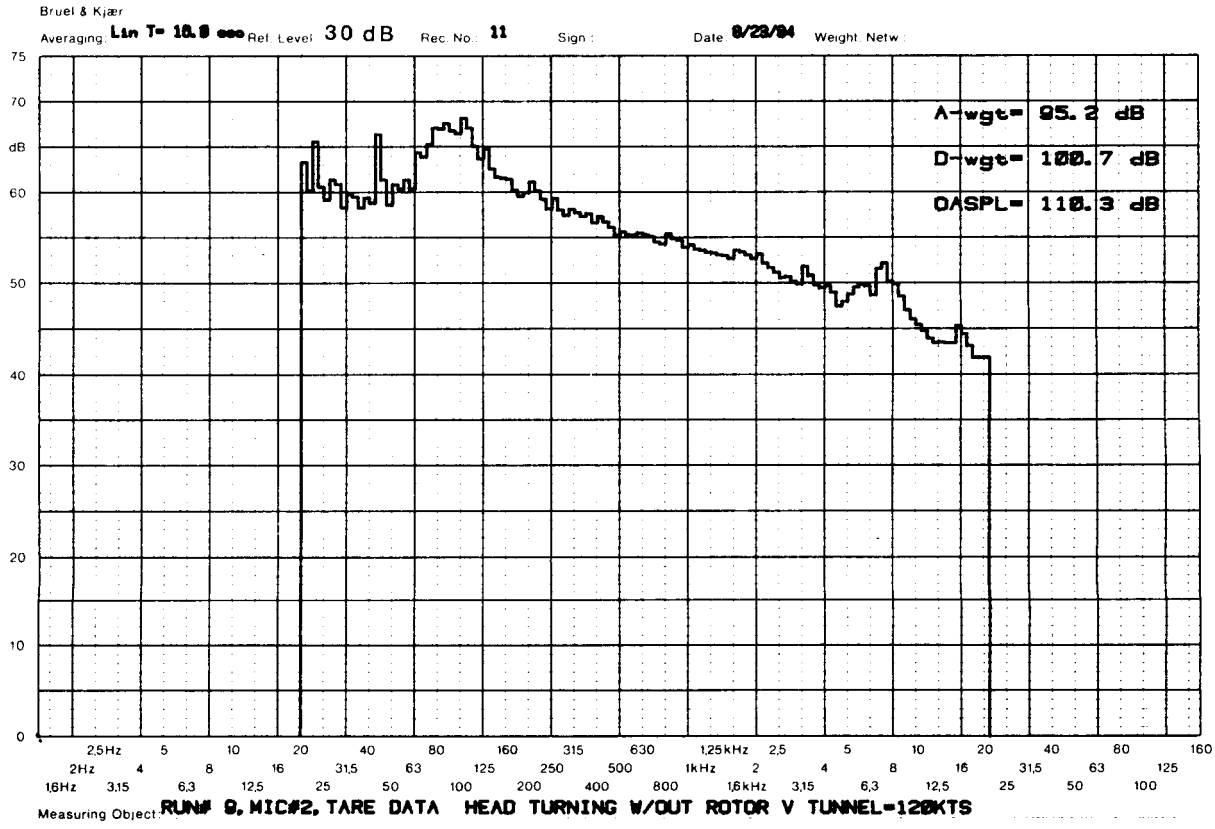

Figure A4. Tunnel Background Noise for 61.2 m/sec (120 Knots) at Microphone 2.

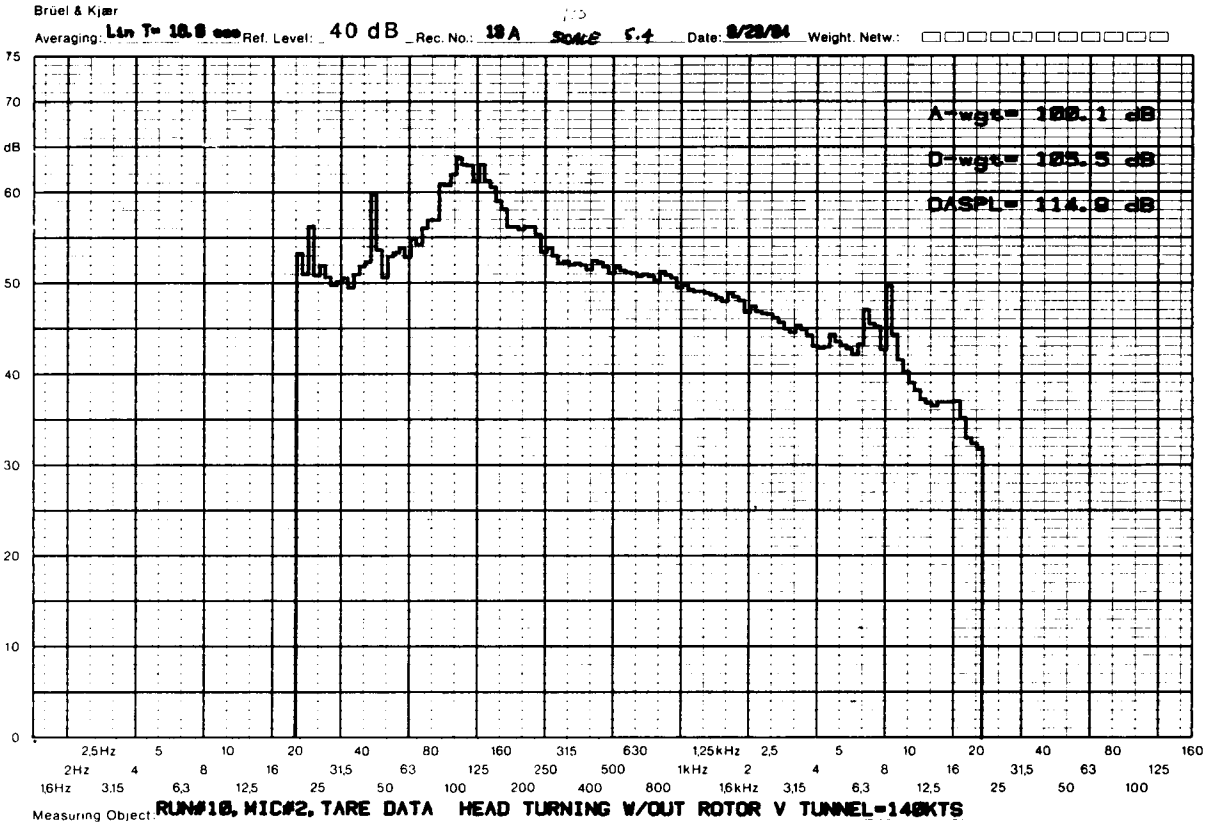

Figure A5. Tunnel Background Noise for 71.4 m/sec (140 Knots) at Microphone 2.

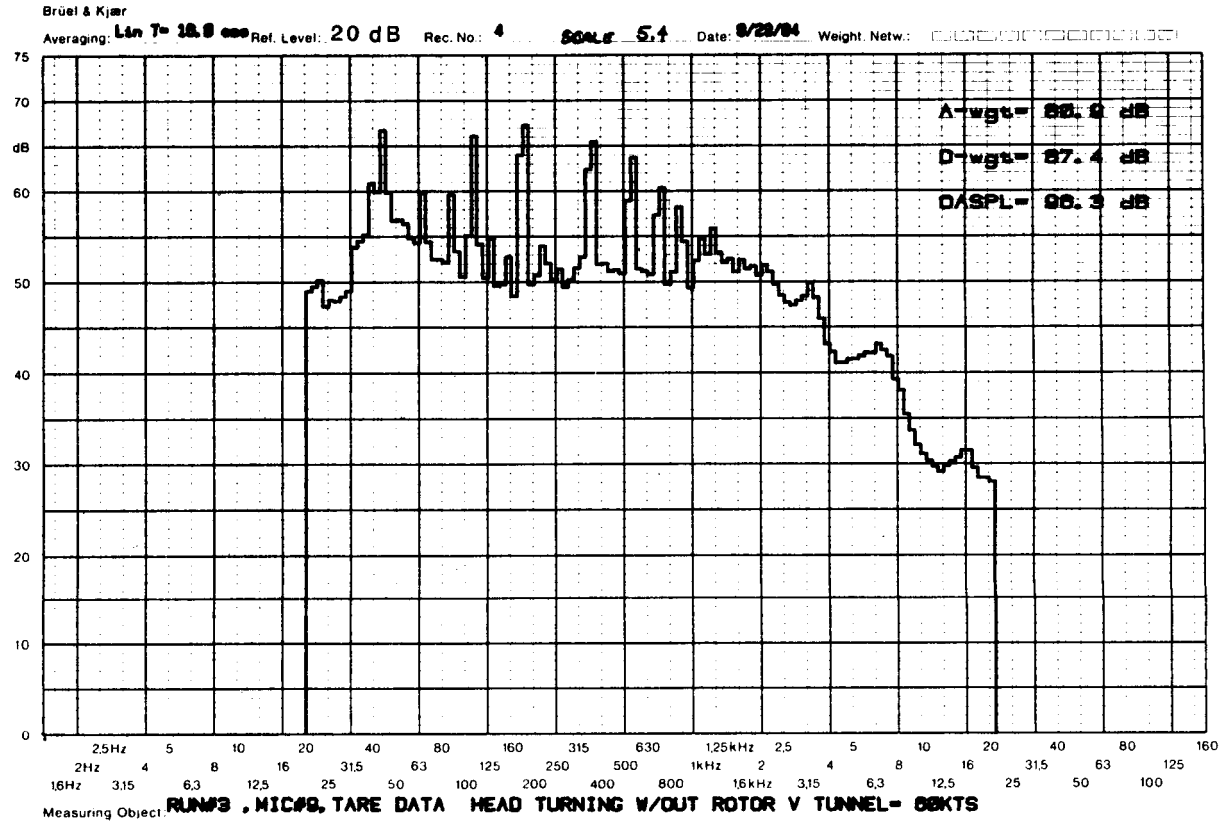

Figure A6. Tunnel Background Noise for 30.6 m/sec (60 Knots) at Microphone 9.

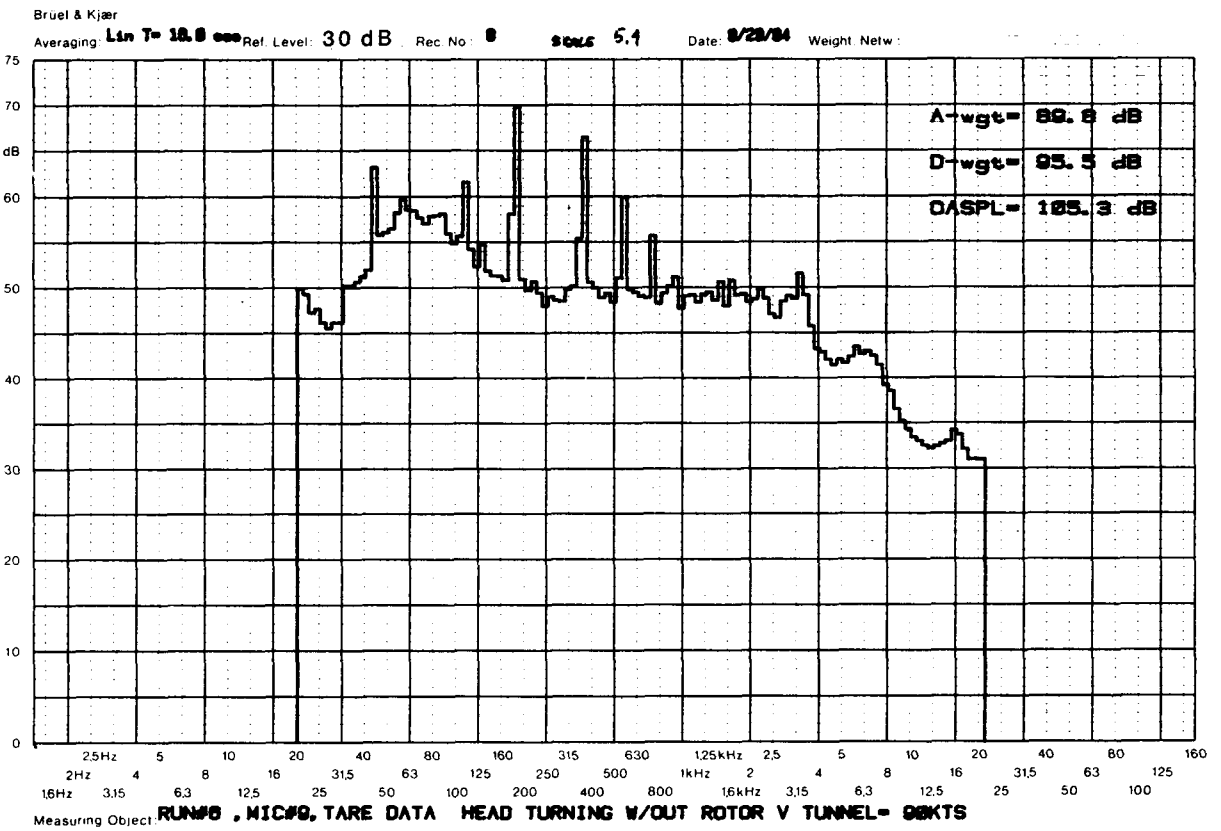

Figure A7. Tunnel Background Noise for 45.9 m/sec (90 Knots) at Microphone 9.

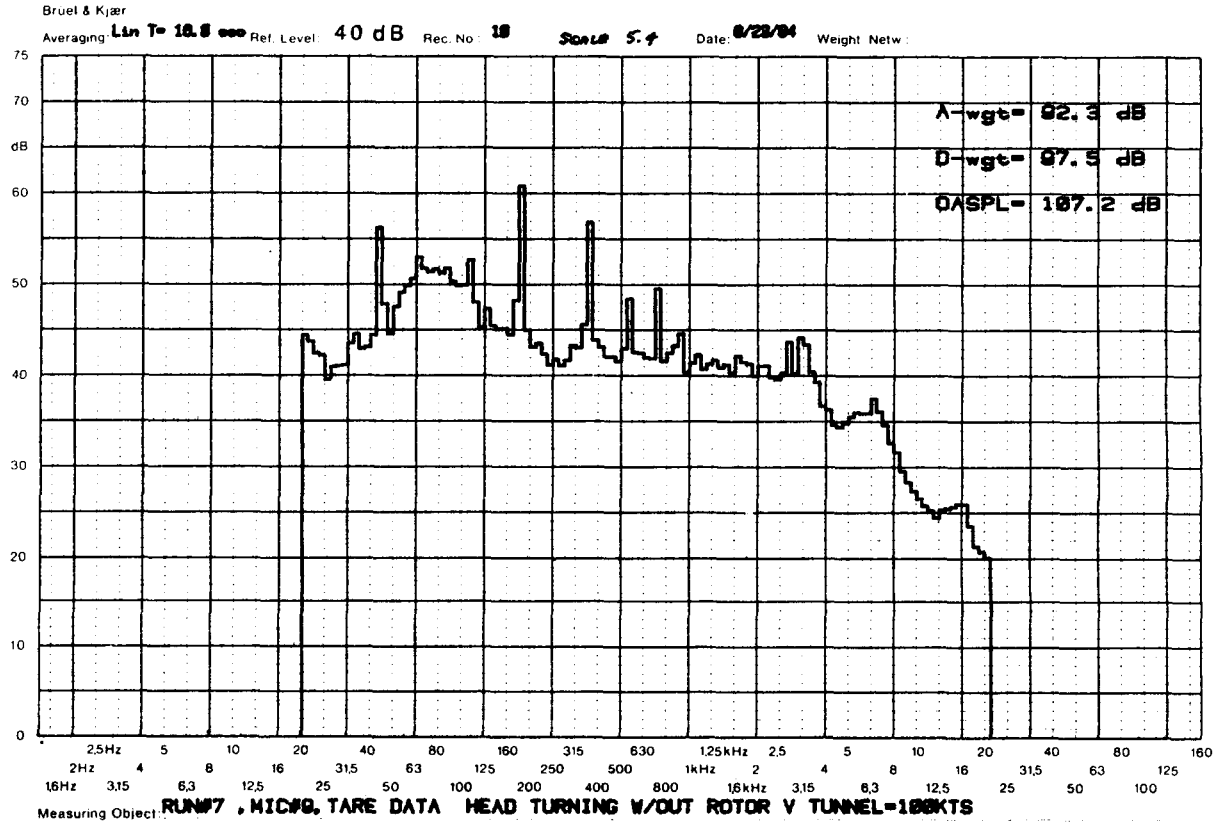

Figure A8. Tunnel Background Noise for 51 m/sec (100 Knots) at Microphone 9.

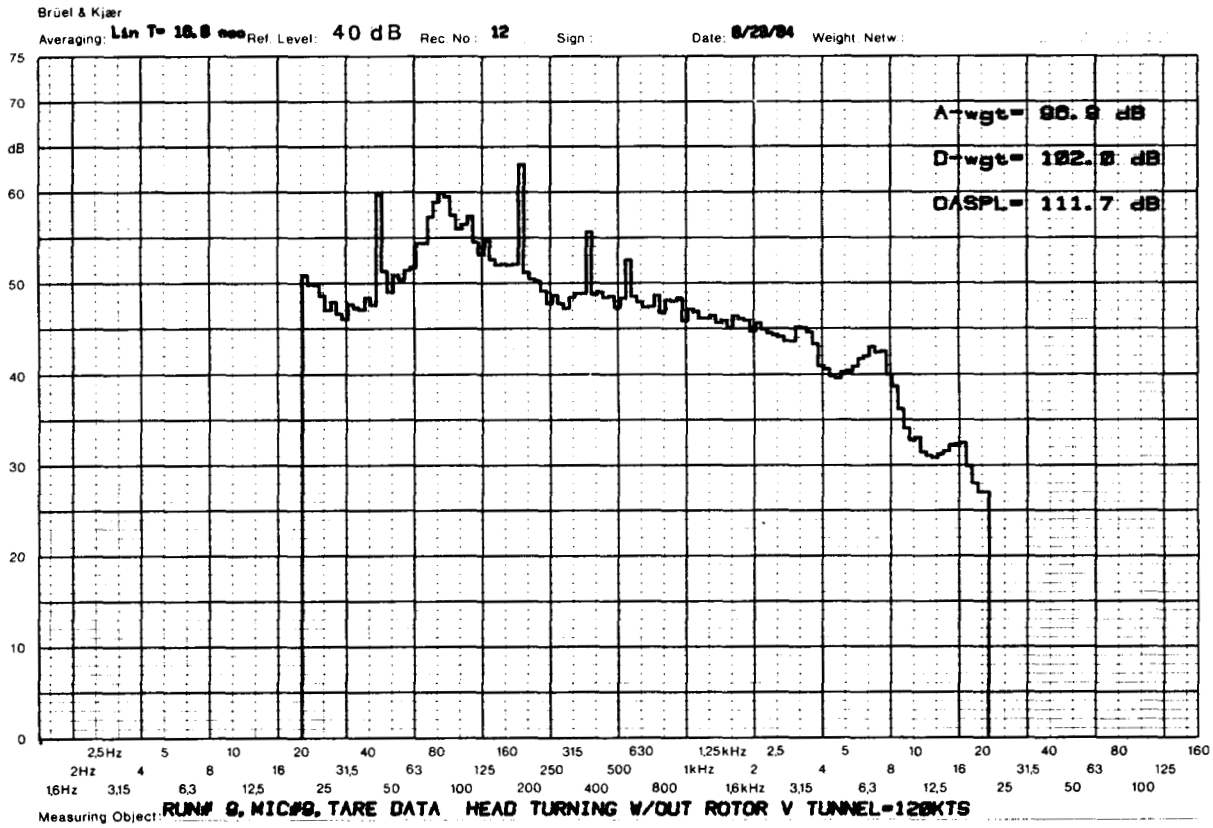

Figure A9. Tunnel Background Noise for 61.2 m/sec (120 Knots) at Microphone 9.

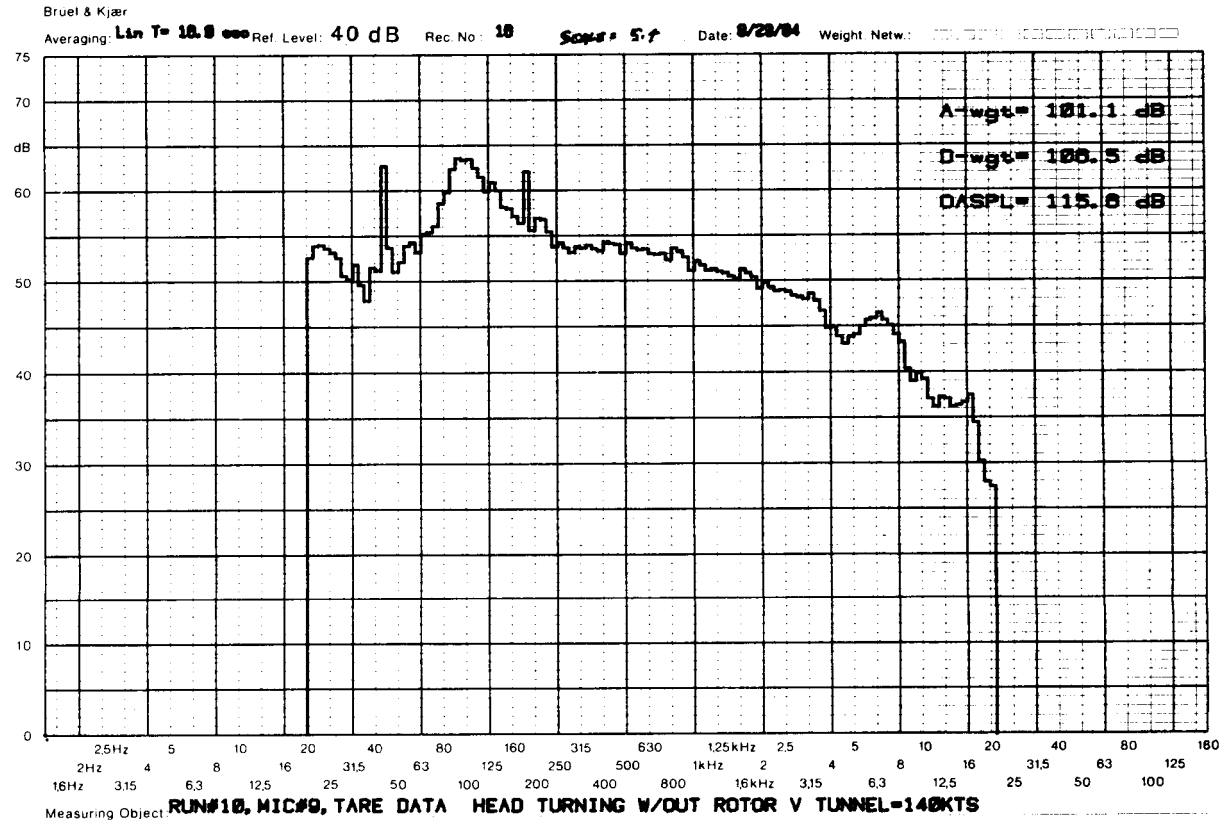

Figure A10. Tunnel Background Noise for 71.4 m/sec (140 Knots) at Microphone 9.

APPENDIX B

NARROWBAND POWER SPECTRAL DENSITY PLOTS

Sample power spectral density plots obtained for each of the rotor models tested are provided here. These plots were obtained by using 3.25 Hz constant band width filters and normalizing the amplitude by the filter band width. Once again the tape was played back at 1/4 the recording speed. All except the UH-1H configuration (#5) were run at 30.6 m/sec (60 knots) while the UH-1H configuration was run at 35.7 m/sec (70 knots) tunnel speed. Similarly the tip path plane angle shown are 3° and 5° for configuration 5 while the same for the other rotors is 4°. Essentially all the configurations show discrete harmonic noise during BVI although the large swept tapered tip configuration with SC1095 airfoil (#4) and the parabolic swept tip configuration (#6) show significant sideband levels in addition to the harmonics. Apparent increase in the broadband noise floor for configurations 4, 5 and 6 are believed to be caused by instrumentation noise floor.

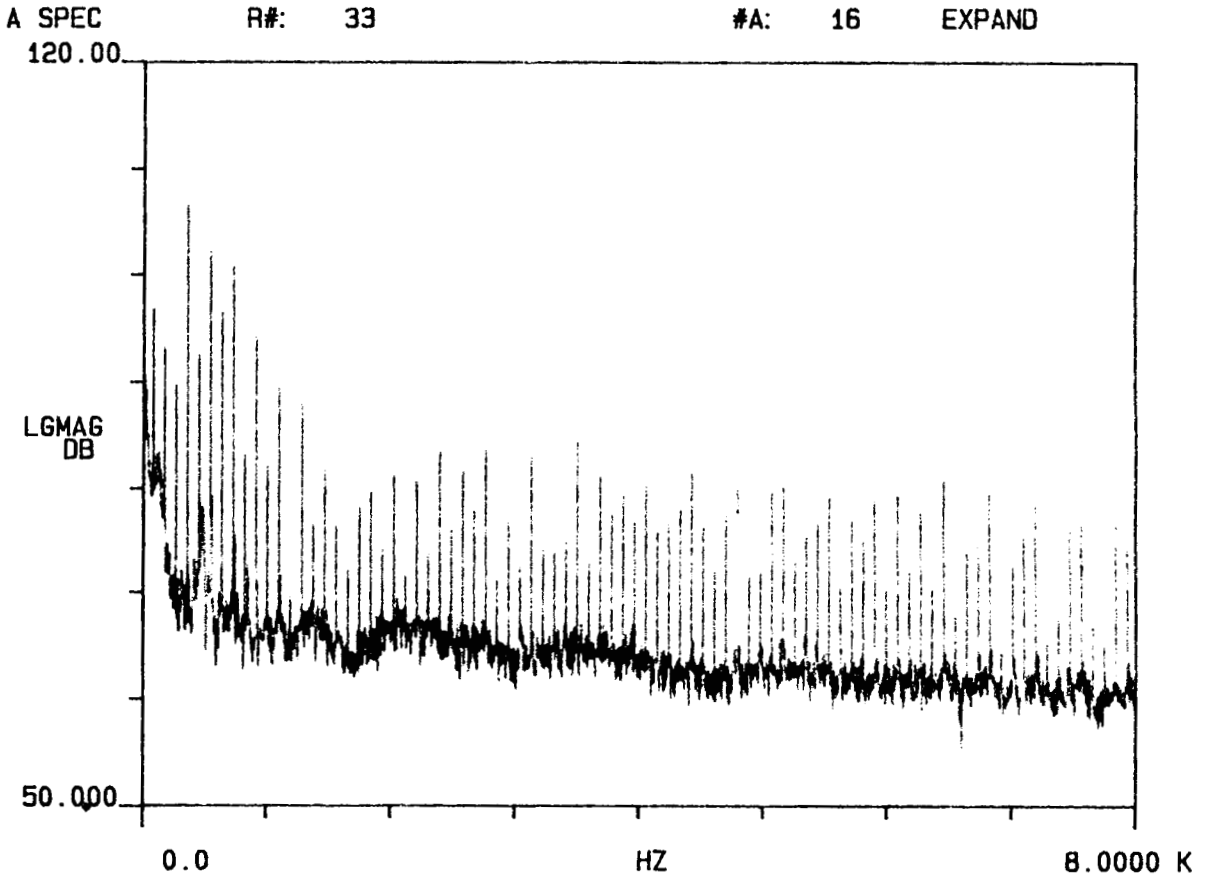

Figure B1. Narrow Band Power Spectral Density for the Baseline Rotor Configuration 1 at C_T = 0.007, $M_{1,90}$ = 0.739, μ = 0.14, and α_{TPP} = 4°.

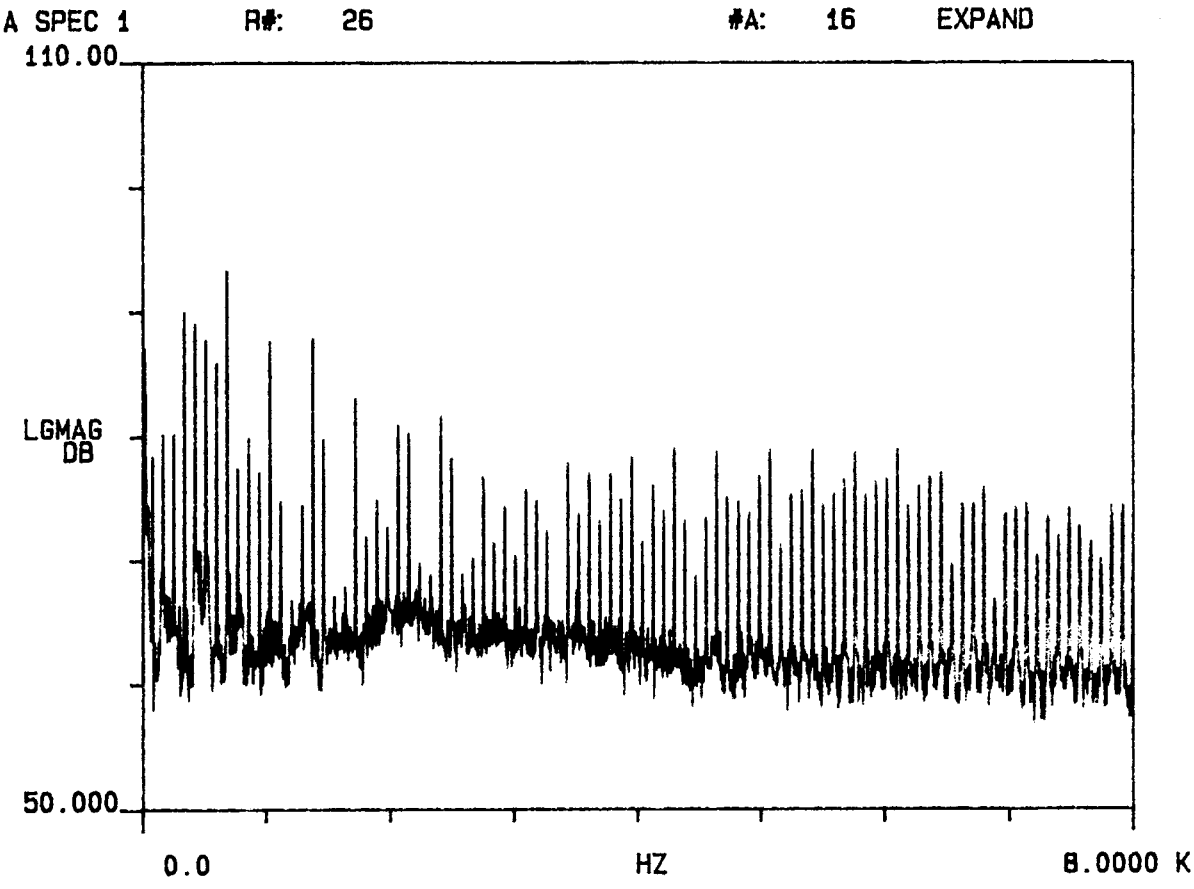

Figure B2. Narrow Band Power Spectral Density for the S-76 Rotor Configuration 2 at C_T = 0.007, $M_{1,90}$ = 0.694, μ = 0.15 and α_{TPP} = 4°.

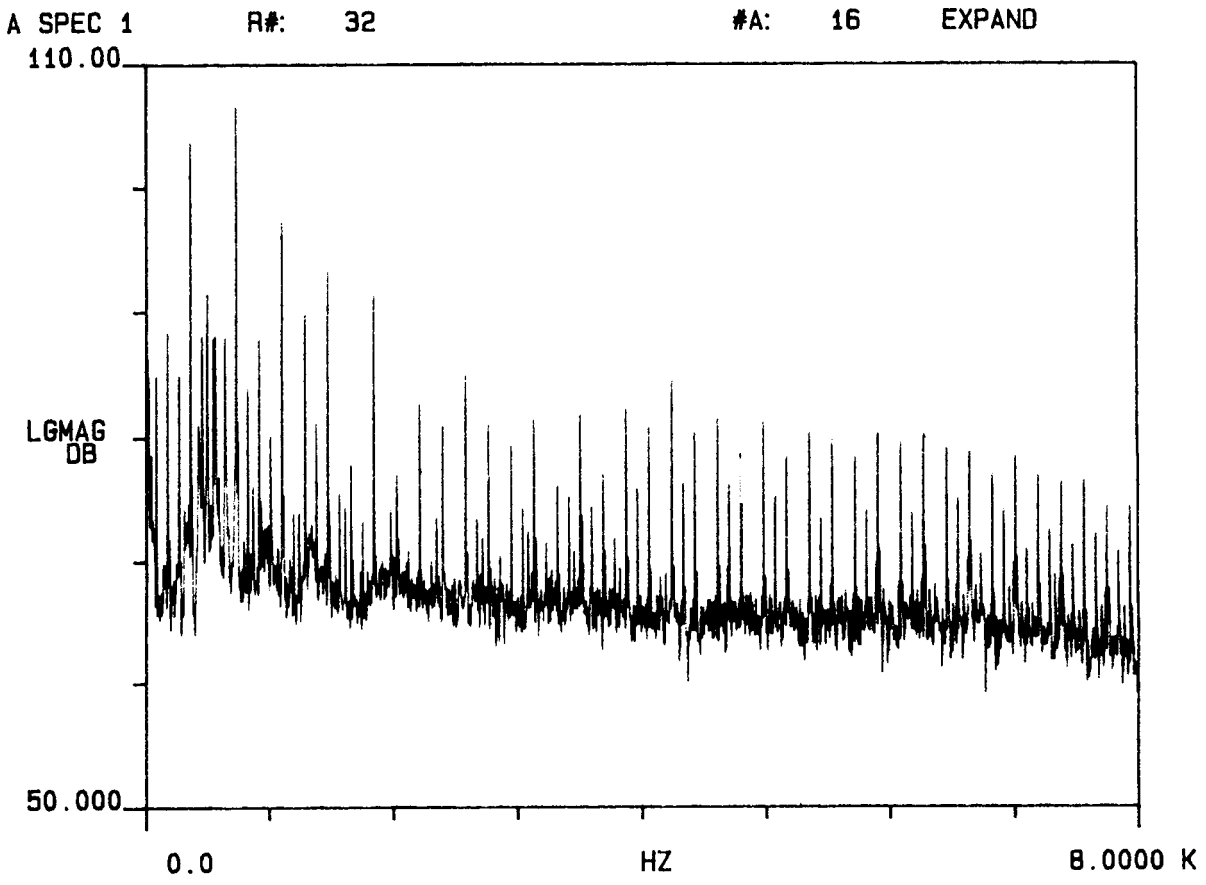

Figure B3. Narrow Band Power Spectral Density for the Large Swept Tapered Tip Configuration 3 with New Airfoils at C_T = 0.007, $M_{1,90}$ = 0.739, μ = 0.14, and α_{TPP} = 4°.

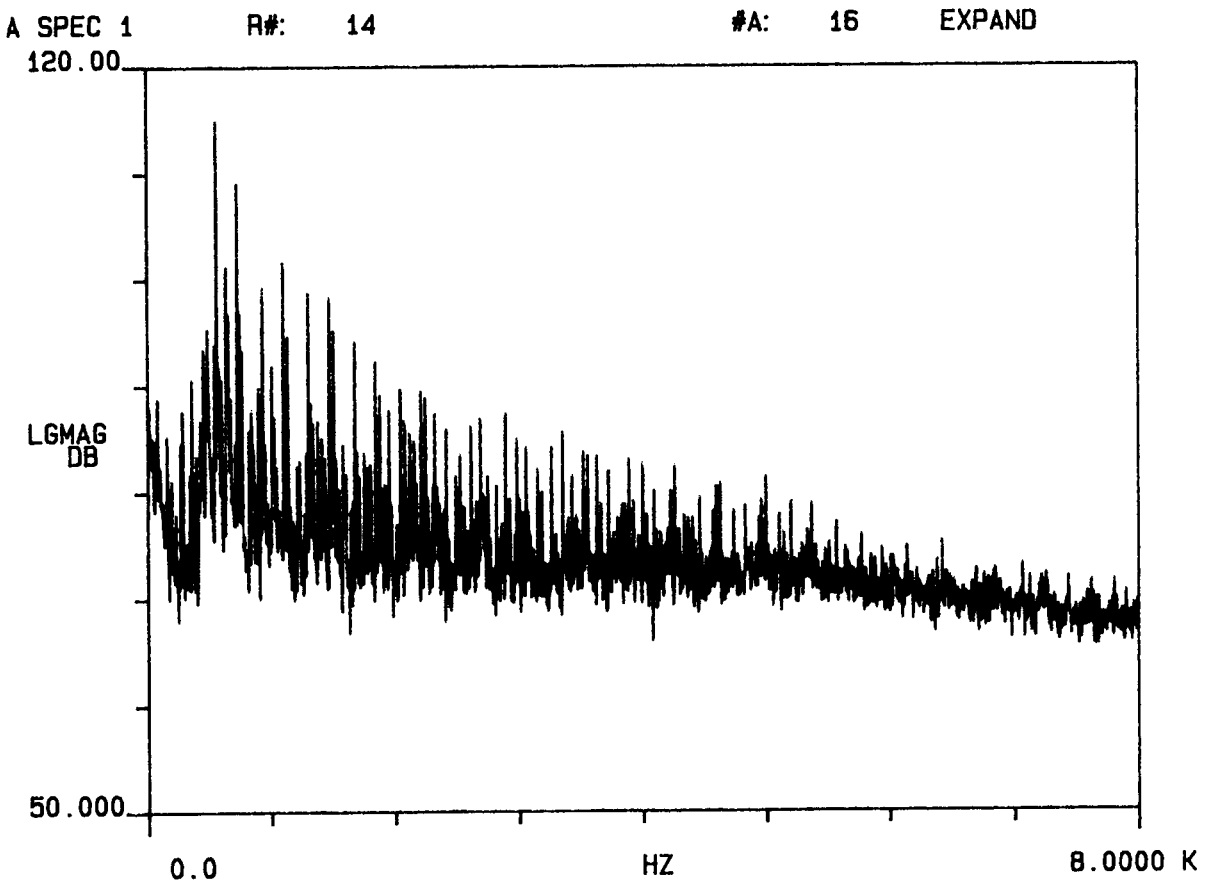

Figure B4. Narrow Band Power Spectral Density for the Large Swept Tapered Tip Configuration 4 with SC1095 Airfoils at C_T = 0.007, $M_{1,90}$ = 0.739, C_T = 0.007 and α_{TPP} = 4°.

C-2

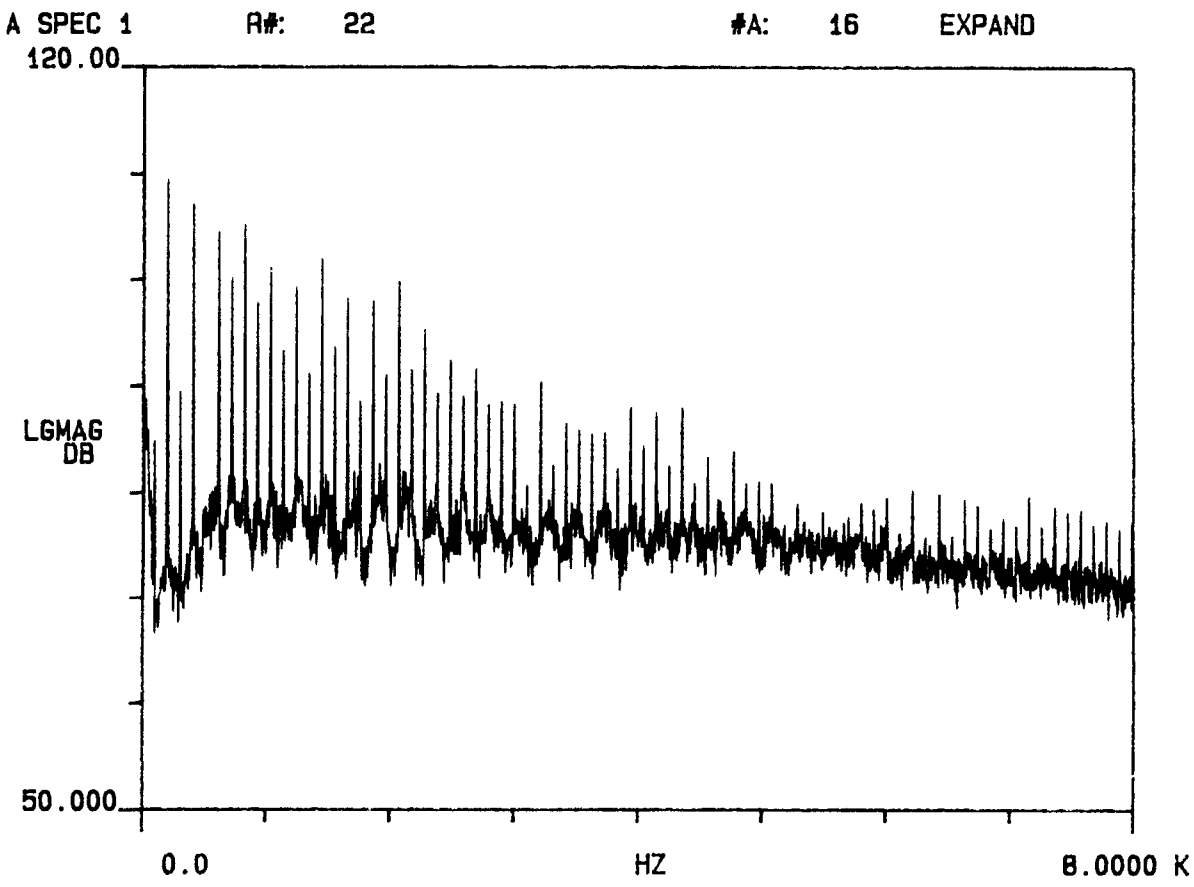

Figure B5. Narrow Band Power Spectral Density for the UH-1H Configuration 5 at C_T = 0.0056, $M_{1,90}$ = 0.833, μ = 0.145, and $\alpha_{TPP} \cong 3°$.

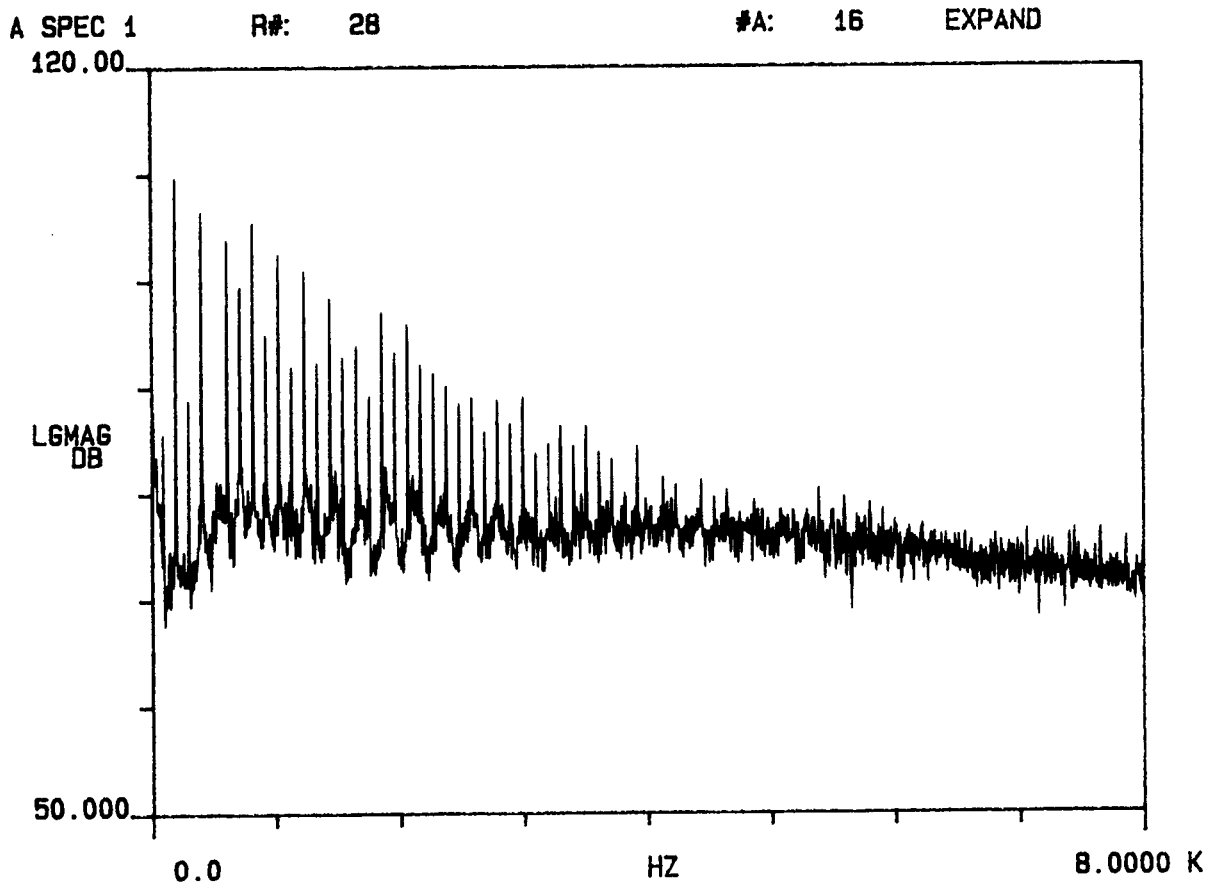

Figure B6. Narrow Band Power Spectral Density for the UH-1H Configuration 5 at $C_T = 0.0056$, $M_{1,90} = 0.833$, $\mu = 0.144$, and $\alpha_{TPP} \doteq 5°$.

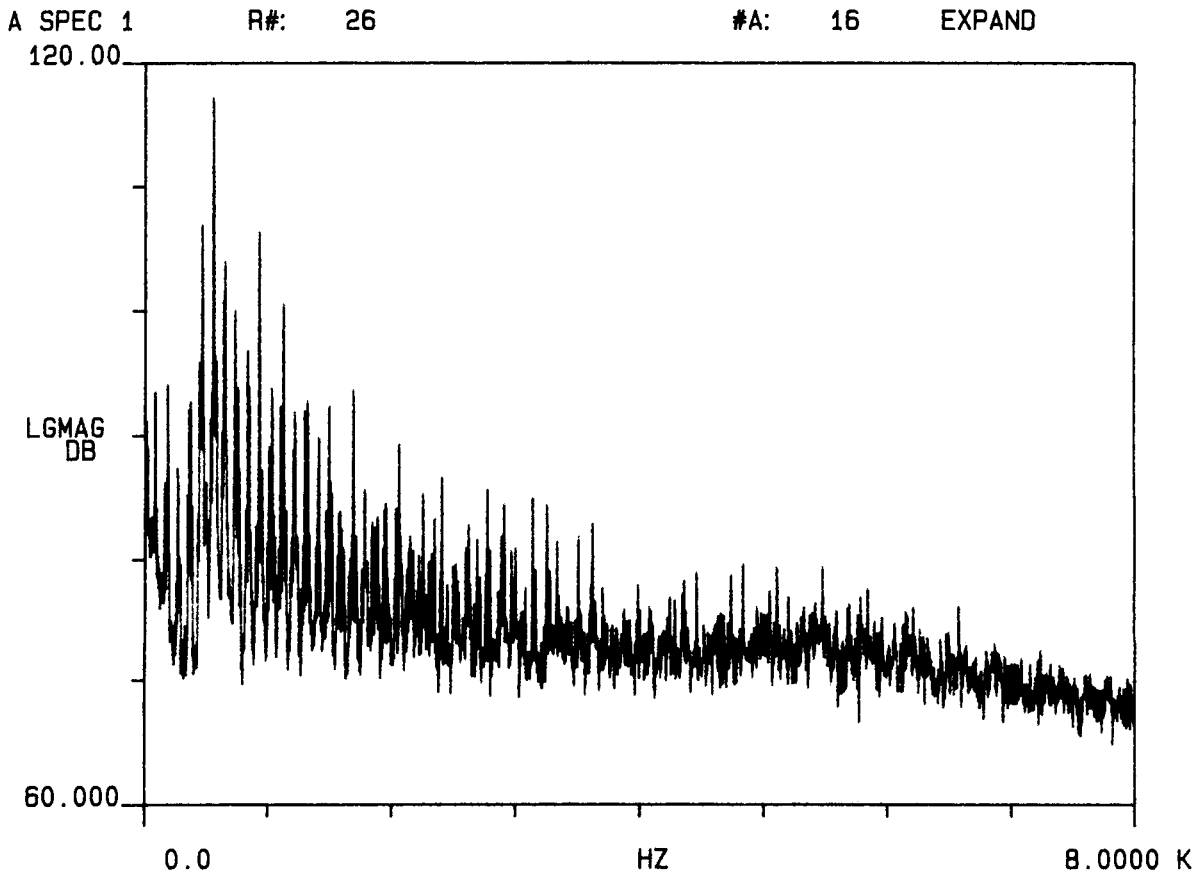

Figure B7. Narrow Band Power Spectral Density for the Parabolic Swept Tip Configuration 6 at $C_T = 0.007$, $M_{1,90} = 0.739$, $\mu = 0.14$, and $\alpha_{TPP} = 4°$.

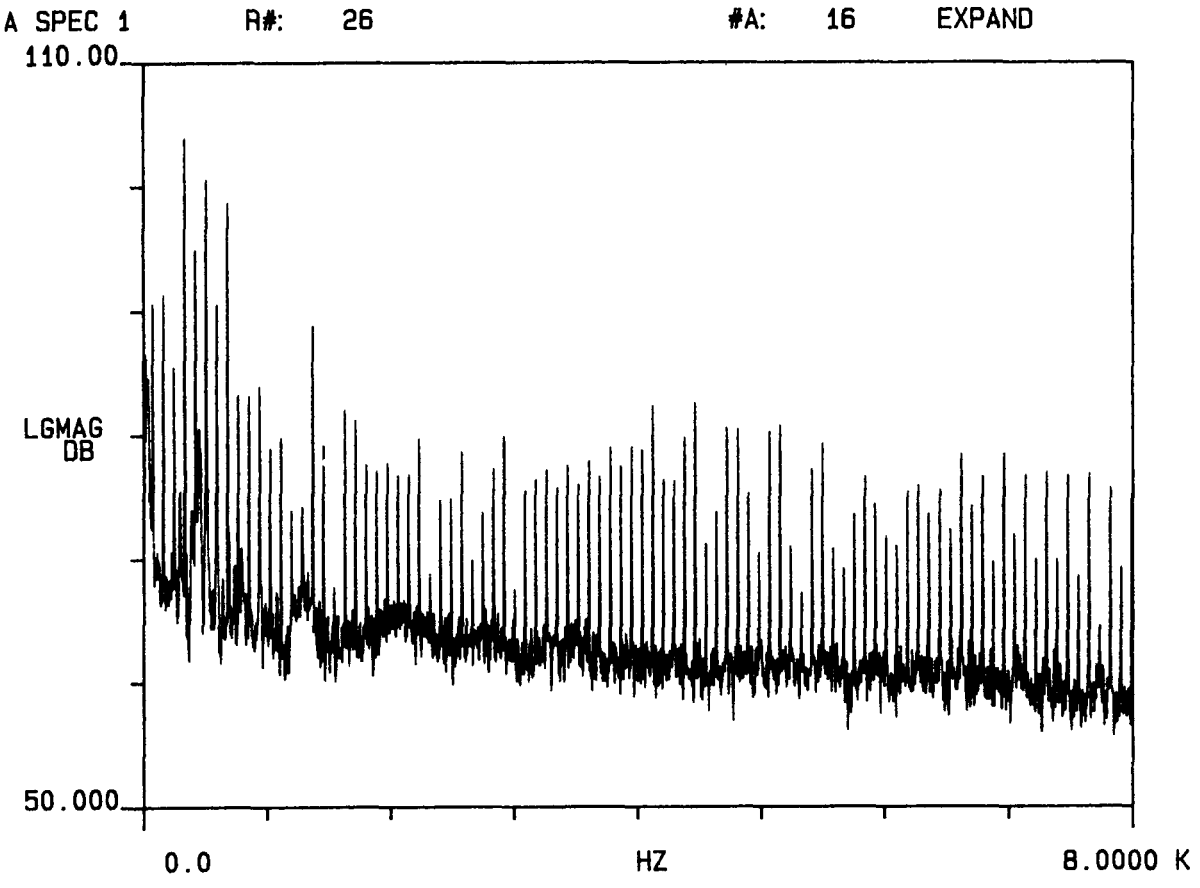

Figure B8. Narrow Band Power Spectral Density for the Baseline Tip Configuration 7 with -10° Twist at C_T = 0.007, $M_{1,90}$ = 0.694, μ = 0.15, and α_{TPP} = 4°.

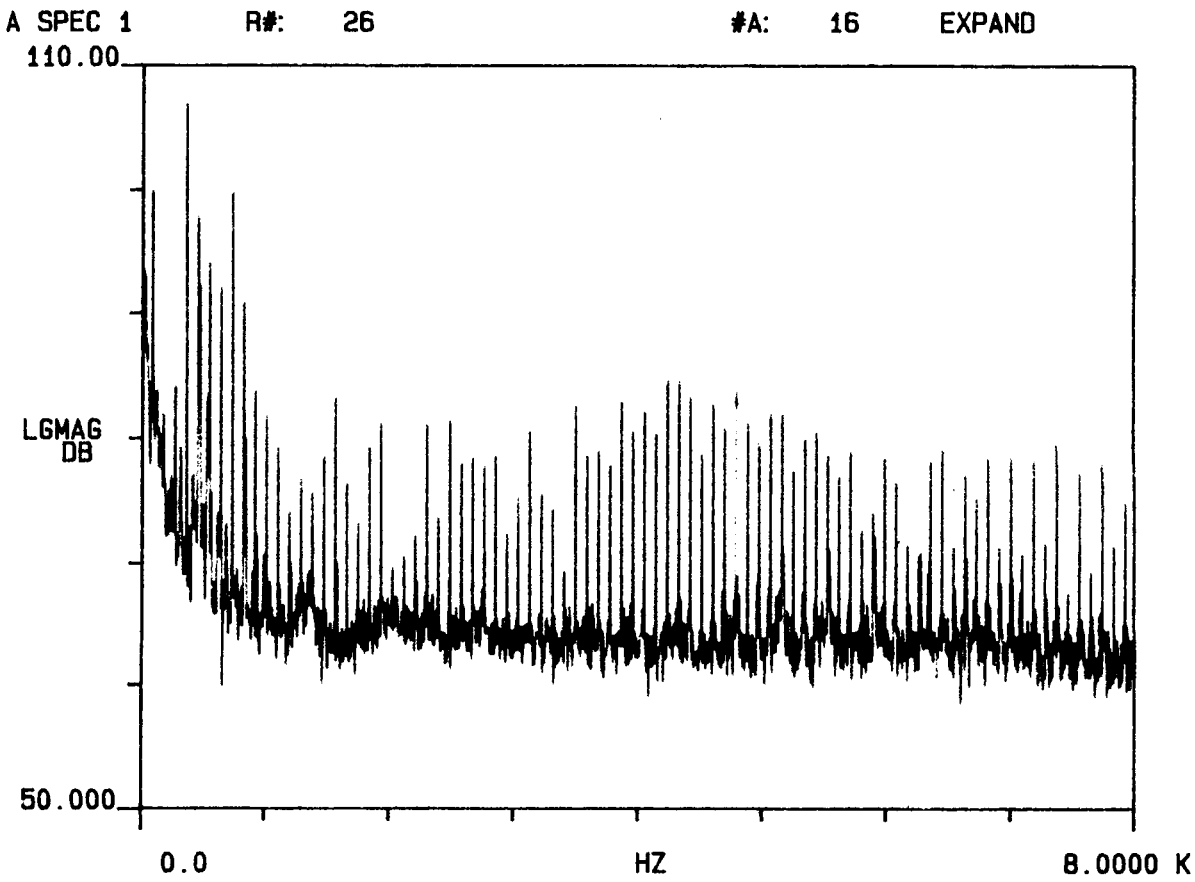

Figure B9. Narrow Band Power Spectral Density for the Baseline Tip Configuration 7 with -10° Twist at C_T = 0.007, $M_{1,90}$ = 0.739, μ = 0.14, and α_{TPP} = 4°.

APPENDIX C

1/12 OCTAVE SPECTRA FOR 1/20 AND 1/5 SCALE MODEL ROTORS

1/12-octave spectral plots at 1/20 and 1/5-scales are provided for the baseline (#1) and Large Swept Tapered Tip (#3) configurations at various tip path plane angles. The tunnel speed used was 30.6 m/sec (60 knots) and the rotor tip speed was 221 m/sec (725 ft/sec). The spectral plots were obtained by operating the tape at 1/4 times the recording speed. The averaging time, over which the spectrum was obtained, is printed on the left hand side top corner of these figures. This is followed by the reference noise level used in the 1/12-octave plots. The record number is of no specific significance since it is only a file code used in storing the data during the data reduction. Finally, the scale is a factor by which the 1/12-octaves are shifted during the computation of the flight scaled A and D metrics. Indeed, at 1/4-tape speed, a scale of say 5.4 means 21.6 (5.4x4). These weighted noise metrics and OASPL are computed and printed on the right hand top quadrant of these plots.

As an example, the first harmonic of the rotor blade passage is plotted at approximately 90 Hz in Figure C1. Since the data was reduced at 1/4-tape speed, this corresponds to 90x4 Hz at 1/20-scale and 90/5.4 at full-scale.

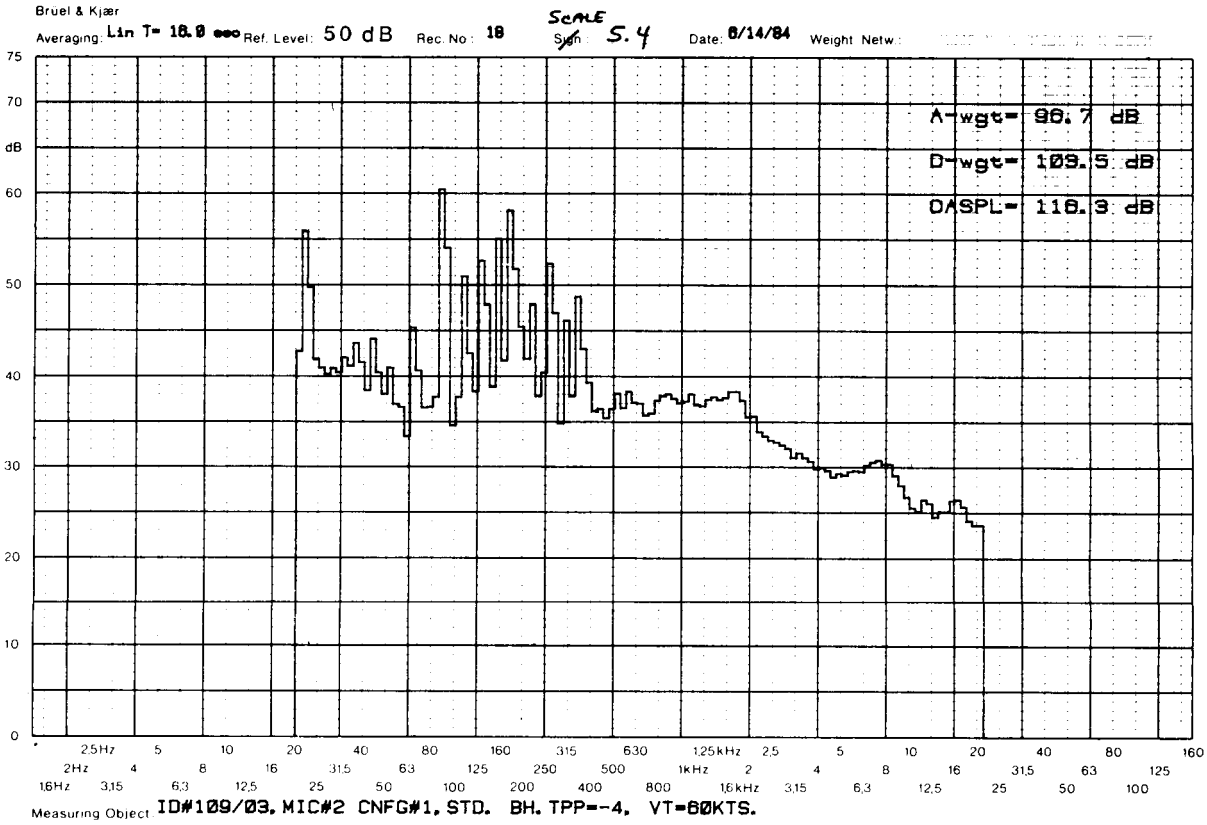

Figure C1. 1/12 Octave Spectra for the 1/20 Scale Baseline Configuration 1 at Microphone 2, M_{QR} = 0.65, C_T = 0.007, μ = 0.14 and α_{TPP} = -4°.

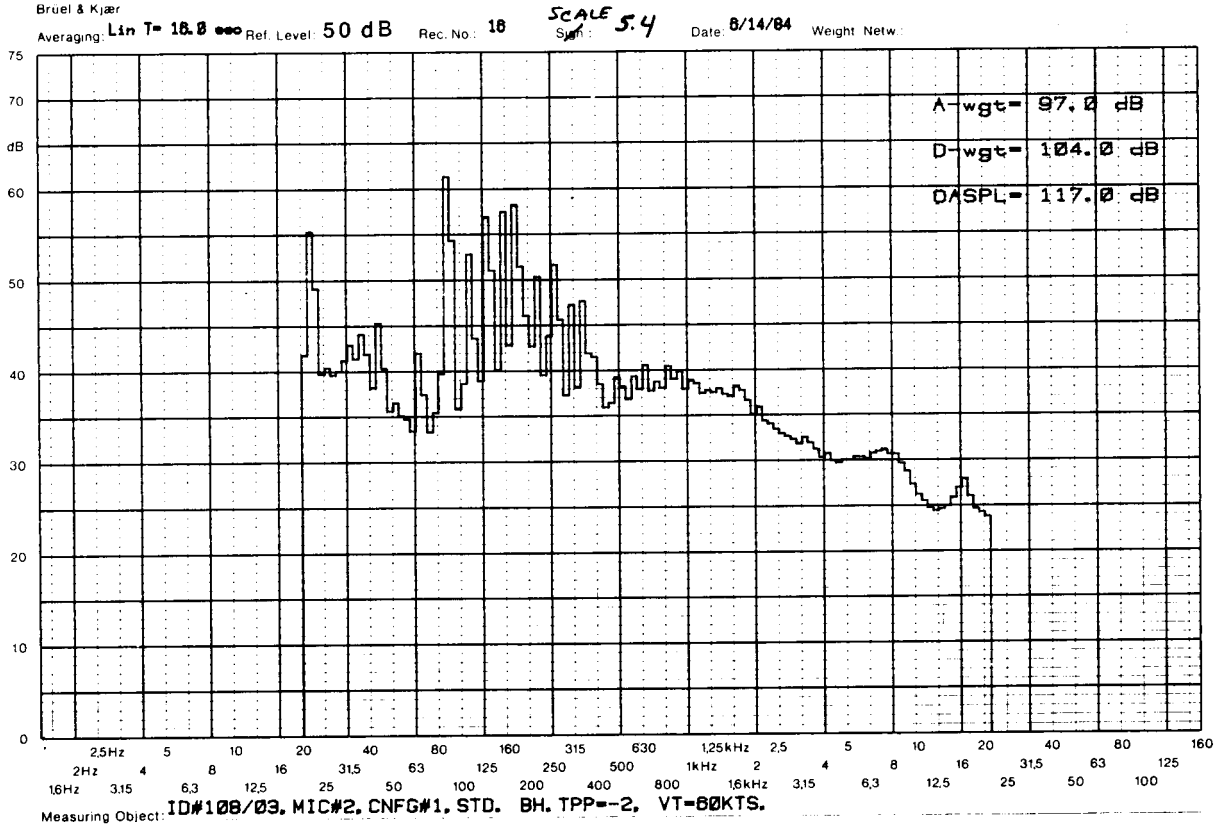

Figure C2. 1/12 Octave Spectra for the 1/20 Scale Baseline Configuration 1 at MIC 2, $M_{\Omega R} = 0.65$, $C_T = 0.007$, $\mu = 0.14$ and $\alpha_{TPP} = -2°$.

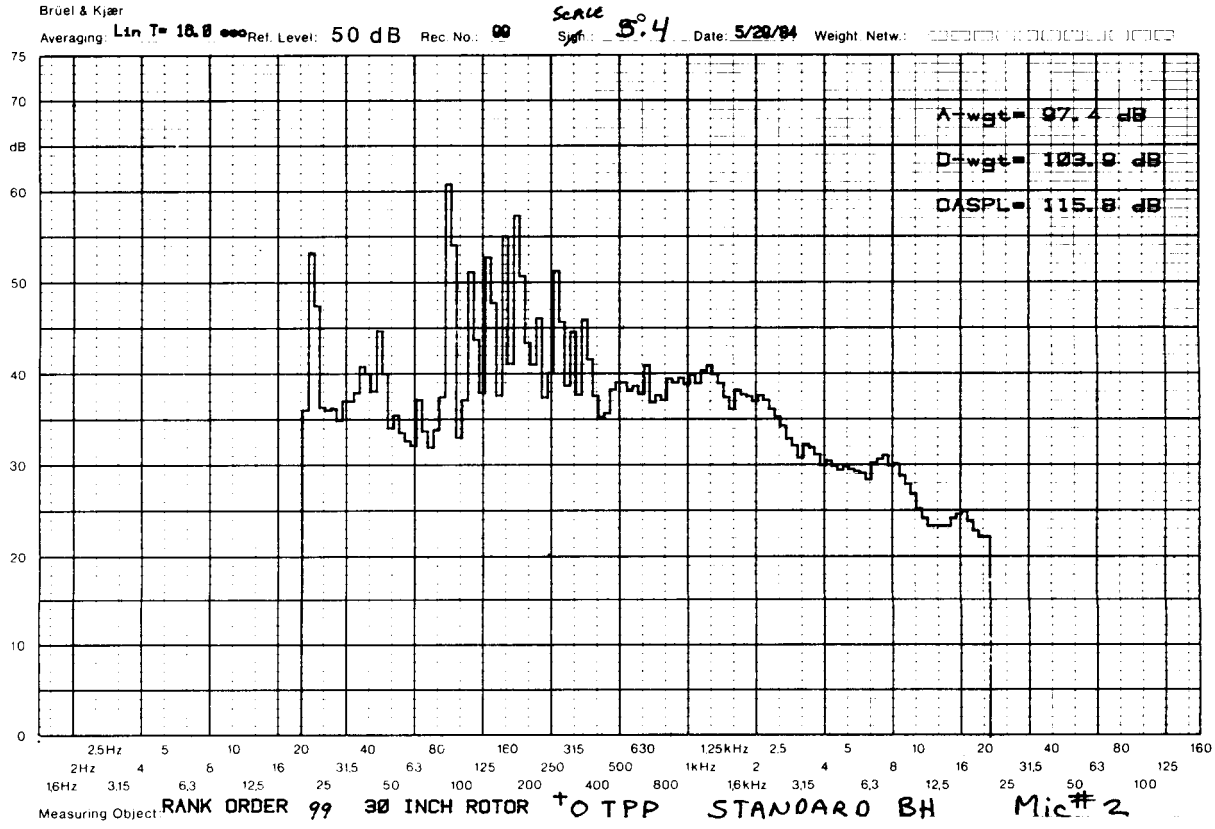

Figure C3. 1/12 Octave Spectra for the 1/20 Scale Baseline Configuration 1 at MIC 2, $M_{\Omega R} = 0.65$, $C_T = 0.007$, $\mu = 0.14$ and $\alpha_{TPP} = 0°$.

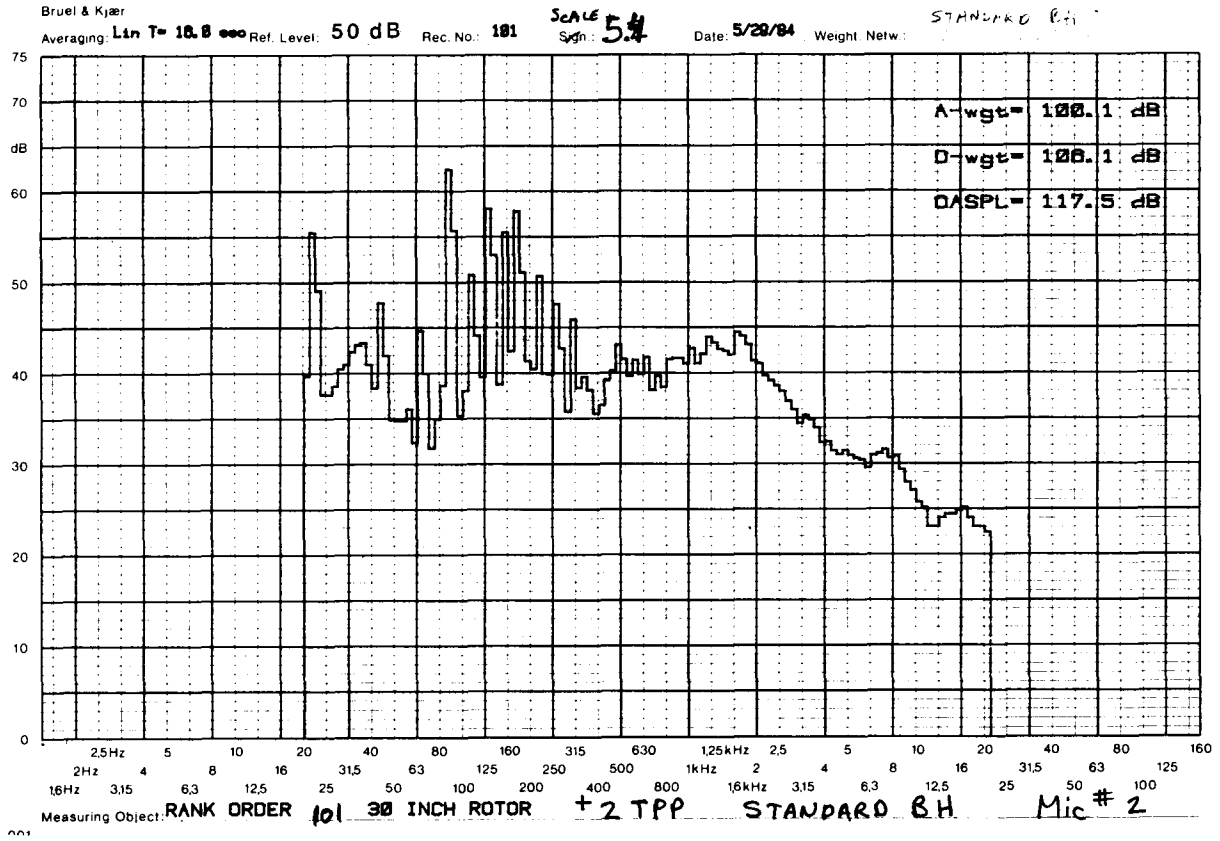

Figure C4. 1/12 Octave Spectra for the 1/20 Scale Baseline Configuration 1 at MIC 2, $M_{\Omega R} = 0.65$, $C_T = 0.007$, $\mu = 0.14$ and $\alpha_{TPP} = 2°$.

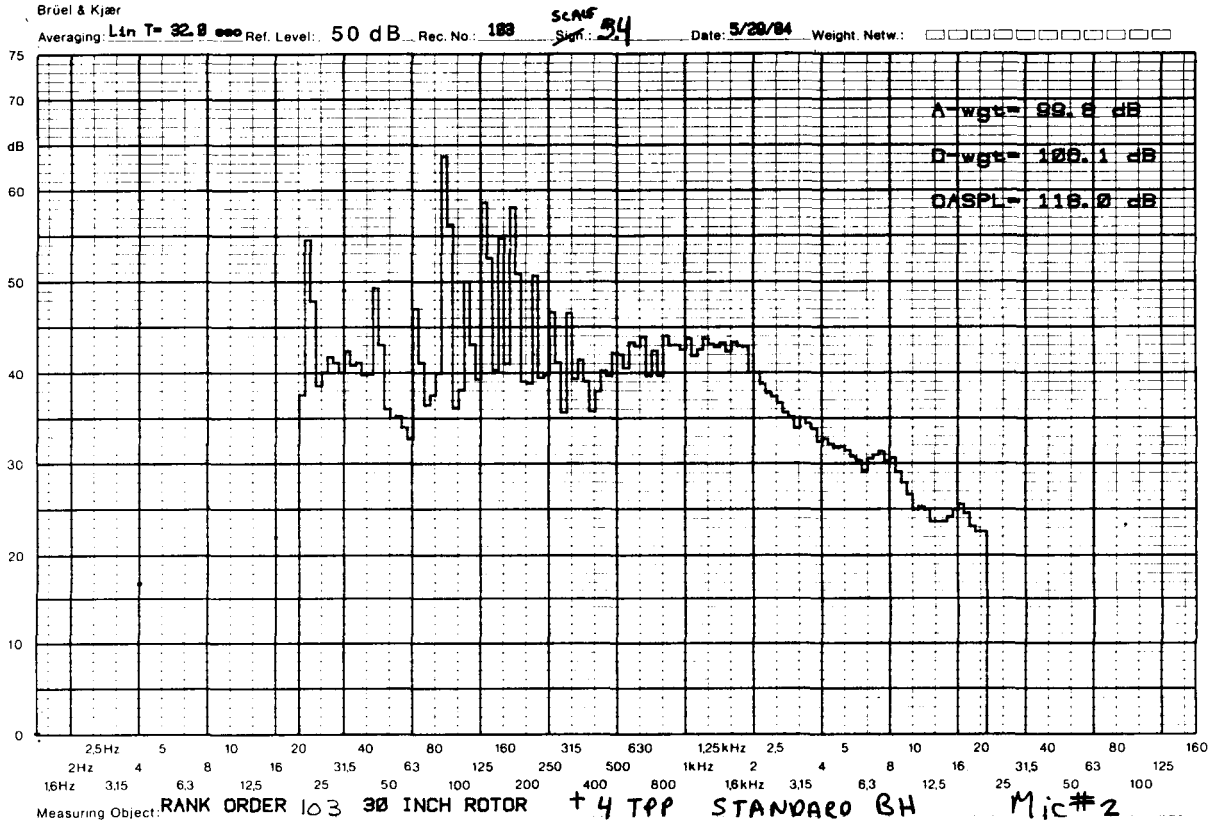

Figure C5. 1/12 Octave Spectra for the 1/20 Scale Baseline Configuration 1 at MIC 2, $M_{\Omega R}$ = 0.65, C_T = 0.007, μ = 0.14 and α_{TPP} = 4°.

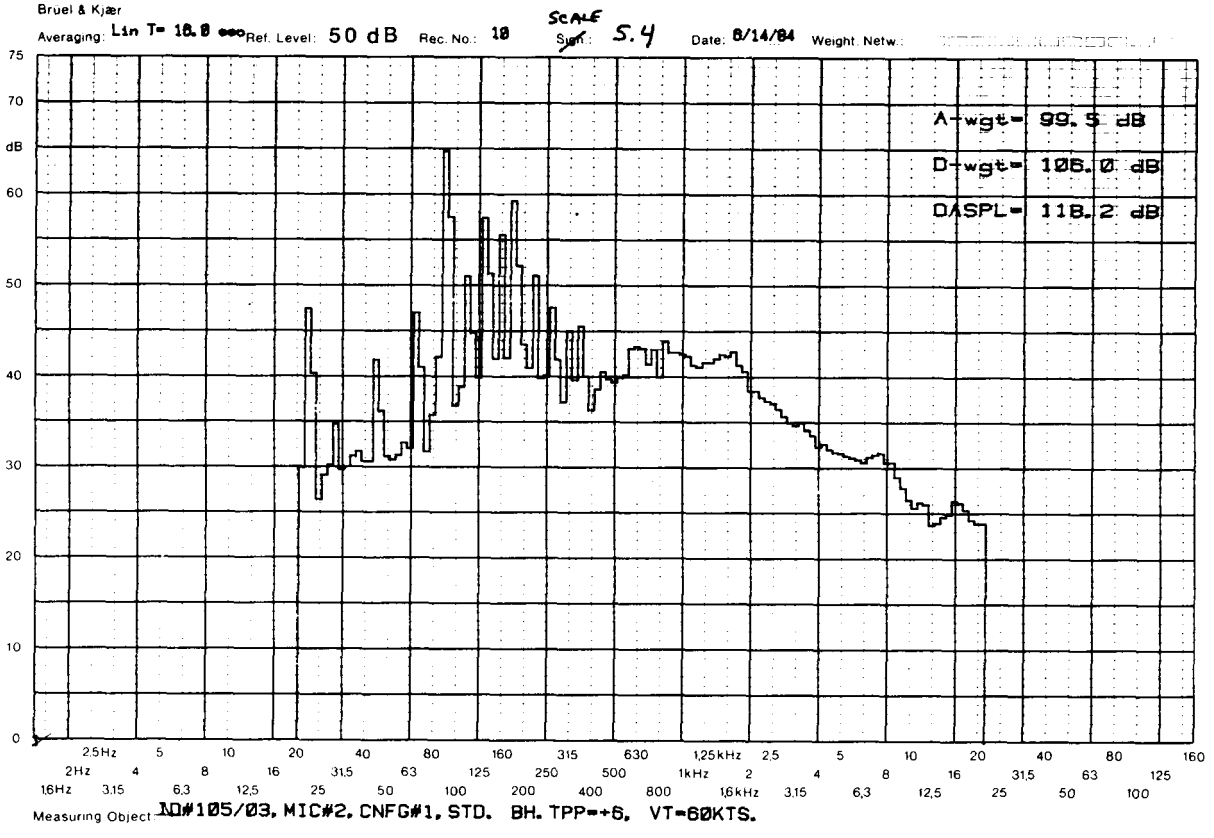

Figure C6. 1/12 Octave Spectra for the 1/20 Scale Baseline Configuration 1 at MIC 2, $M_{\Omega R} = 0.65$, $C_T = 0.007$, $\mu = 0.14$ and $\alpha_{TPP} = 6°$.

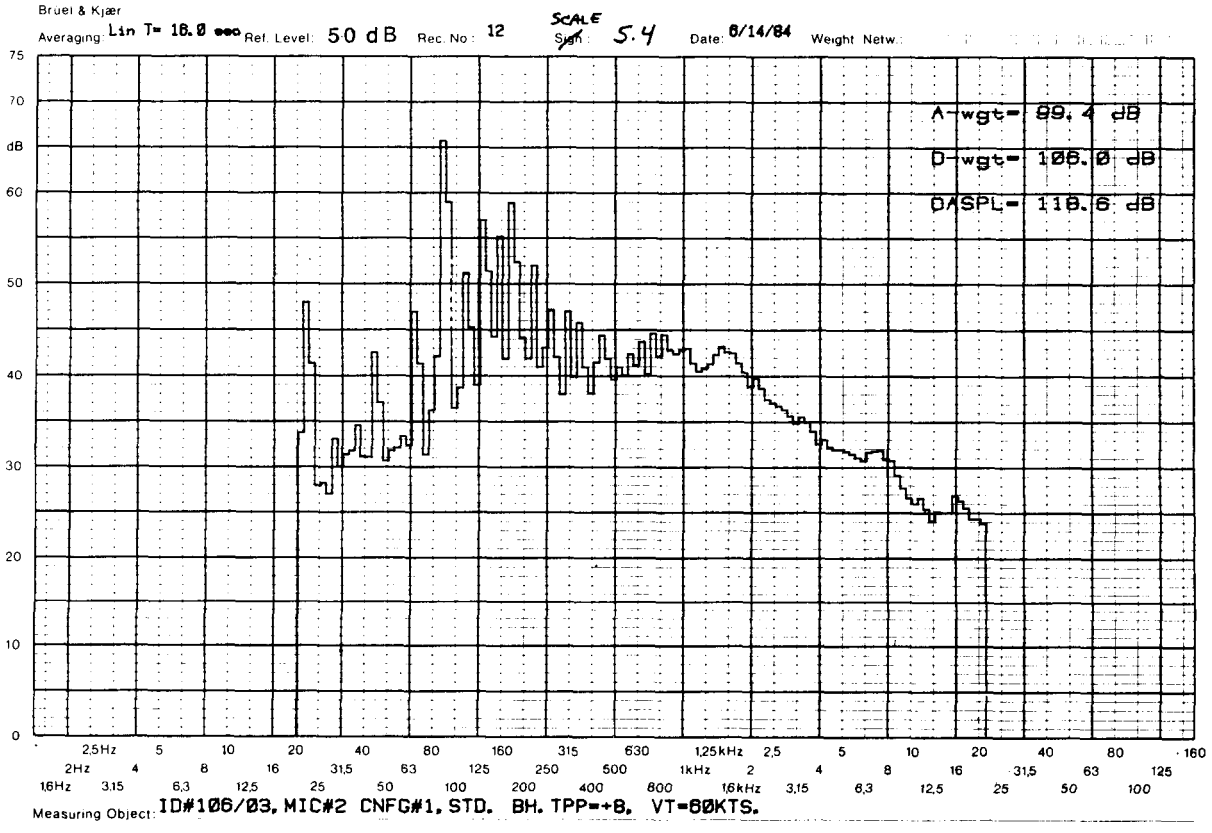

Figure C7. 1/12 Octave Spectra for the 1/20 Scale Baseline Configuration 1 at MIC 2, $M_{\Omega R} = 0.65$, $C_T = 0.007$, $\mu = 0.14$ and $\alpha_{TPP} = 8°$.

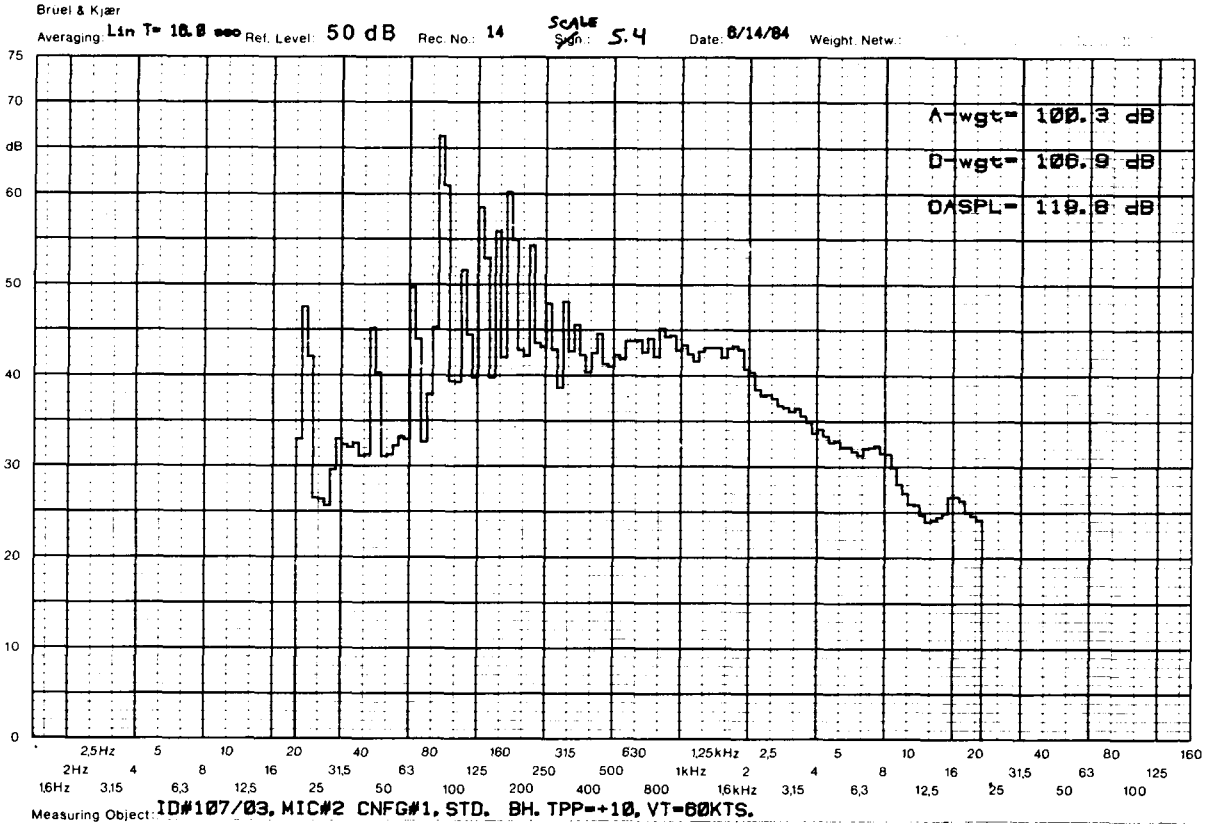

Figure C8. 1/12 Octave Spectra for the 1/20 Scale Baseline Configuration 1 at MIC 2, $M_{\Omega R}$ = 0.65, C_T = 0.007, μ = 0.14 and α_{TPP} = 10°.

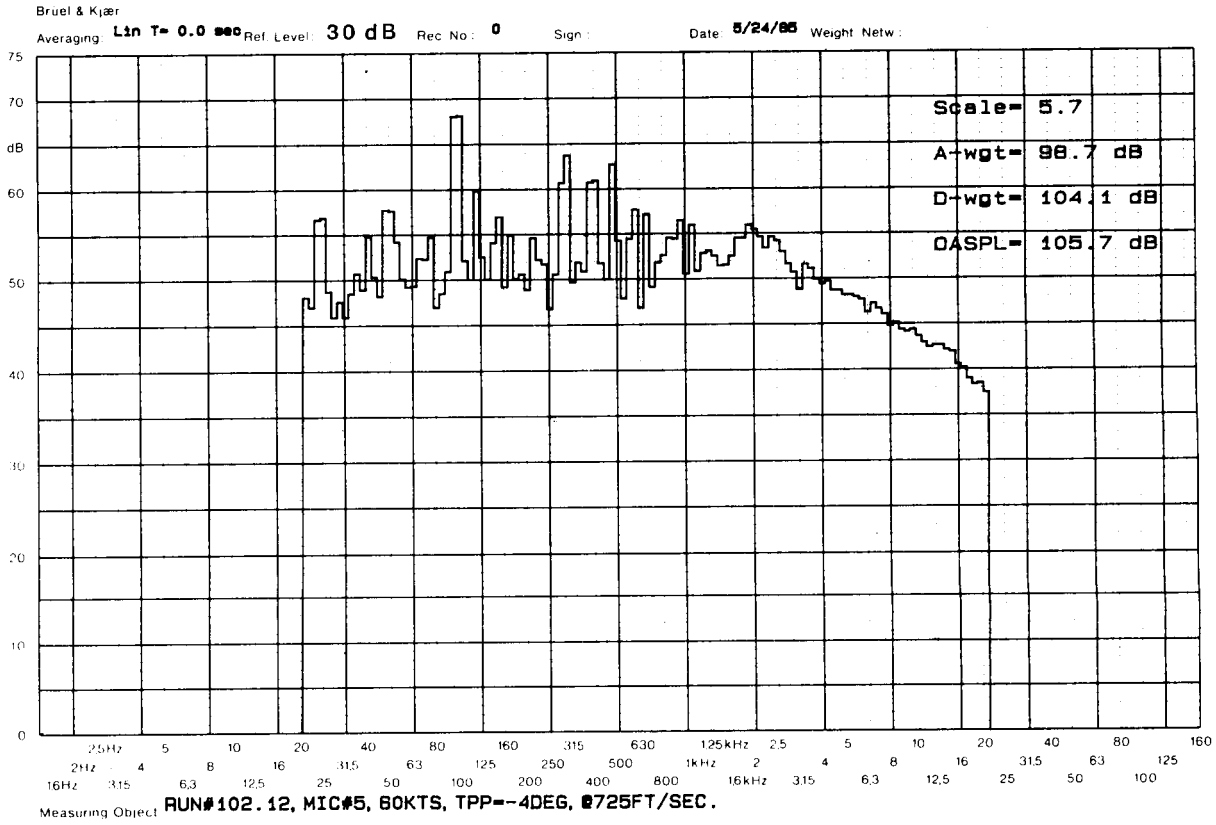

Figure C9. 1/12 Octave Spectra for the 1/5 Scale Baseline Configuration 1 at MIC 5, $M_{\Omega R}$ = 0.63, C_T = 0.007, μ = 0.14 and α_{TPP} = -4°.

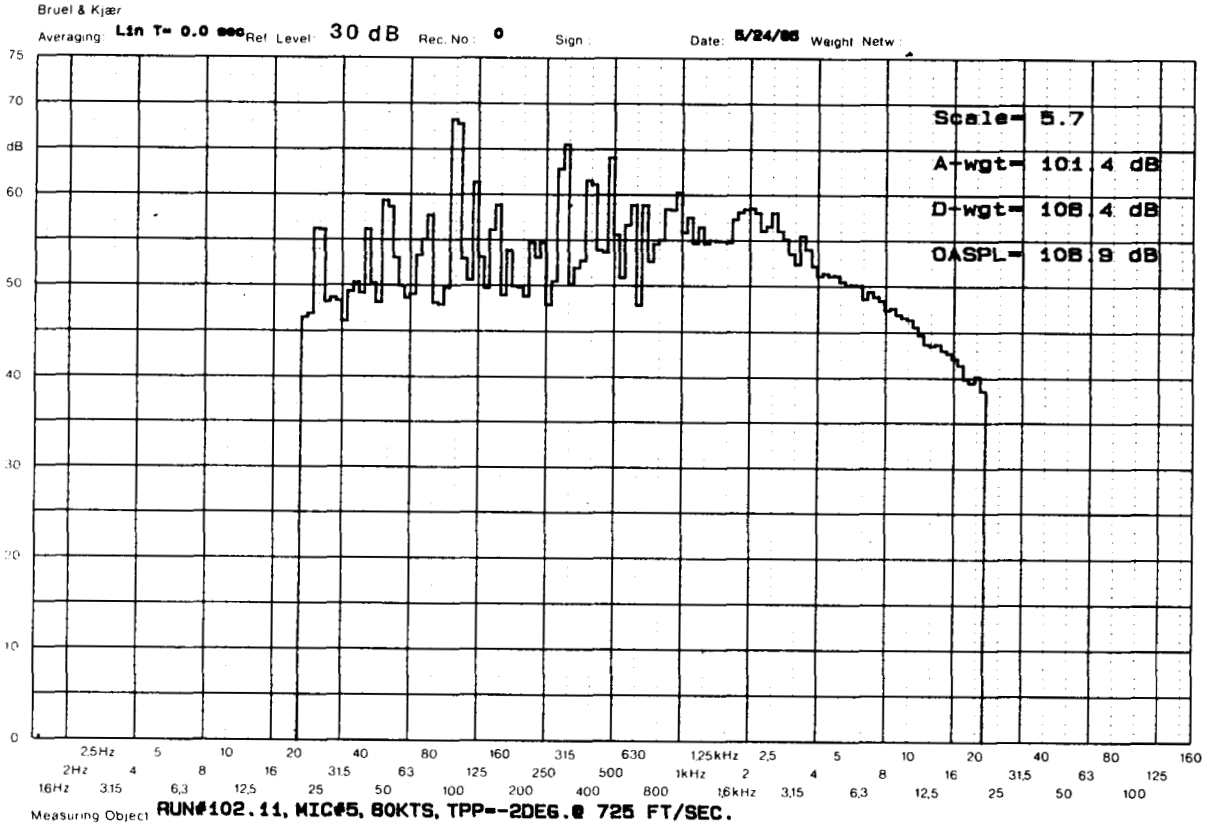

Figure C10. 1/12 Octave Spectra for the 1/5 Scale Baseline Configuration 1 at MIC 5, $M_{\Omega R} = 0.63$, $C_T = 0.007$, $\mu = 0.14$ and $\alpha_{TPP} = -2°$.

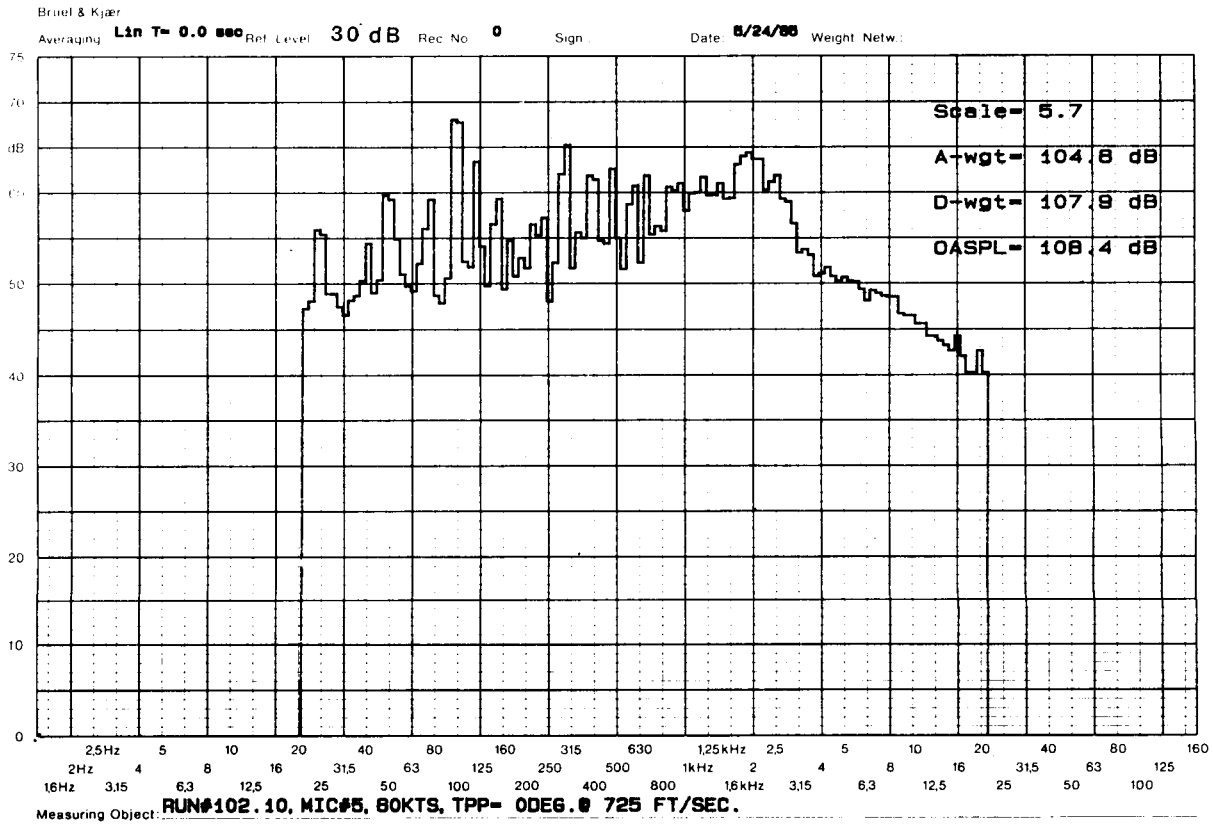

Figure C11. 1/12 Octave Spectra for the 1/5 Scale Baseline Configuration 1 at MIC 5, $M_{\Omega R}$ = 0.63, C_T = 0.007, μ = 0.14 and α_{TPP} = 0°.

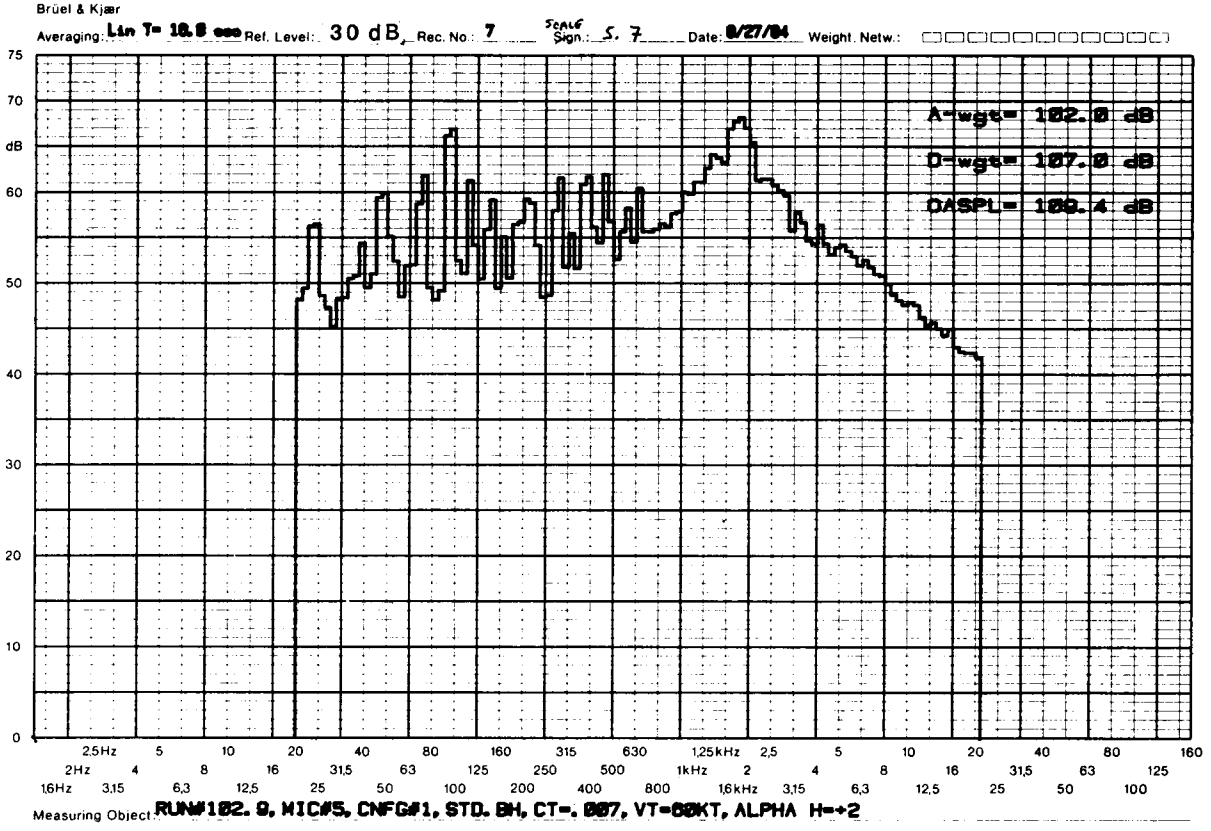

Figure C12. 1/12 Octave Spectra for the 1/5 Scale Baseline Configuration 1 at MIC 5, $M_{\Omega R} = 0.63$, $C_T = 0.007$, $\mu = 0.14$ and $\alpha_{TPP} = 2°$.

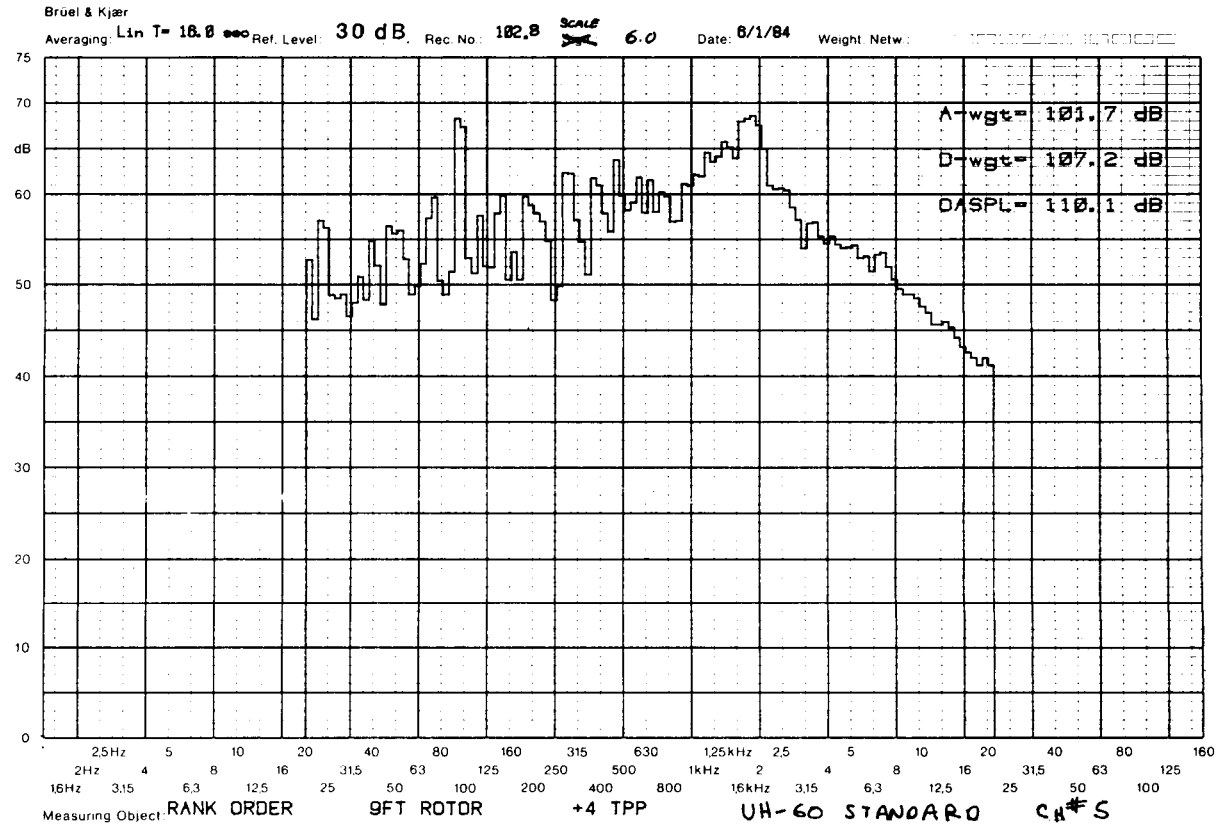

Figure C13. 1/12 Octave Spectra for the 1/5 Scale Baseline Configuration 1 at MIC 5, $M_{\Omega R} = 0.63$, $C_T = 0.007$, $\mu = 0.14$ and $\alpha_{TPP} = 4°$.

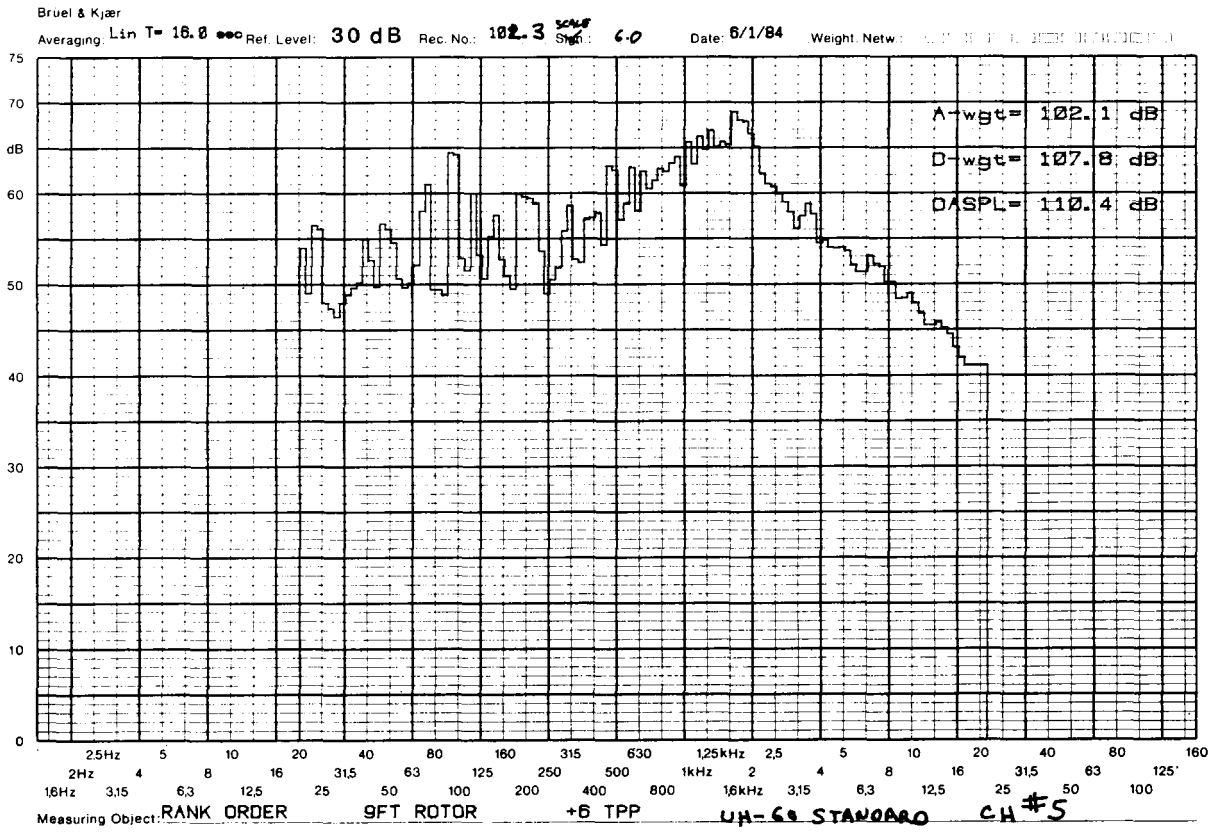

Figure C14. 1/12 Octave Spectra for the 1/5 Scale Baseline Configuration 1 at MIC 5, $M_{\Omega R} = 0.63$, $C_T = 0.007$, $\mu = 0.14$ and $\alpha_{TPP} = 6°$.

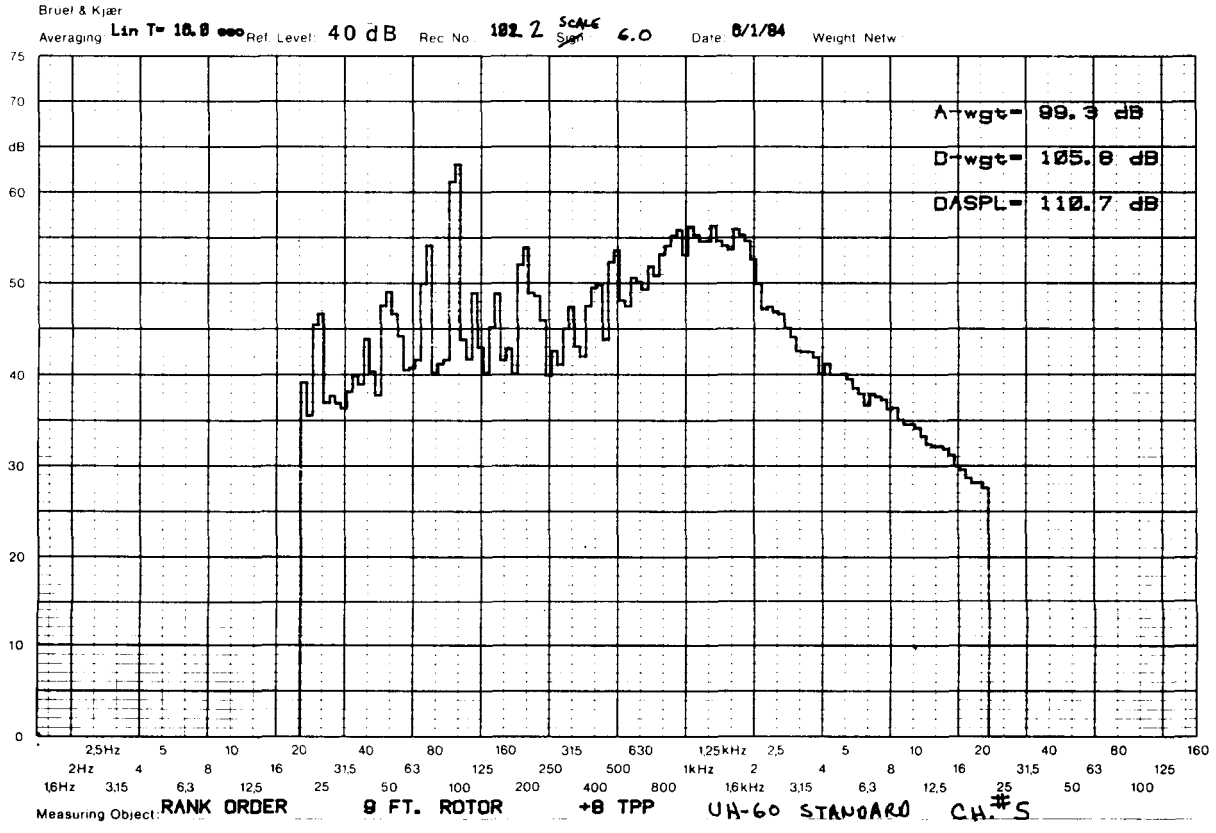

Figure C15. 1/12 Octave Spectra for the 1/5 Scale Baseline Configuration 1 at MIC 5, $M_{\Omega R} = 0.63$, $C_T = 0.007$, $\mu = 0.14$ and $\alpha_{TPP} = 8°$.

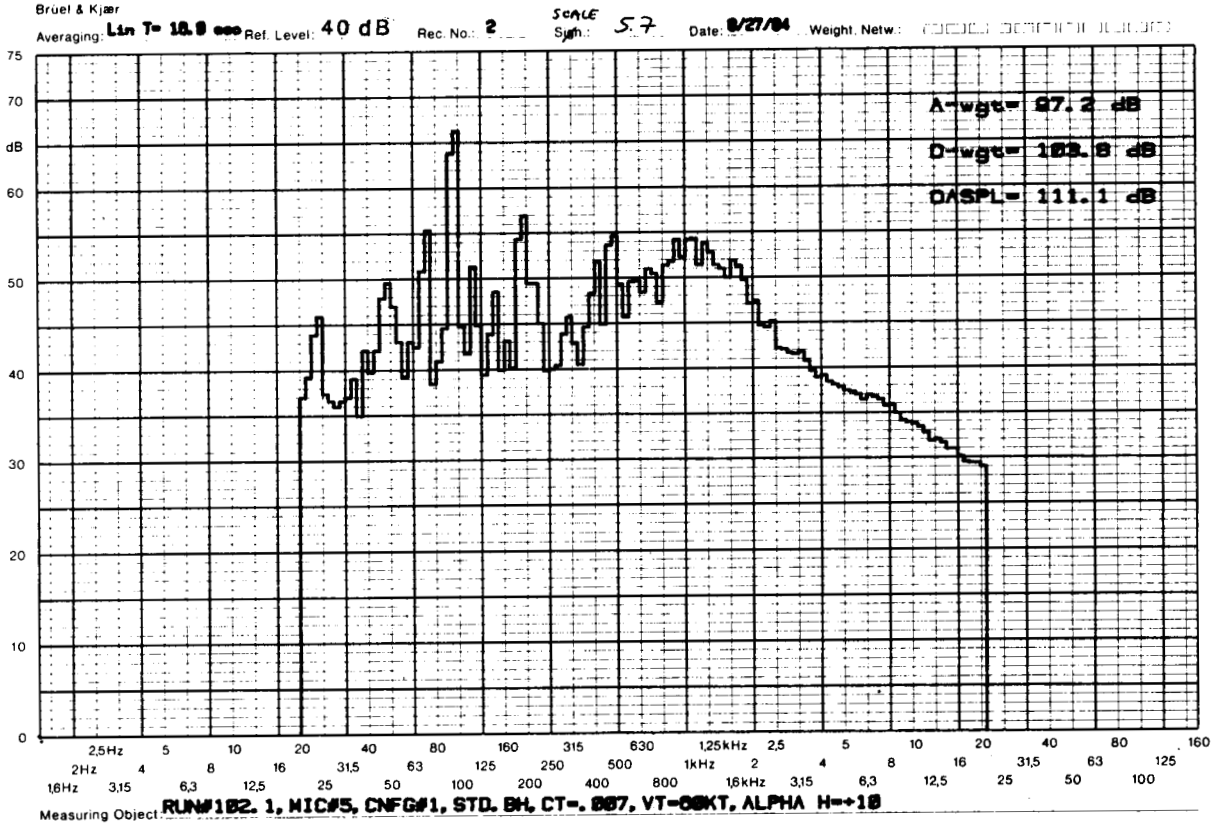

Figure C16. 1/12 Octave Spectra for the 1/5 Scale Baseline Configuration 1 at MIC 5, $M_{\Omega R}$ = 0.63, C_T = 0.007, μ = 0.14 and α_{TPP} = 10°.

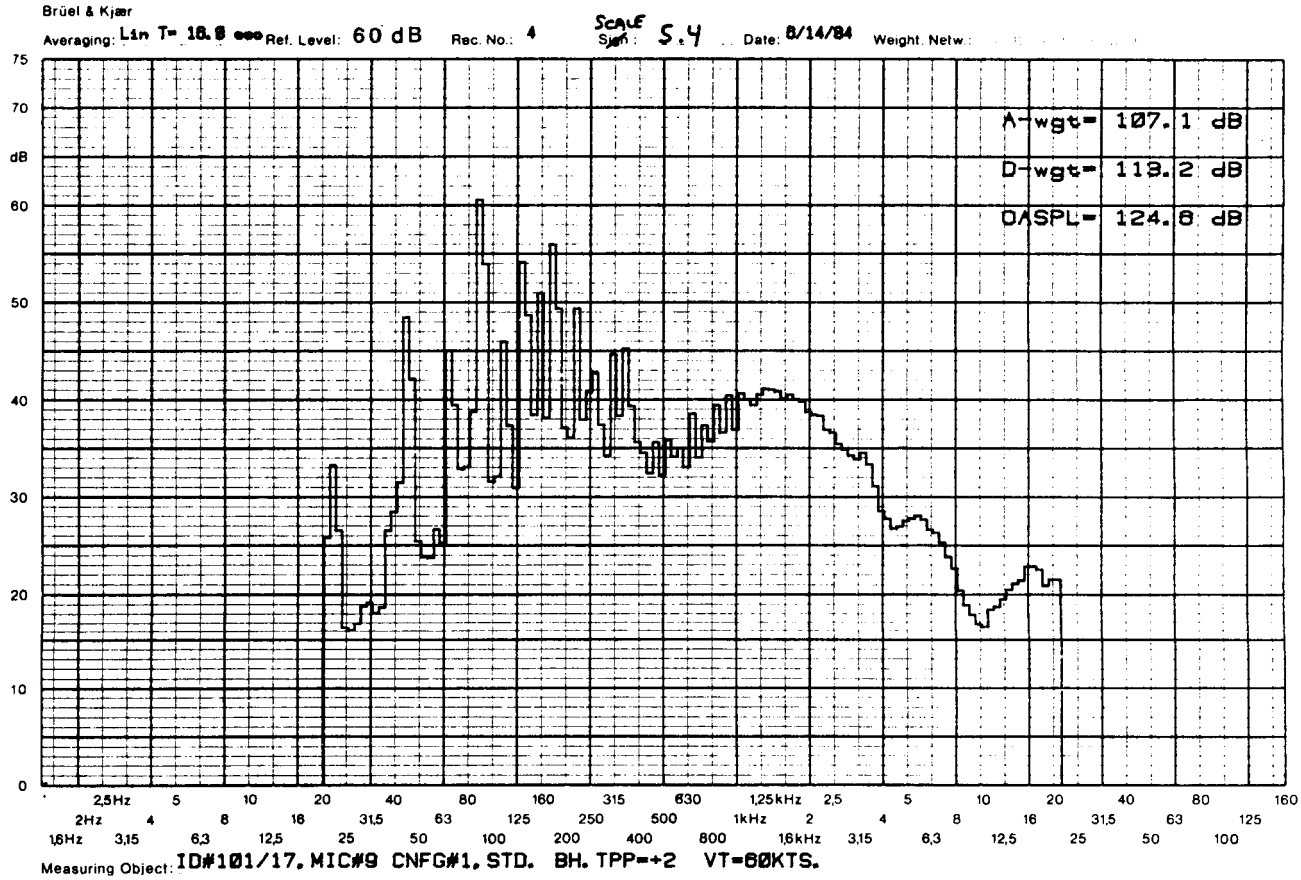

Figure C17. 1/12 Octave Spectra for the 1/20 Scale Baseline Configuration 1 at MIC 9, $M_{\Omega R}$ = 0.65, C_T = 0.007, μ = 0.14 and α_{TPP} = 2°.

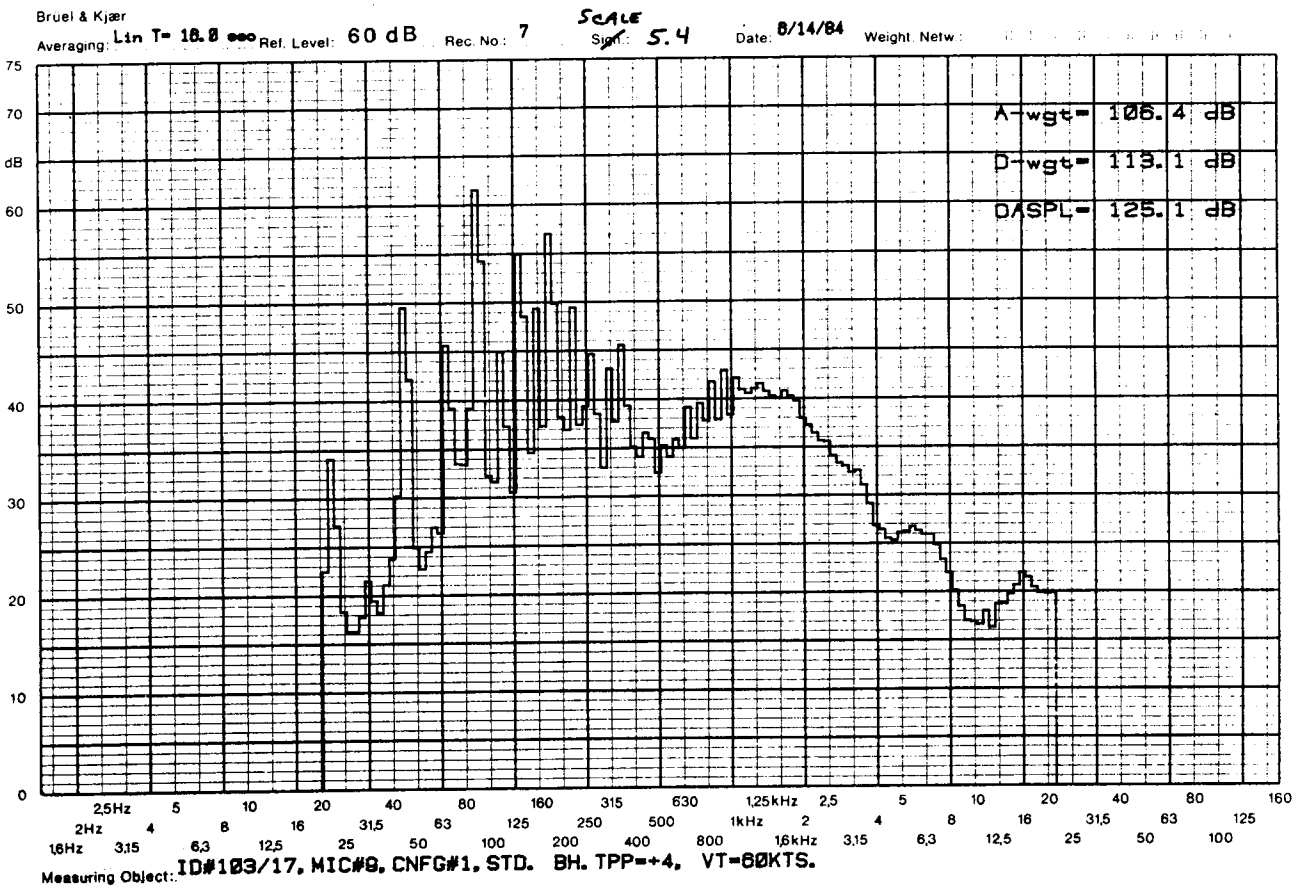

Figure C18. 1/12 Octave Spectra for the 1/20 Scale Baseline Configuration 1 at MIC 9, $M_{\Omega R}$ = 0.65, C_T = 0.007, μ = 0.14 and α_{TPP} = 4°.

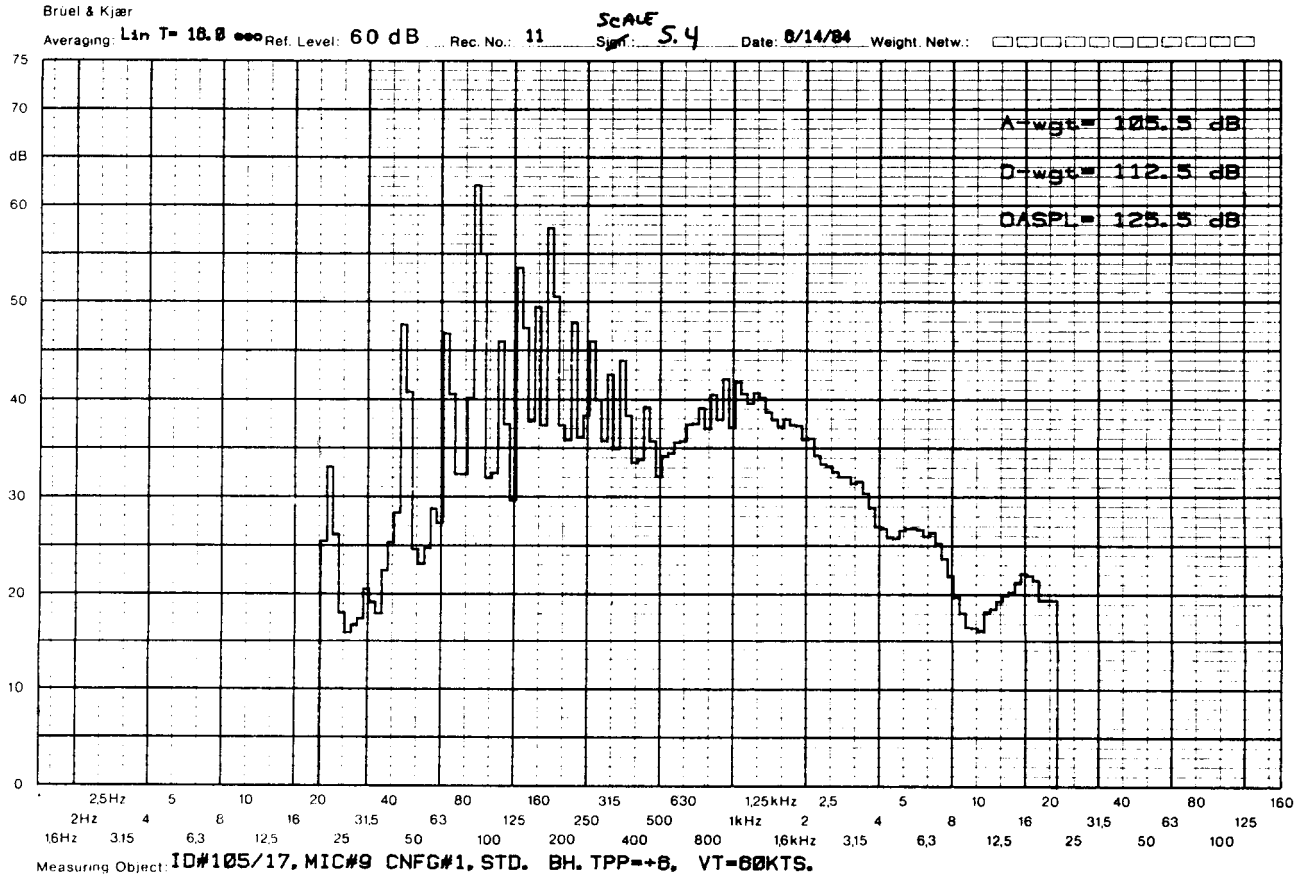

Figure C19. 1/12 Octave Spectra for the 1/20 Scale Baseline Configuration 1 at MIC 9, $M_{\Omega R} = 0.65$, $C_T = 0.007$, $\mu = 0.14$ and $\alpha_{TPP} = 6°$.

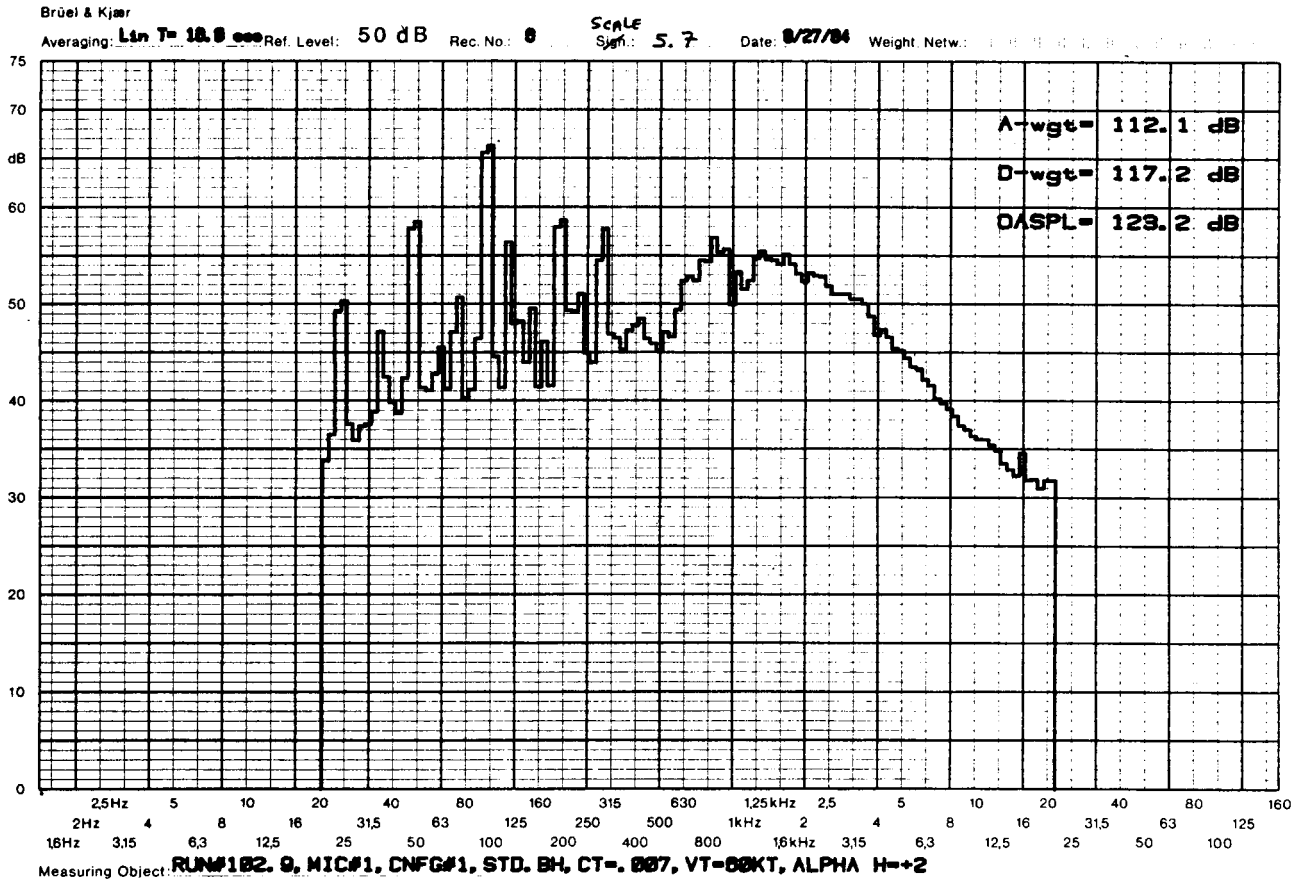

Figure C20 1/12 Octave Spectra for the 1/5 Scale Baseline Configuration 1 at MIC 1, $M_{\Omega R} = 0.63$, $C_T = 0.007$, $\mu = 0.14$ and $\alpha_{TPP} = 2°$.

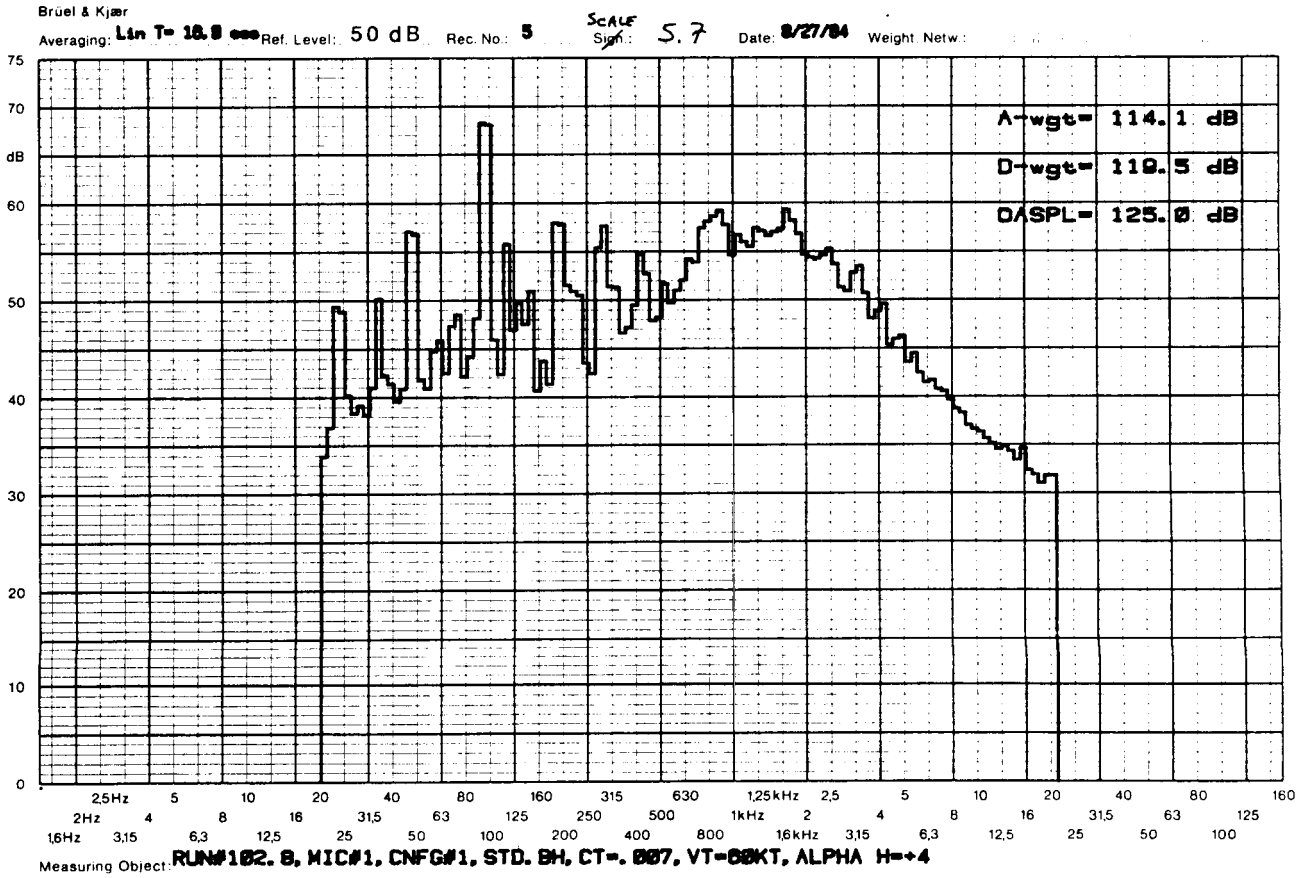

Figure C21. 1/12 Octave Spectra for the 1/5 Scale Baseline Configuration 1 at MIC 1, $M_{\Omega R}$ = 0.63, C_T = 0.007, μ = 0.14 and α_{TPP} = 4°.

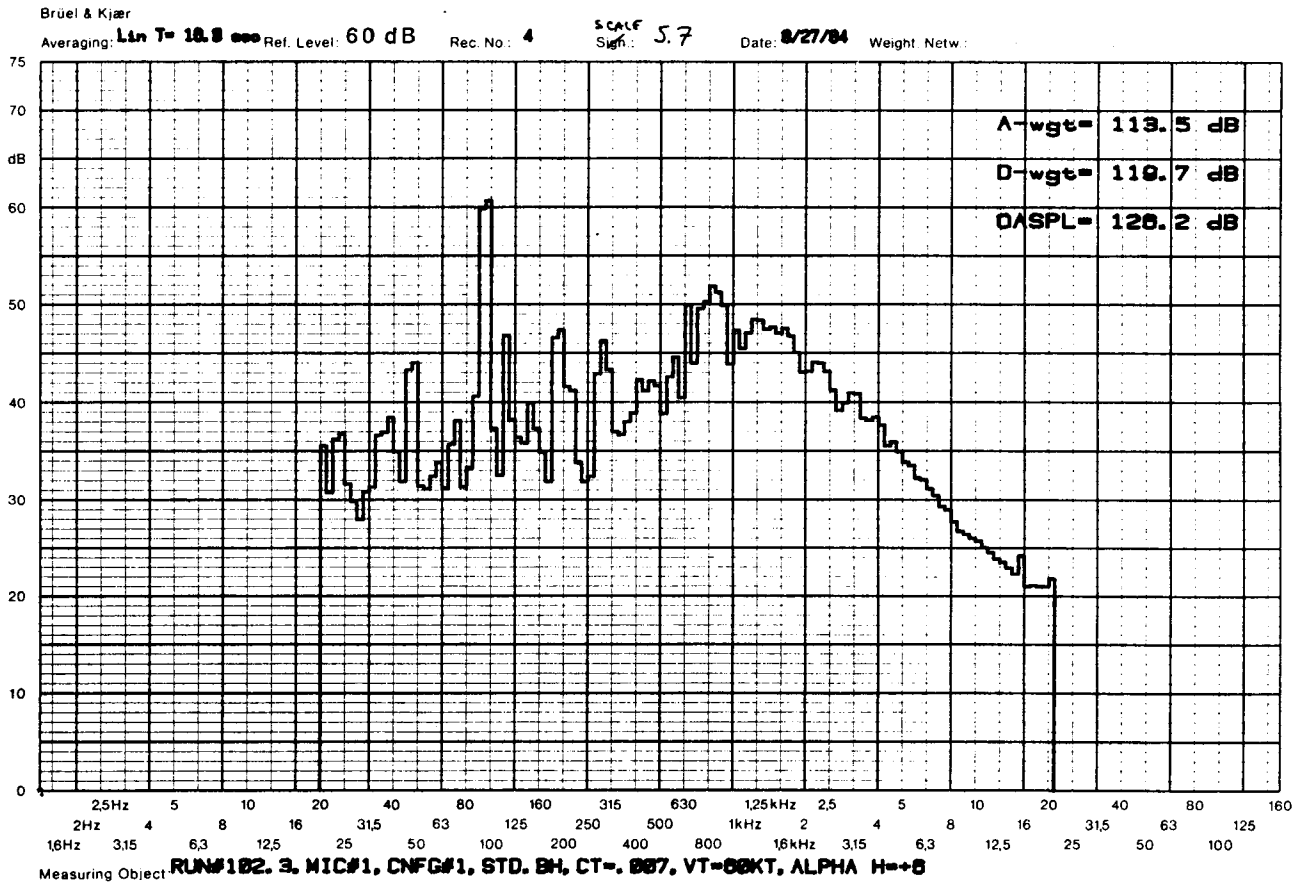

Figure C22. 1/12 Octave Spectra for the 1/5 Scale Baseline Configuration 1 at MIC 1, $M_{\Omega R} = 0.63$, $C_T = 0.007$, $\mu = 0.14$ and $\alpha_{TPP} = 6°$.

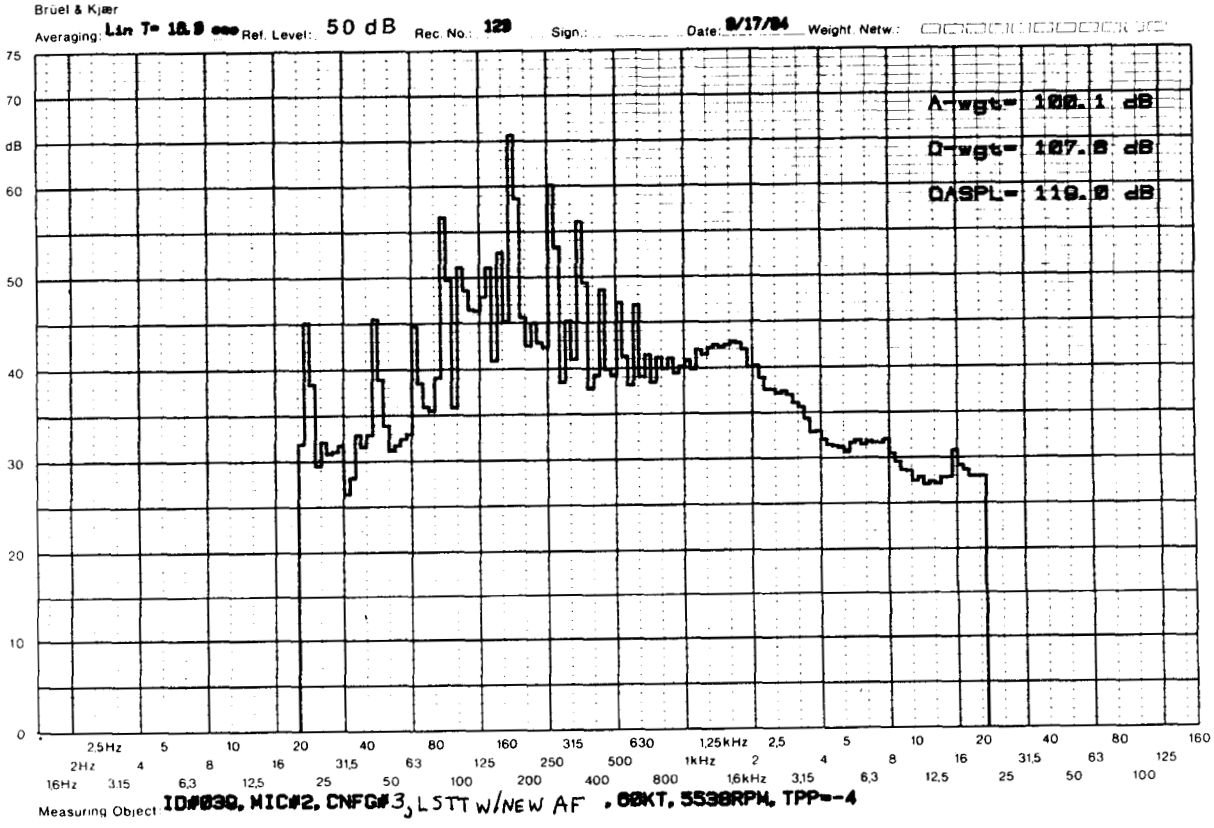

Figure C23. 1/12 Octave Spectra for the 1/20 Scale Large Swept Tapered Tip Configuration 3 with New Airfoils at Microphone 2, $M_{\Omega R} = 0.65$, $C_T = 0.007$, $\mu = 0.14$ and $\alpha_{TPP} = -4°$.

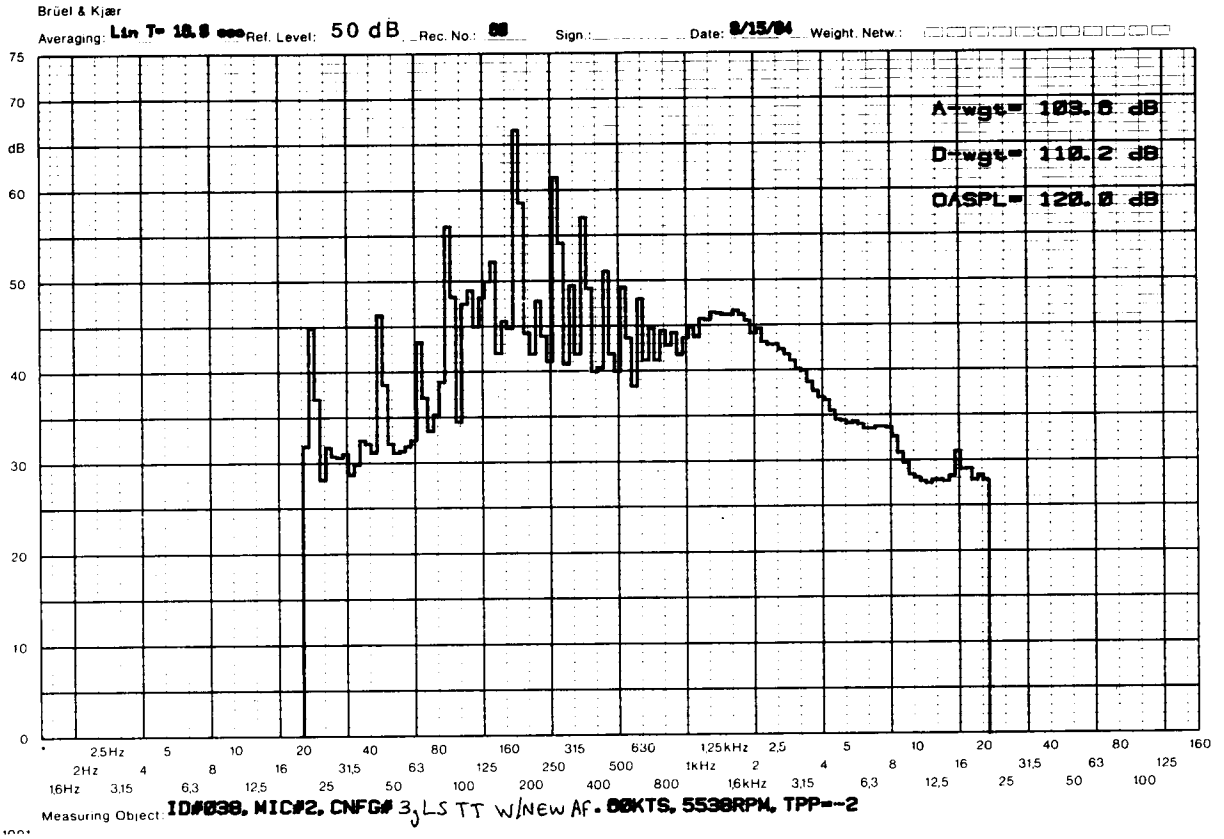

Figure C24. 1/12 Octave Spectra for the 1/20 Scale Large Swept Tapered Tip Configuration 3 with New Airfoils at Microphone 2, $M_{\Omega R} = 0.65$, $C_T = 0.007$, $\mu = 0.14$ and $\alpha_{TPP} = -2°$.

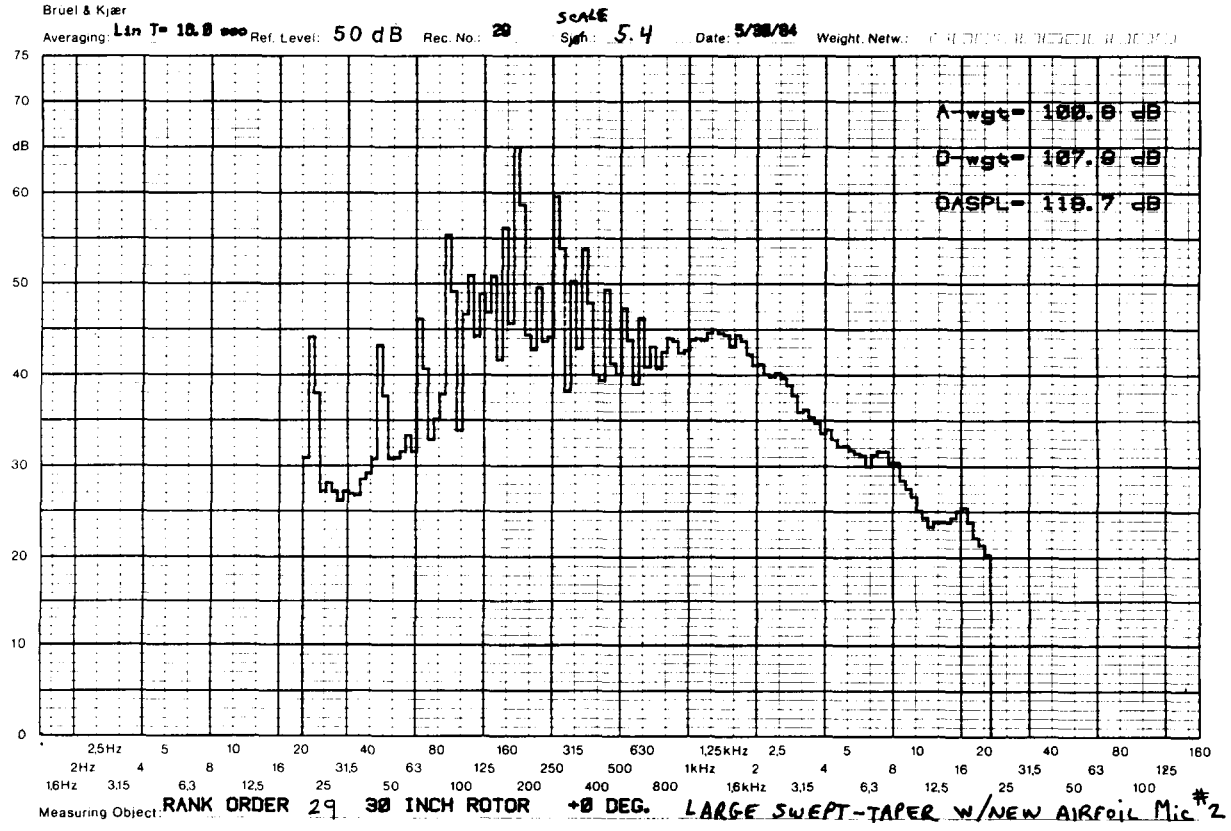

Figure C25. 1/12 Octave Spectra for the 1/20 Scale Large Swept Tapered Tip configuration 3 with New Airfoils at Microphone 2, $M_{\Omega R} = 0.65$, $C_T = 0.007$, $\mu = 0.14$ and $\alpha_{TPP} = 0°$.

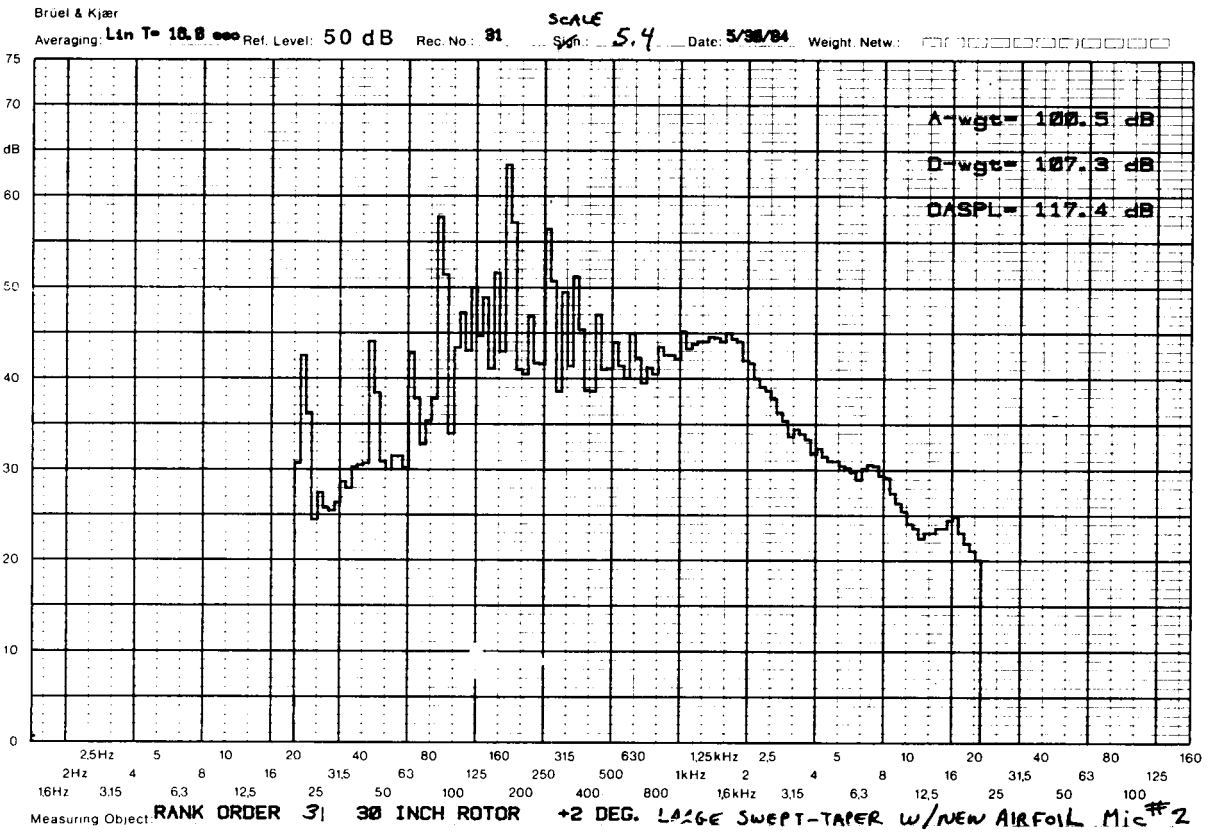

Figure C26. 1/12 Octave Spectra for the 1/20 Scale Large Swept Tapered Tip configuration 3 with New Airfoils at Microphone 2, $M_{\Omega R} = 0.65$, $C_T = 0.007$, $\mu = 0.14$ and $\alpha_{TPP} = 2°$.

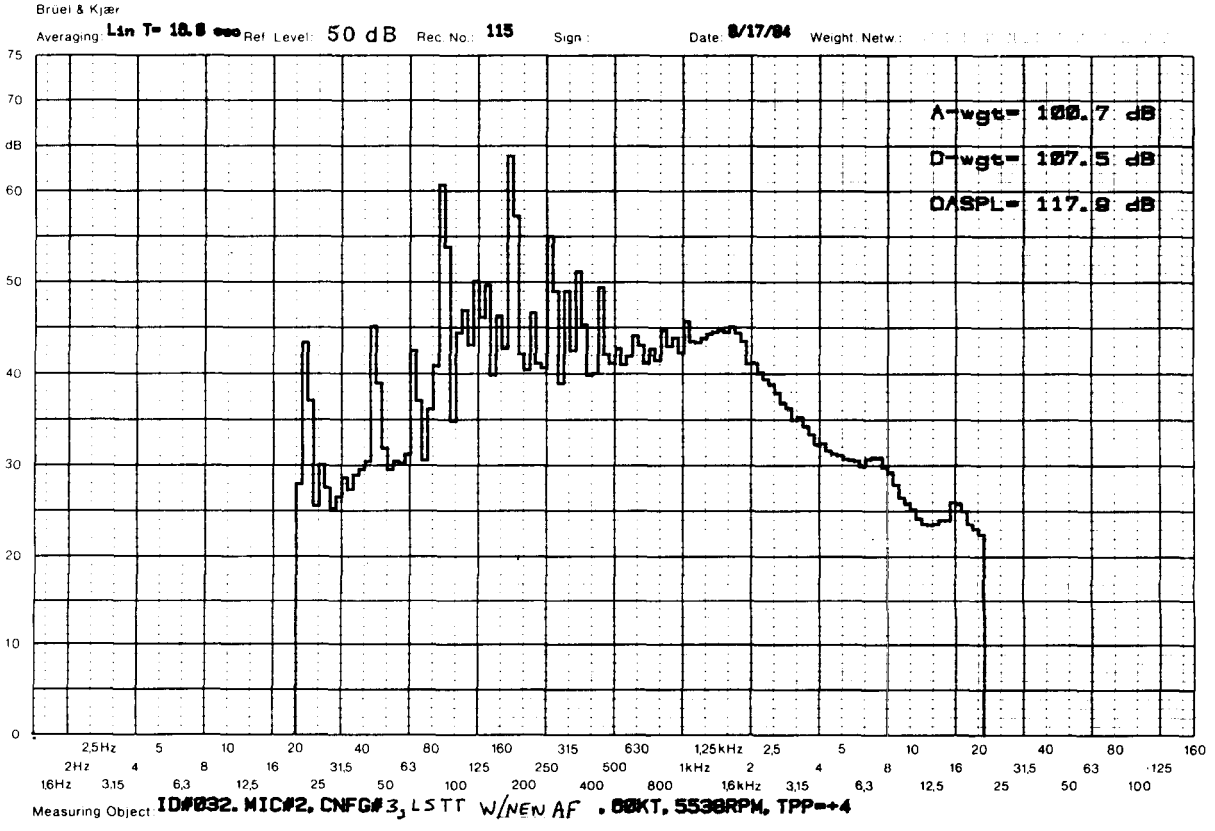

Figure C27. 1/12 Octave Spectra for the 1/20 Scale Large Swept Tapered Tip configuration 3 with New Airfoils at Microphone 2, $M_{\Omega R} = 0.65$, $C_T = 0.007$, $\mu = 0.14$ and $\alpha_{TPP} = 4°$.

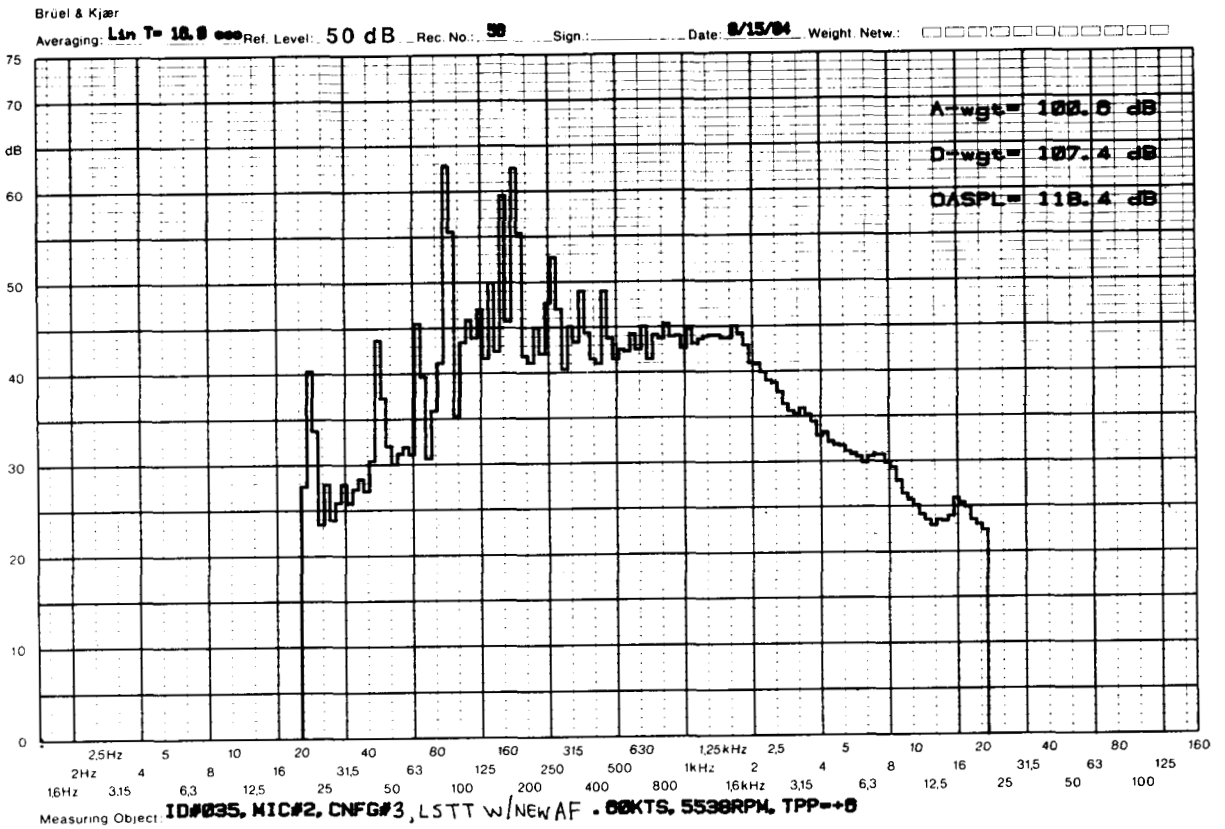

Figure C28. 1/12 Octave Spectra for the 1/20 Scale Large Swept Tapered Tip configuration 3 with New Airfoils at Microphone 2, $M_{\Omega R} = 0.65$, $C_T = 0.007$, $\mu = 0.14$ and $\alpha_{TPP} = 6°$.

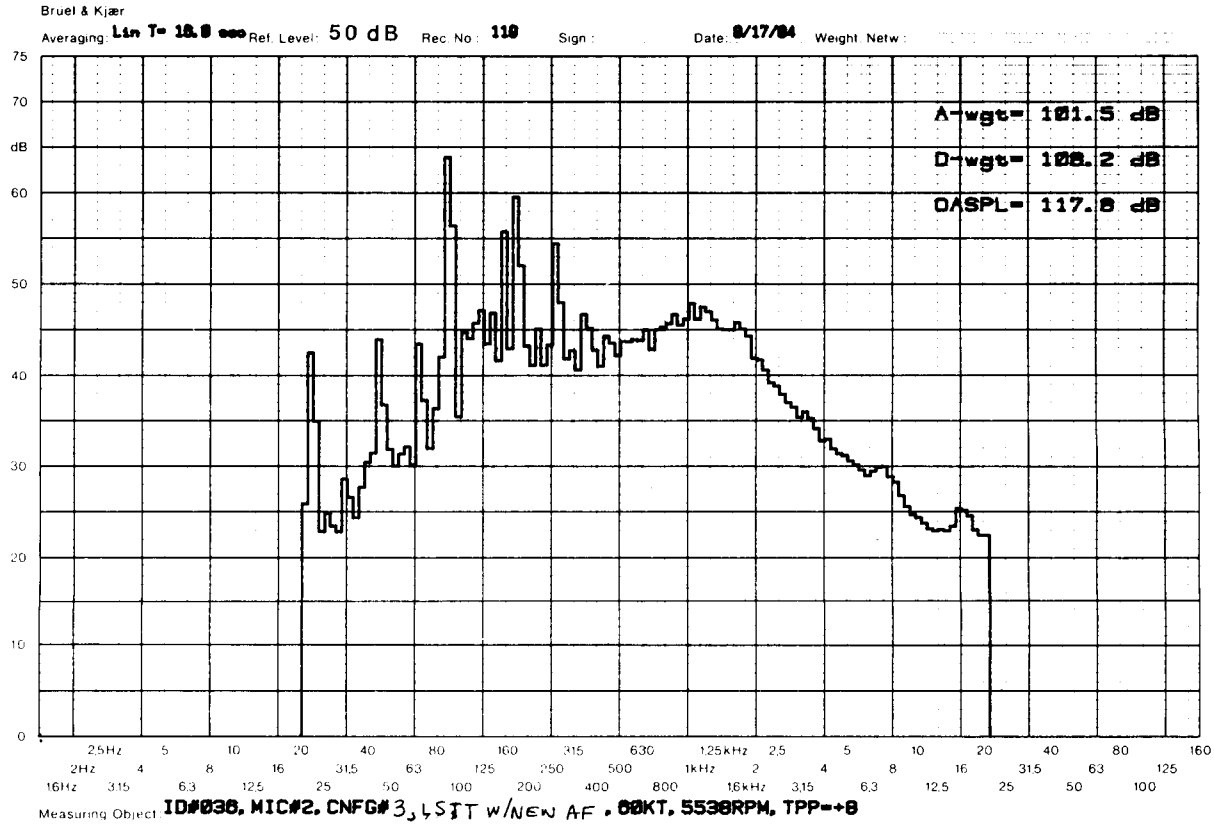

Figure C29. 1/12 Octave Spectra for the 1/20 Scale Large Swept Tapered Tip configuration 3 with New Airfoils at Microphone 2, $M_{\Omega R} = 0.65$, $C_T = 0.007$, $\mu = 0.14$ and $\alpha_{TPP} = 8°$.

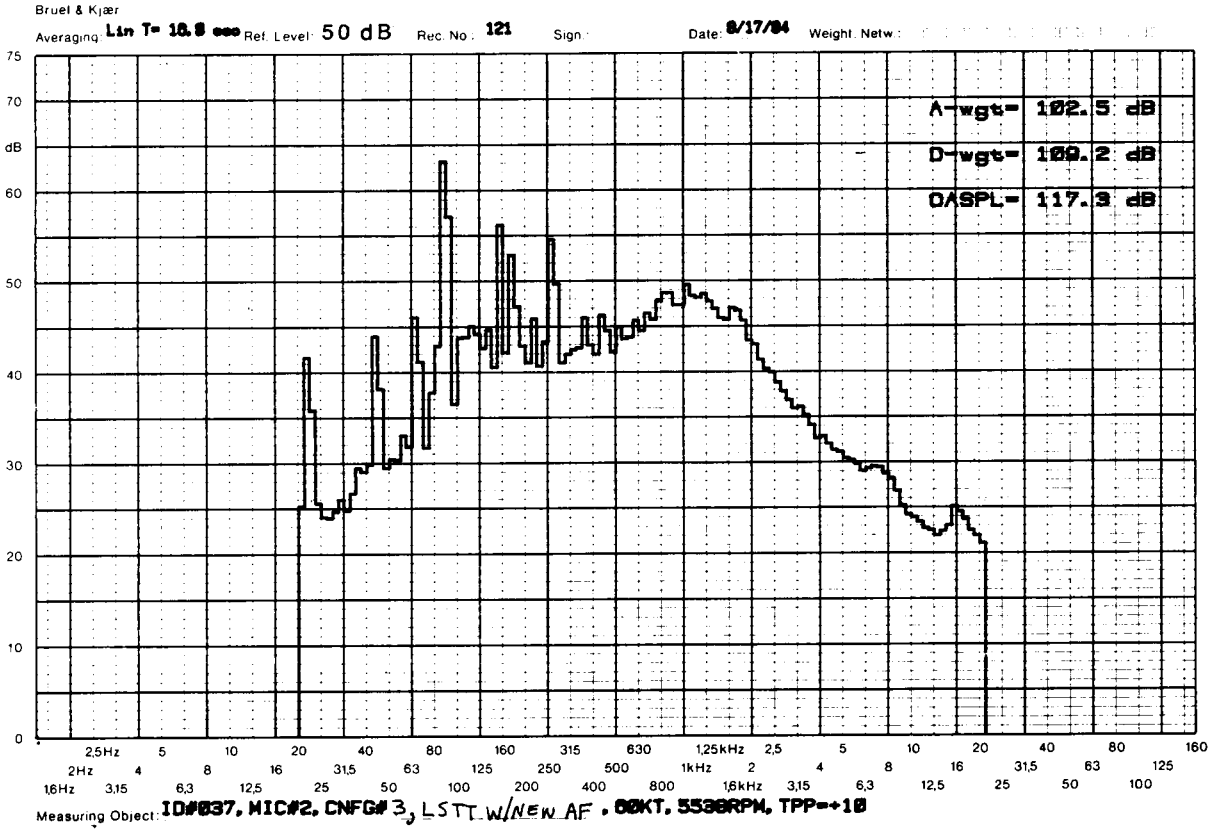

Figure 30. 1/12 Octave Spectra for the 1/20 Scale Large Swept Tapered Tip configuration 3 with New Airfoils at Microphone 2, $M_{\Omega R} = 0.65$, $C_T = 0.007$, $\mu = 0.14$ and $\alpha_{TPP} = 10°$.

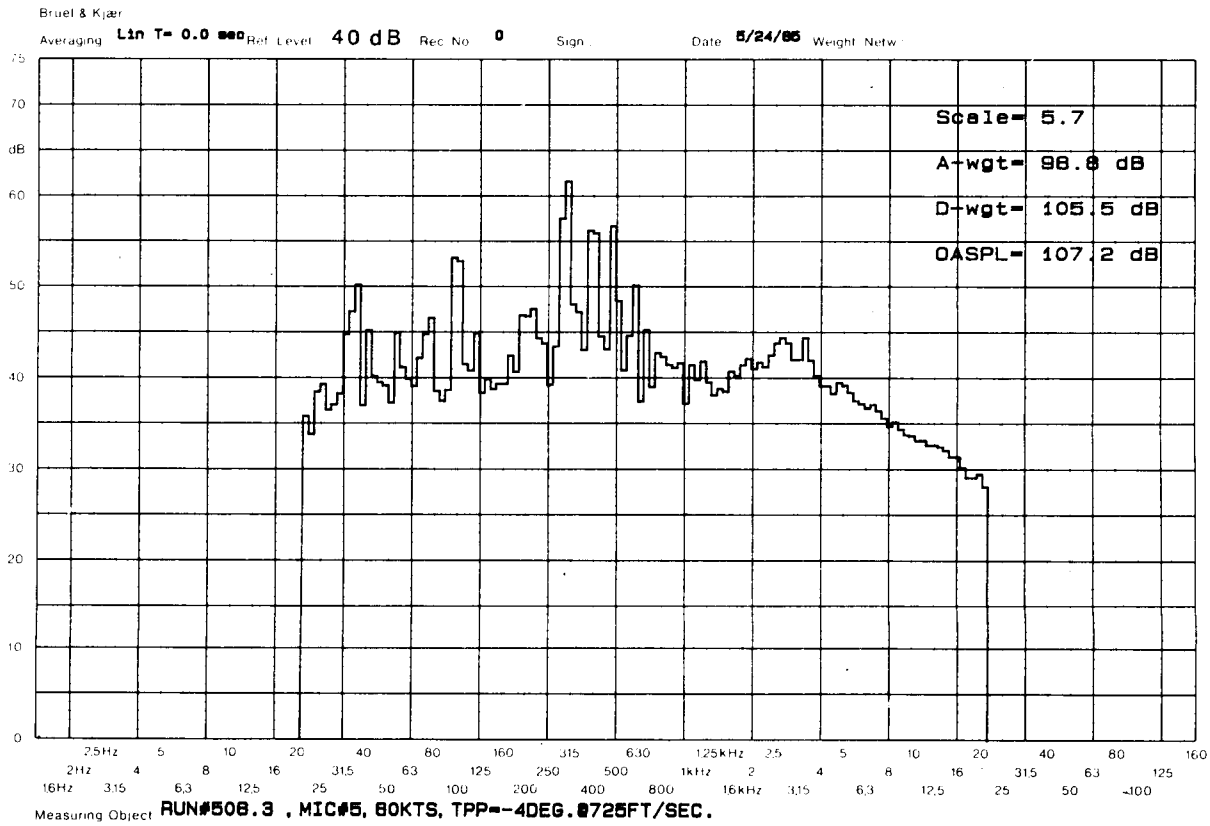

Figure C31. 1/12 Octave Spectra for the 1/5 Scale Large Swept Tapered Tip configuration 3 with New Airfoils at Microphone 5, $M_{\Omega R} = 0.63$, $C_T = 0.007$, $\mu = 0.14$ and $\alpha_{TPP} = -4°$.

ORIGINAL PAGE IS
OF POOR QUALITY

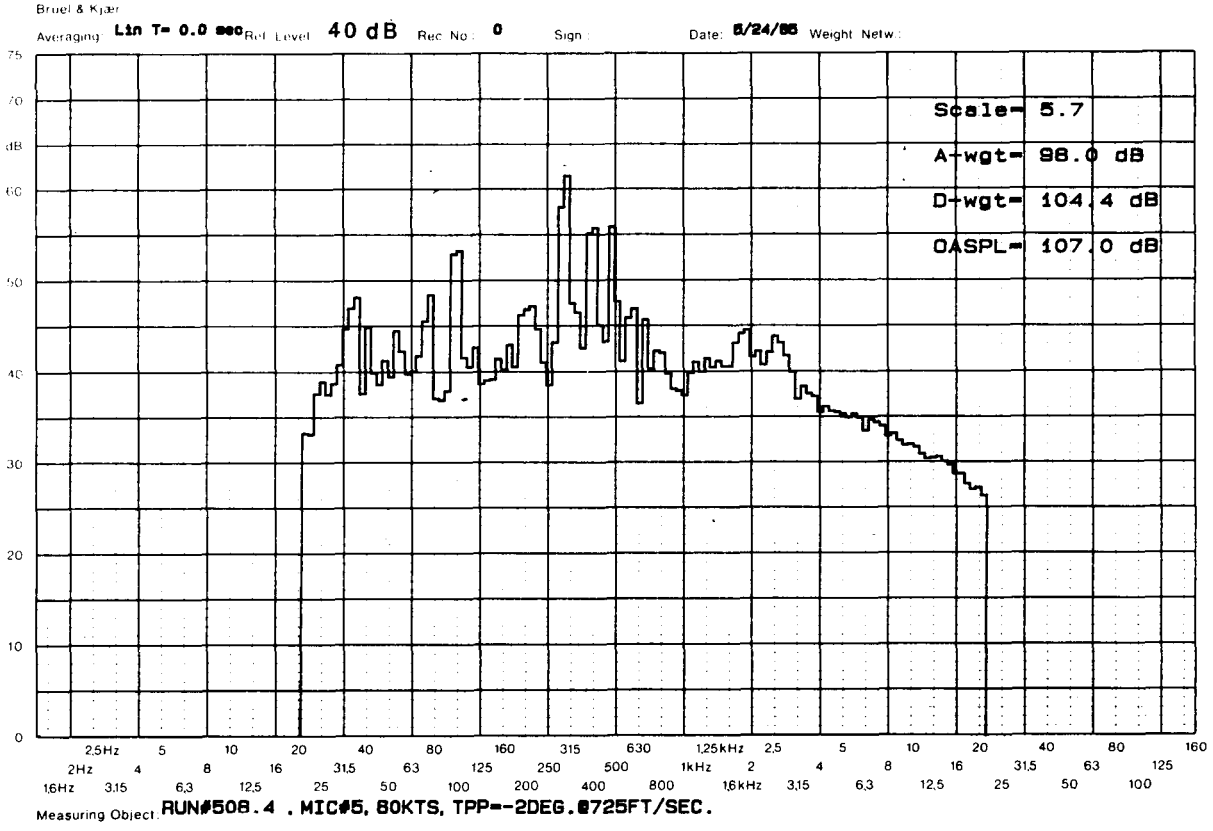

Figure C32. 1/12 Octave Spectra for the 1/5 Scale Large Swept Tapered Tip configuration 3 with New Airfoils at Microphone 5, $M_{\Omega R} = 0.63$, $C_T = 0.007$, $\mu = 0.14$ and $\alpha_{TPP} = -2°$.

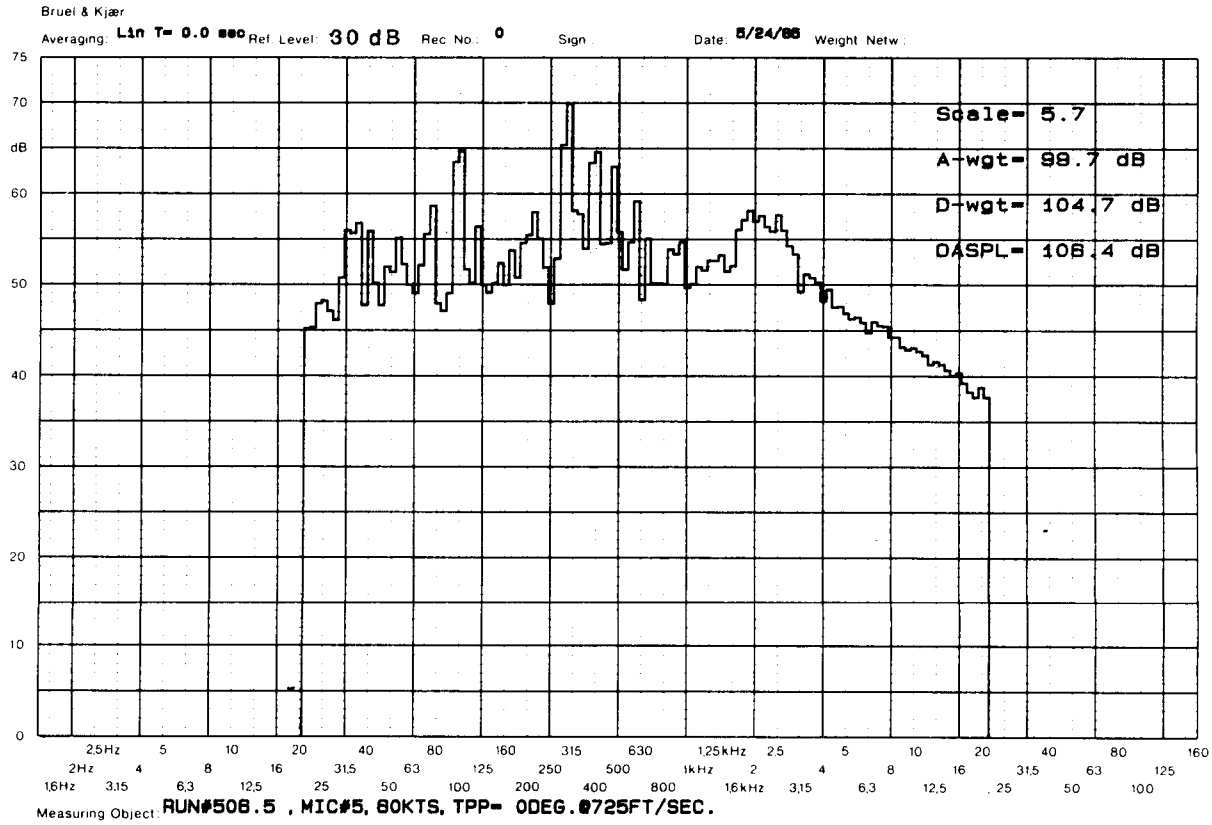

Figure C33. 1/12 Octave Spectra for the 1/5 Scale Large Swept Tapered Tip configuration 3 with New Airfoils at Microphone 5, $M_{\Omega R} = 0.63$, $C_T = 0.007$, $\mu = 0.14$ and $\alpha_{TPP} = 0°$.

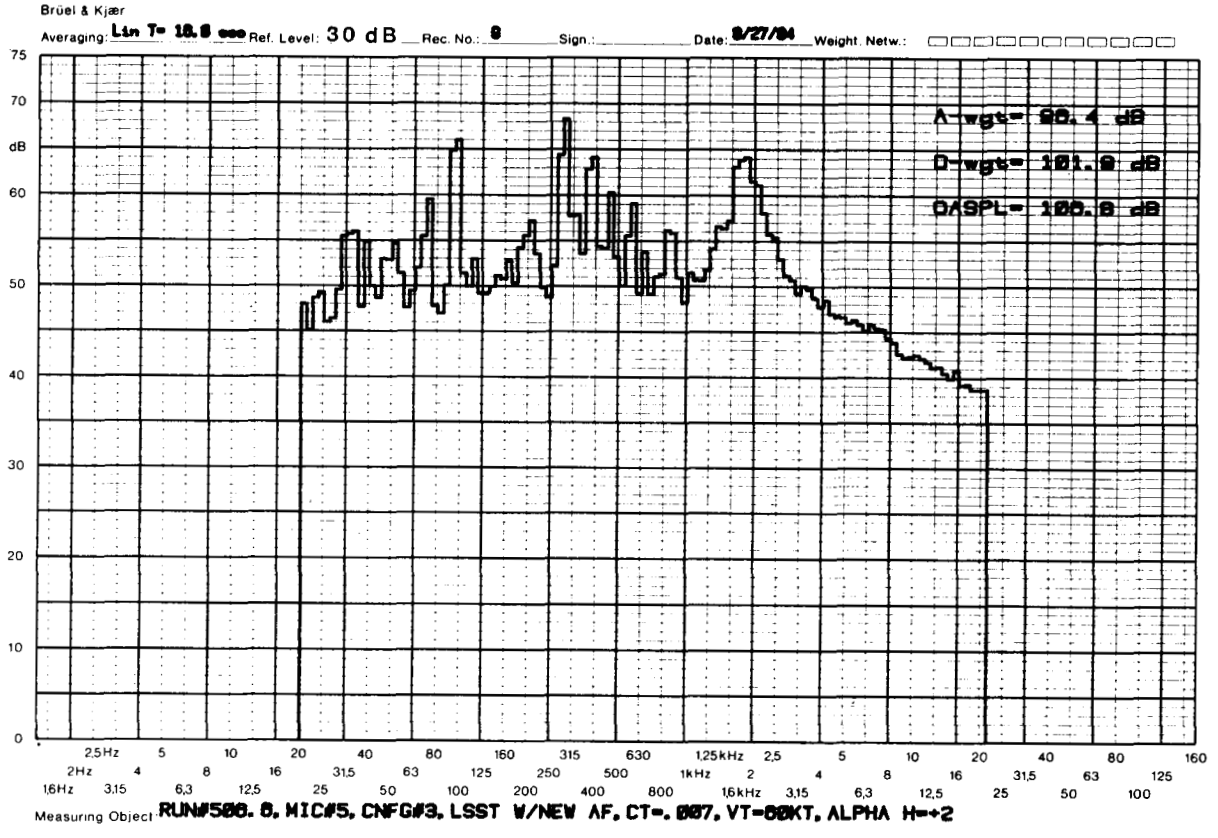

Figure C34. 1/12 Octave Spectra for the 1/5 Scale Large Swept Tapered Tip configuration 3 with New Airfoils at Microphone 5, $M_{\Omega R} = 0.63$, $C_T = 0.007$, $\mu = 0.14$ and $\alpha_{TPP} = 2°$.

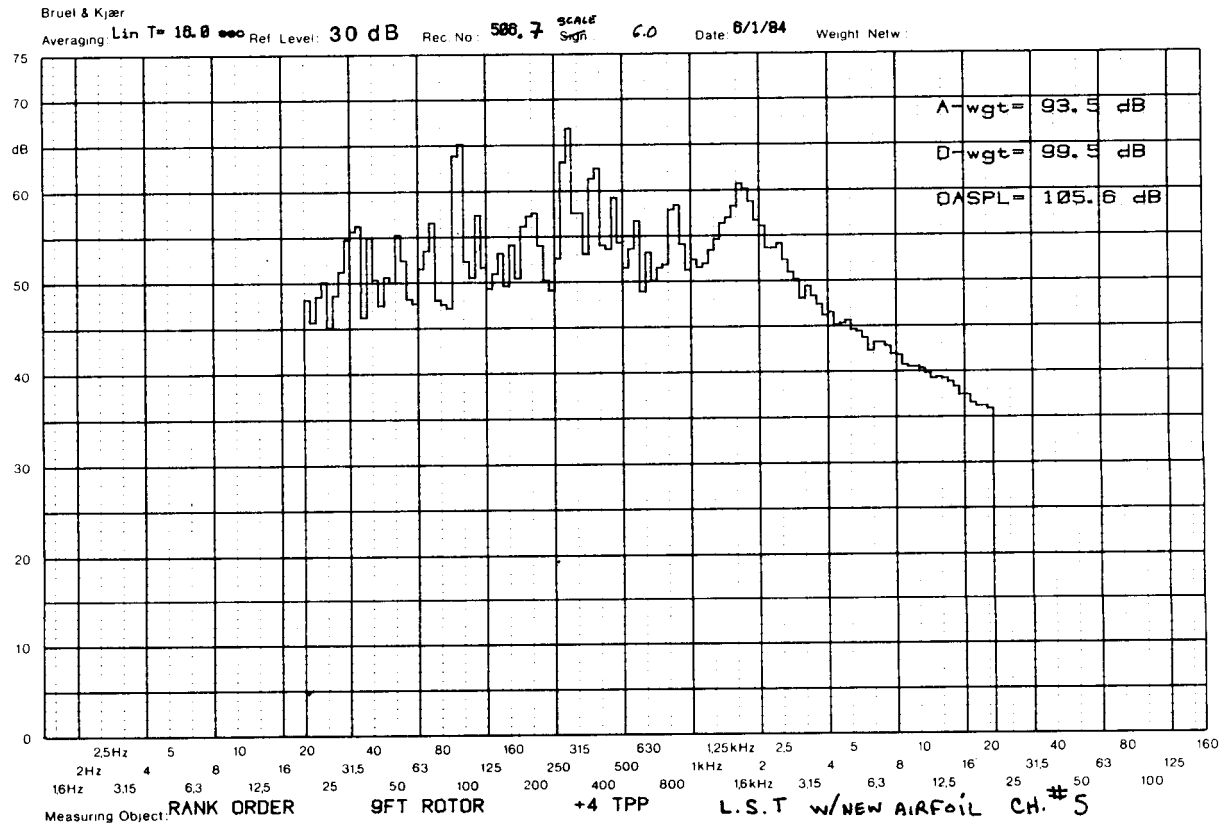

Figure C35. 1/12 Octave Spectra for the 1/5 Scale Large Swept Tapered Tip configuration 3 with New Airfoils at Microphone 5, $M_{\Omega R} = 0.63$, $C_T = 0.007$, $\mu = 0.14$ and $\alpha_{TPP} = 4°$.

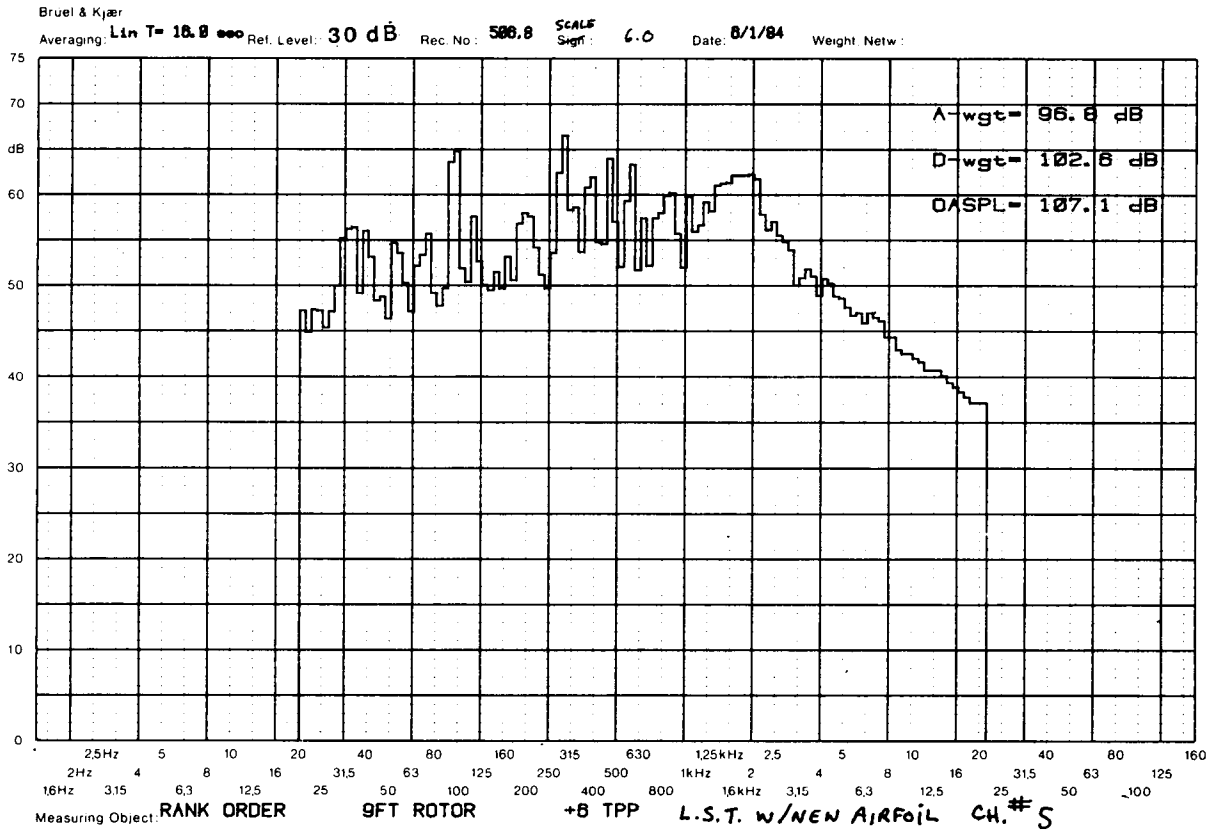

Figure C36. 1/12 Octave Spectra for the 1/5 Scale Large Swept Tapered Tip configuration 3 with New Airfoils at Microphone 5, $M_{\Omega R} = 0.63$, $C_T = 0.007$, $\mu = 0.14$ and $\alpha_{TPP} = 6°$.

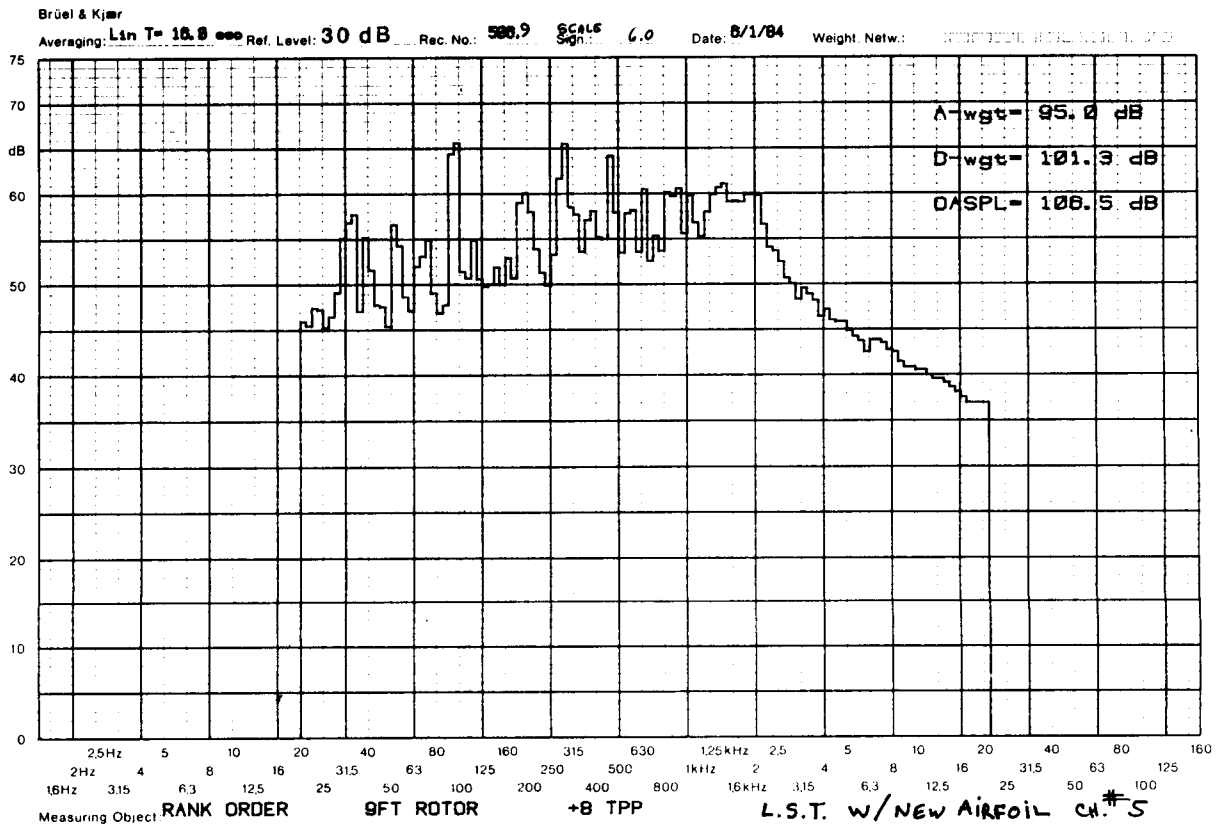

Figure C37. 1/12 Octave Spectra for the 1/5 Scale Large Swept Tapered Tip configuration 3 with New Airfoils at Microphone 5, $M_{\Omega R} = 0.63$, $C_T = 0.007$, $\mu = 0.14$ and $\alpha_{TPP} = 8°$.

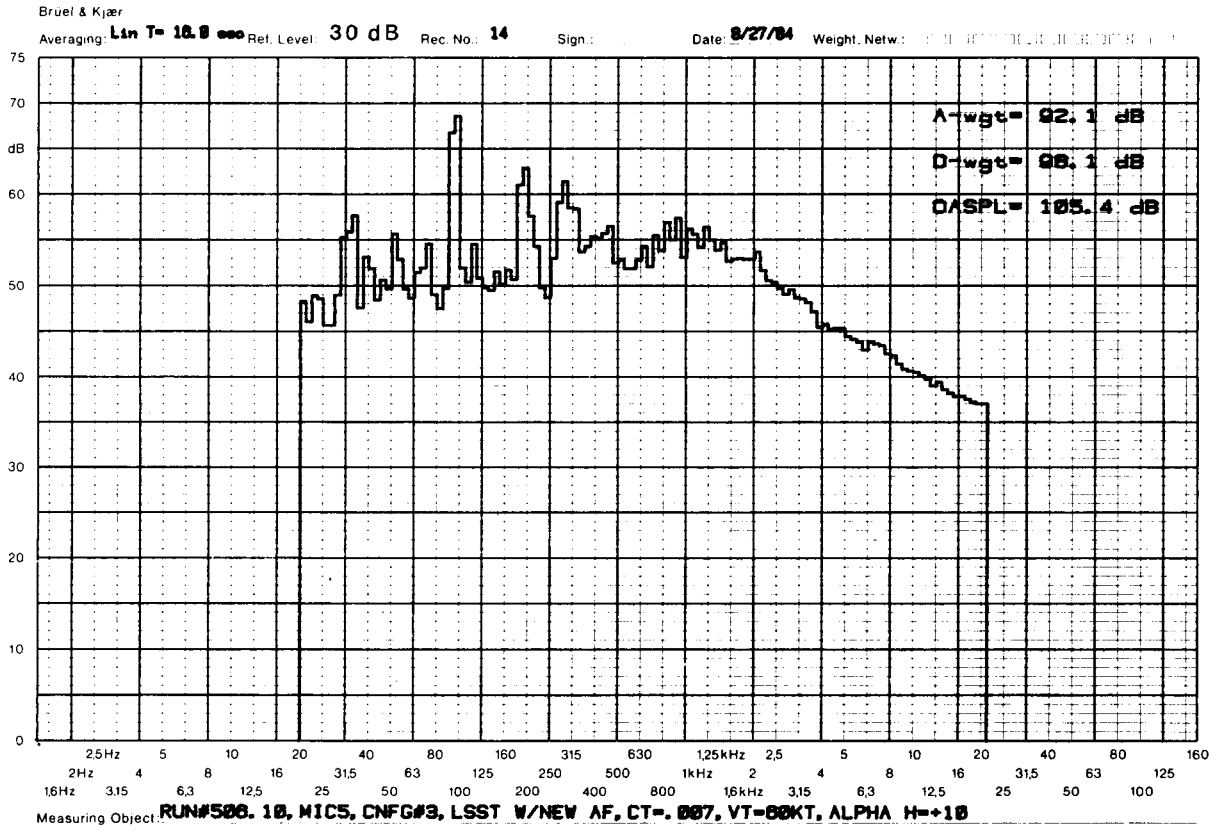

Figure C38. 1/12 Octave Spectra for the 1/5 Scale Large Swept Tapered Tip configuration 3 with New Airfoils at Microphone 5, $M_{\Omega R} = 0.63$, $C_T = 0.007$, $\mu = 0.14$ and $\alpha_{TPP} = 10°$.

1. Report No.	2. Government Accession No.	3. Recipient's Catalog No.
NASA CR-177355		

4. Title and Subtitle	5. Report Date
Acoustic Characteristics of 1/20-Scale Model Helicopter Rotors	August 1986
	6. Performing Organization Code

7. Author(s)	8. Performing Organization Report No.
R.K. Shenoy, F.W. Kohlhepp and K.P. Leighton	SER-510248
	10. Work Unit No.

9. Performing Organization Name and Address	11. Contract or Grant No.
Sikorsky Aircraft Division United Technologies Corporation No. Main Street, Stratford, CT 06601	NAS2-11310
	13. Type of Report and Period Covered
12. Sponsoring Agency Name and Address	Contractor Report
National Aeronautics and Space Administration Washington, D.C. 20546	14. Sponsoring Agency Code
	505-42-11, 505-61-11

15. Supplementary Notes

Point of Contact: Technical Monitor, Marianne Mosher
TR-32 Ames Research Center, Moffett Field, CA 94035
(415) 694-6719 FTS 464-6719

16. Abstract

A wind tunnel test to study the effect of geometric scale on acoustics and to investigate the applicability of very small scale models for the study of acoustic characteristics of helicopter rotors was conducted in the United Technologies Research Center Acoustic Research Tunnel. The results show that the Reynolds number effects significantly alter the Blade-Vortex-Interaction (BVI) Noise characteristics by enhancing the lower frequency content and suppressing the higher frequency content. In the time domain this is observed as an "inverted" thickness noise impulse rather than the typical positive-negative impulse of BVI noise. At higher advance ratio conditions, in the absence of BVI, the 1/20 scale model acoustic trends with Mach Number follow those of larger scale models. However, the 1/20 scale model acoustic trends appear to indicate stall at higher thrust and advance ratio conditions.

17. Key Words (Suggested by Author(s))	18. Distribution Statement
Helicopter Rotor, Acoustics, Scaling Effects, Blade-Vortex-Interaction Acoustics, Model Testing, Anechoic Wind Tunnel	Unclassified - Unlimited Subject Category 71

19. Security Classif. (of this report)	20. Security Classif. (of this page)	21. No. of Pages	22. Price*
Unclassified	Unclassified	118	

*For sale by the National Technical Information Service, Springfield, Virginia 22161